Coordination Chemistry Reviews 255 (2011) 203–240

Contents lists available at ScienceDirect

Coordination Chemistry Reviews

journal homepage: www.elsevier.com/locate/ccr

Review

Spin crossover active iron(II) complexes of selected pyrazole-pyridine/pyrazine ligands

Juan Olguín, Sally Brooker*

Department of Chemistry, The MacDiarmid Institute for Advanced Materials and Nanotechnology, University of Otago, PO Box 56, Dunedin, New Zealand

Contents

ARTICLE INFO

Article history:
Received 25 May 2010
Accepted 5 August 2010
Available online 17 August 2010

Keywords:
Iron(II)
Spin crossover
Pyrazole
Synthesis
Structure
Magnetic
Mössbauer

ABSTRACT

This review begins with a brief introduction to pyrazole and to spin crossover. The focus then moves to a detailed consideration of the synthesis and magnetic properties of structurally characterized iron(II) spin crossover (SCO) active complexes of pyrazole- and pyrazolate-based ligands that also contain at least one pyridine or pyrazine unit within the ligand motif. The syntheses and crystallization methods reported in the original publications are emphasized in this review. The reason for this is that these factors often affect the exact nature of the final product, including the amount and nature of the crystallization solvent molecules present and/or what polymorph is obtained, and hence they can impact strongly on the SCO properties of the resulting materials, as can be seen in this review.

1. Introductory remarks and scope of the review

1.1. Introductory remarks on pyrazoles

Pyrazole (Fig. 1A) is one of the most versatile molecules in inorganic chemistry so, not surprisingly, there are many reviews of the coordination and organometallic chemistry of pyrazole

* Corresponding author. Tel.: +64 3 479 7919; fax: +64 3 479 7906.
E-mail address: sbrooker@chemistry.otago.ac.nz (S. Brooker).

0010-8545/$ – see front matter © 2010 Elsevier B.V. All rights reserved.
doi:10.1016/j.ccr.2010.08.002

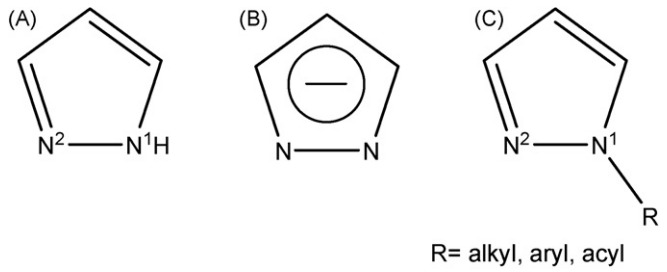

Fig. 1. (A) Pyrazole; (B) Pyrazolate anion; (C) *N*-substituted pyrazole.

[1–9]. Pyrazole containing ligands have been used for the synthesis of inorganic models of metallo-enzymes and as synthons in supramolecular chemistry and catalysis. The wide use of the pyrazole moiety is due to the convenient, adjacent positioning of two nitrogen donors, a deprotonable NH (*N*1) and an aromatic-like N (*N*2). Either the *N2* donor atom only, or, on deprotonation of *N*1, both of these nitrogen donor atoms are capable of coordinating to metal centres.

Neutral pyrazole ligands coordinate in acid media to metal ions and metalloids only through the aromatic-like nitrogen *N*2 (Fig. 2A). The resulting complex can form H-bonding interactions thanks to the N–H donor at the *N*1 position.

On the other hand, deprotonation of *N*1 results in the pyrazolate anion and facilitates the synthesis of dinuclear and/or polynuclear pyrazolate-bridged metal complexes (eg. Fig. 2B) with relatively short M···M separations (typically from 3.5 to 4.7 Å for first row transition metal ions). However it should be noted that a wide range of binding modes, over 20, has been observed for pyrazole/pyrazolate to date, including a mode in which a single pyrazolate unit coordinates to 4 metal centres. The reader is referred to comprehensive surveys, by Halcrow [10] and by Meyer and co-workers [11], of these binding modes. Those that are relevant to the present survey are shown in Fig. 2.

A wide range of aryl, acyl and alkyl substituents have been introduced to the *N*1 position of pyrazole. The resulting '*N*1-blocked' pyrazole remains neutral and can only coordinate through the aromatic-like *N*2 so the resulting metal complexes are usually mononuclear (*N*-blocked neutral monodentate binding mode, Fig. 2C). Exceptions to this arise when the substituent at *N*1 is a ditopic connector or another bridging ligand that provides donor atoms to the coordination sphere of the metal ion.

1.2. Introductory remarks on spin crossover

In addition to the aforementioned interests, it is well known that pyrazole- and pyrazolate-derived ligands can generate iron(II) spin crossover (SCO) active complexes [9,12], in which the paramagnetic $t_{2g}^4\ e_g^2$ high spin state (HS) can be switched to the diamagnetic t_{2g}^6 low spin state (LS) by means of an external stimulus like temperature, pressure, light or applied magnetic field [13].

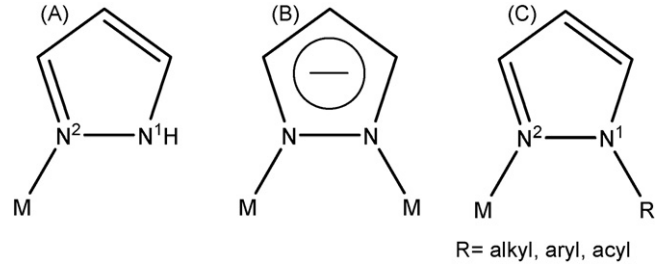

Fig. 2. Selected coordination modes which are relevant to the present survey: (A) neutral monodentate; (B) anionic *exo*-bidentate; (C) *N*-blocked neutral monodentate.

Change in temperature is the most commonly employed external stimulus, probably because the technical requirements involved in the detection and characterisation of a temperature dependent spin transition (ST) are readily met. Typically, variable temperature (VT) magnetic (e.g. using a SQUID magnetometer), X-ray crystallographic and Mössbauer spectroscopic studies are carried out. SCO events can be gradual or abrupt, complete or incomplete, and with or without hysteresis [14]. The most desirable are abrupt, complete and with hysteresis. It is generally found that cooperativity between metal centres (either via bridging ligands or via packing interactions, such as hydrogen bonding [15,16]) greatly aids both the abruptness and the chances of observing hysteresis. Such properties are usually seen for crystalline samples rather than powders.

Spin transition curves are most readily obtained from VT magnetic studies and are often plotted as a $\chi_M T$ vs T graph. The expected magnetic moment value for a HS mononuclear iron(II) complex (HS is observed at higher temperatures) is around 5.0 BM, consistent with the presence of 4 unpaired electrons (paramagnetic). Upon cooling and undergoing SCO to the LS state this value drops to close to 0 BM, consistent with the presence of no unpaired electrons (diamagnetic). Samples do not need to be single crystals, but this usually improves the quality of the SCO transition.

Another important technique for the characterisation of this event is X-ray crystallography as the Fe–N bond lengths and N–Fe–N bond angles for the two spin states are usually unequivocally distinguishable. In the case of HS iron(II) the bond lengths are usually 2.00–2.20 Å and the bond angles are characteristic of a distorted octahedron (angles not particularly close to 90°/180°). In contrast, for LS iron(II) the expected bond lengths are about 1.80–2.00 Å and the bond angles are normally far closer to those of an ideal octahedron (90°/180° [13]). Such studies can be carried out at more than one temperature, allowing structural characterisation of the complex in the different spin states. The key limitation with regard to unleashing this technique is the growth of single crystals of the complex, something which seems to be harder for SCO complexes than in general (for example, the famous Kahn SCO-active triply-triazole-bridged iron(II) polymer [17] has never been crystallized, but a single crystal X-ray structure determination has been carried out on the copper(II) analogue [18]).

VT ^{57}Fe Mössbauer spectroscopy is also very powerful, not least as it does not require single crystals. As the name suggests, this technique focuses in on the ^{57}Fe centres (natural abundance 2% so in some cases complexes are prepared using isotopically enriched ^{57}Fe salts). Typically the spectra of HS iron(II) samples show relatively high quadrupole splitting ($\Delta E_Q = 2–3\ mm\ s^{-1}$) and isomer shift ($\delta = 1\ mm\ s^{-1}$), while in LS iron(II) samples these parameters are usually smaller ($\Delta E_Q \leq 1\ mm\ s^{-1}$, $\delta \leq 0.5\ mm\ s^{-1}$ [14]).

Such SCO systems are very interesting, not only from theoretical and fundamental research perspectives, but also because of the technological applications that ultimately may arise, such as memory devices, molecular switches, MRI contrast agents, and other uses in devices [16,19]. The reader is referred to recent reviews of SCO-active complexes for reviews of the range of types of SCO-active complexes and their possible applications [12,13,16,20].

1.3. Scope of this review

A survey of the CSD (5.30, update September 2009 [21,22]) revealed a total of 85 structurally characterized iron(II) complexes of pyrazole- and pyrazolate-based ligands that contain at least one pyridine or pyrazine unit within the ligand motif. Of these, 42 are SCO-active and these complexes are the focus of this review.

To set the scene we first give an overview of the 19 different ligands that have been used to generate these 42 structurally char-

acterized SCO-active iron(II) complexes, and in doing so briefly survey the most common structural types observed for coordination complexes of these, and two related, ligands with a wide range of transition metal ions (Section 2). Then we present and discuss in detail the syntheses, structures and properties of the 42 iron(II) complexes of these 19 ligands (Section 3).

The magnetic properties of SCO-active complexes can be critically dependent on the exact nature of the interactions present in the crystal lattice, such as hydrogen bonding, π–π and anion–π interactions. These interactions can change when a different solvate or a different polymorph is obtained. Hence a detailed description of the synthesis and crystallization methods, as well as the space group and packing interactions present in the crystal lattice of these structurally characterized SCO-active iron(II) complexes, is presented in this review.

It is pertinent to note that there are no examples of *macrocyclic* iron(II) complexes of pyrazole/pyrazolate-based ligands containing at least one pyridine or pyrazine unit in the ligand motif, let alone any that are also SCO-active. That is, all of the ligands employed in such studies to date are *acyclic*. Finally, please note that complexes of pyrazolylborate and pyrazolylmethane ligands have been excluded from this review [23].

2. Acyclic ligands and non-iron(II) transition metal complexes

In this section the structures of non-iron(II) transition metal complexes of the 19 ligands (Fig. 3) plus two closely related ligands, derived from pyrazole and pyridine or pyrazine, that have permitted the synthesis of the 42 structurally characterized SCO-active iron(II) complexes, are analysed to provide background information for the subsequent analysis of the iron(II) complexes (Section 3).

A classic approach to the development of ligands that on coordination might induce SCO in iron(II) is the replacement of some six-membered heterocycles in a LS-inducing ligand by five-membered heterocycles. This reduces the σ-donor and π-acceptor character of the system and introduces more strain into the resulting chelate ring, reducing the ligand field experienced by the iron(II) centre. The topic of this review fits nicely within this area as all 21 ligands of interest contain at least one six-membered (pyridine or pyrazine) and one five-membered (pyrazole) ring.

Replacement of the two terminal pyridine rings in the 2,2′:6′6″-terpyridine (terpy) structure by two pyrazole rings can be done in two different ways: forming either a $N_{pyrazole}$–$C_{pyridine}$ (L^1–L^{14}, Fig. 3) or $C_{pyrazole}$–$C_{pyridine}$ (H_2L^{15}, Fig. 3) connection. Both approaches produce terdentate ligands capable of forming mononuclear iron(II) SCO-active complexes (in contrast, all iron(II) complexes of terpy are low spin [24]). However, the $N_{pyrazole}$–$C_{pyridine}$ linked ligands, L^1–L^{14}, can no longer be deprotonated, and provide only one of the two pyrazole nitrogen atoms for coordination (*N*-blocked neutral monodentate binding mode, Fig. 2C). In contrast, the $C_{pyrazole}$–$C_{pyridine}$ ligands, H_2L^{15}, can either remain neutral on coordination, with the N–H available for hydrogen bonding (neutral monodentate binding mode, Fig. 2A), or deprotonate, potentially providing two pyrazolate nitrogen atoms for coordination to metal ions (anionic *exo*-bidentate binding mode, Fig. 2B).

According to the CSD version 5.31 (updates September 2009) there are at least 80 structurally characterized transition metal complexes of the 2,6-bis(pyrazol-1-yl)pyridine derived-ligands ($N_{pyrazole}$–$C_{pyridine}$ linked), L^1–L^5 and L^{10}–L^{14}. Of these 36 are iron(II) complexes, of which 21 are SCO-active (see Section 3.1.1). Of the remaining complexes there are 22 of copper(II), 6 of ruthenium(II), 6 of cobalt(II), 2 of each of platinum(II), nickel(II), zinc(II) and cadmium(II), 1 of mercury(II) and 1 dimetallic complex of rhenium(V). The most common structural type observed is $[M^{II}(L^n)_2]^{2+}$, with the transition metal ion six coordinate, surrounded by two terdentate ligands, and resulting complex being dicationic (Fig. 4A). The second most common structural type is again mononuclear, but in these complexes the metal centre is coordinated to only one 2,6-bis(pyrazol-1-yl)pyridine derived-ligand and the remaining vacant positions are occupied by anions or solvent molecules or by a bidentate ligand such as 2,2′-bipyridine (Fig. 4B–E). The third and final structural type comprises dinuclear complexes, $[M^{II}(L^n)(X)(\mu_2\text{-}X)]_2^{x+}$, in which each metal centre is coordinated to one 2,6-bis(pyrazol-1-yl)pyridine derived-ligand, two vacant positions are occupied by a bridging ligand X (halogen, pseudo-halogen, 4,4′-bipyridine, azide or oxo group), and the last position is occupied by a terminal anion or solvent molecule, X (Fig. 4F). The charge on the resulting complex is clearly variable depending on the nature of X.

In the case of the 2,6-bis(pyrazol-1-yl)pyrazine derived-ligands, L^6–L^9, there are only 9 structurally characterized metal complexes. All 9 of them are of iron(II) and of the type $[Fe^{II}(L^{6-9})_2]X_2$ (X = SbF_6, BF_4 or ClO_4, Fig. 4A), and 3 of them are SCO-active so will be analysed in Section 3.1.1.

For 2,6-bis(pyrazol-3-yl)pyridine derived-ligands ($C_{pyrazole}$–$C_{pyridine}$ connector), 27 structurally characterized transition metal and lanthanide complexes were found (CSD version 5.31). Of these complexes, 15 are iron(II) complexes of H_2L^{15} (i.e. with no substituents on the pyridine or pyrazole ring), of which 10 are SCO-active so are discussed in detail later (Section 3.1.2). There are also 3 ruthenium(II), 3 copper(II) and 1 of each of silver(I), cobalt(II), nickel(II), europium(III), gadolinium(III) and holmium(III) complexes, all of which are of H_2L^{15}, except for one complex of Ag(II) and one complex of Ru(II) in which the pyrazole ring is substituted in the 3 and/or 4-positions. The most common structural type here is $[M^{II}(H_2L^{15})_2]^{2+}$ in which the metal ion is coordinated to two neutral terdentate 2,6-bis(pyrazol-3-yl)pyridine derived-ligands, resulting in a dicationic complex (Fig. 5A). Lanthanide ions require a greater coordination number so those structures feature $[Ln^{III}(H_2L^{15})_3]^{3+}$, with three neutral terdentate 2,6-bis(pyrazol-3-yl)pyridine derived-ligands coordinated to the nine-coordinate lanthanide ion (Fig. 5B). There are only 3 examples of complexes in which only one 2,6-bis(pyrazol-3-yl)pyridine derived-ligand is coordinated to the metal centre, 2 of these are copper(II) complexes where Cl^- or Br^- completes the five-coordination and 1 is a silver(I) complex where two pyridine molecules complete the five coordination (Fig. 5C). Finally, the only example of a dinuclear system incorporating this type of ligand is an SCO-active iron(II) complex, $\{[Fe^{II}(H_2L^{15})(NCS)_2]_2(\mu\text{-}4,4'\text{-bipy})\}$, in which each metal centre is coordinated to a 2,6-bis(pyrazol-3-yl)pyridine derived-ligand, along with two isothiocyanato anions and a bridging 4,4′-bipyridine ligand (Fig. 5D), and it will be analysed in Section 3.1.2. For this particular family no pyrazine analogues were structurally characterized.

A more flexible version of the 2,6-bis(pyrazol-1-yl)pyridine ligand is 2,6-bis(1-pyrazolylmethyl)pyridine, L^{16}, which features a flexible methylene linker between the $N_{pyrazole}$ and $C_{pyridine}$ atoms. For this ligand, and some related ligands in which the 3,4 and/or 5 positions of the pyrazole ring are substituted (eg. L^{17}, Fig. 3), 33 structurally characterized transition metal complexes were found in the CSD (version 5.31, updates February 2010). There are 14 complexes of copper(II), 6 complexes of copper(I), 5 complexes of palladium(II), and 1 complex each of zinc(II), nickel(II), platinum(II) and cadmium(II). Finally, there are 4 complexes of iron(II), of which only one is SCO-active (analysed in Section 3.1.3). The most common structural type is mononuclear $[M(L)(X)_n]^{m+}$ where $n = 1$ or 2 and L = unsubstituted L^{16} or analogues that are substituted at the 3, 4 and/or 5 positions of the pyrazole rings (Fig. 6A).

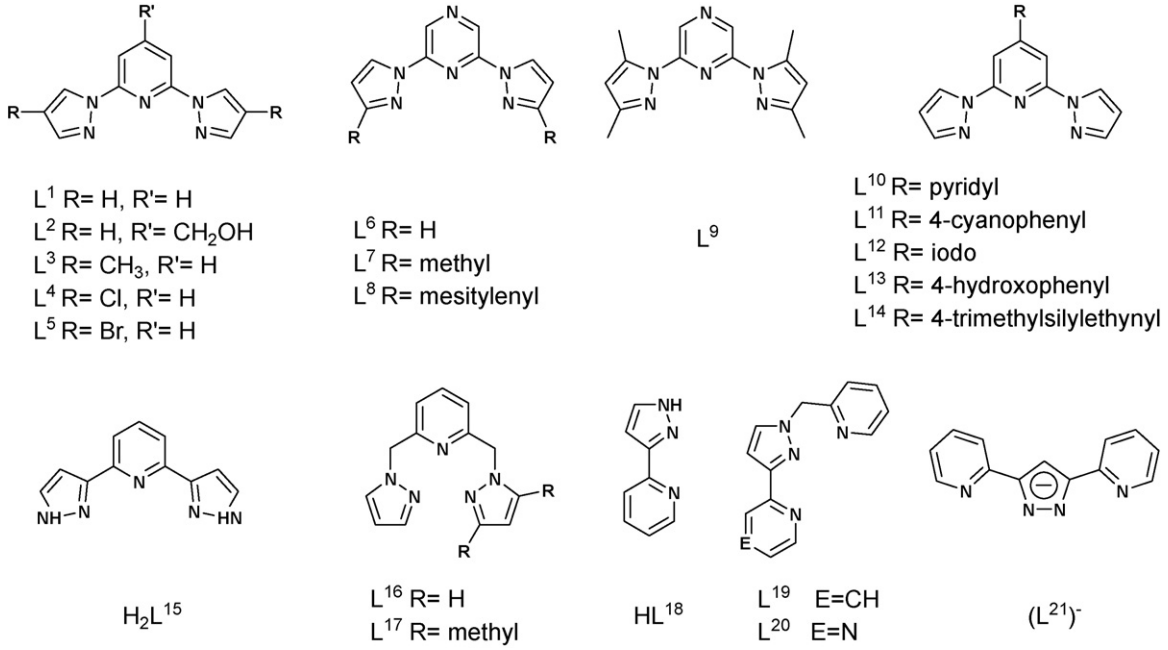

Fig. 3. The 19 pyrazole-pyridine or -pyrazine based ligands used to prepare the 41 structurally characterized SCO-active iron(II) complexes reviewed herein, plus 2 related ligands L^8 and L^{17}.

In these complexes the metal ion is coordinated to the central pyridine unit and to both pyrazole rings of the 2,6-bis(pyrazol-1-yl)pyridine-based ligand and the rest of the positions, X, are either occupied by terminal ligands, such as counteranions and/or solvent molecules, or by bridging ligands (e.g. 4,4′-bipyridine or azide). The second most common structural type, $[M(L)_2]^{2+}$, is also mononuclear, but the metal centre is coordinated to *two* terdentate 2,6-bis(1-pyrazolylmethyl)pyridine-based ligands (Fig. 6B). There are no structurally characterized complexes of the pyrazine based analogues of these pyridine based ligands.

Another classic system is generated by the replacement of one pyridine ring in the 2,2′-bipyridine (bpy) ligand by a pyrazole ring (unsubstituted or 3- and/or 4-substituted), resulting in 2-(pyrazol-3-yl)pyridine derived-ligands, HL^{18} and pyrazole-substituted analogues. Some of the resulting mononuclear and dinuclear iron(II) complexes of unsubstituted HL^{18} are SCO-active (see Section 3.2.1). This type of ligand can either remain neutral and bind as a simple bidentate ligand, where the metal centre is coordinated to the pyridine nitrogen and the aromatic-like *N*2 of the pyrazole ring, or it can be deprotonated (at *N*1 of the pyrazole ring) and bridge two metal centres.

According to a search of the CSD (version 5.30), there are at least 58 structurally characterized transition and lanthanide metal complexes in which the unsubstituted HL^{18} or 3- and/or 4-substituted pyrazole derivatives of HL^{18} act as neutral bidentate ligands (*N*1 remaining protonated). There are 13 complexes of cadmium(II), 10 of copper(II), 10 of manganese(II), 4 of iron(II), from which 3 are SCO-active (see Section 3.2.1), 4 of zinc(II), 3 of nickel(II), 2 of each of lead(II), platinum(II) and iron(III), 1 of each of cobalt(II), palladium(II), ruthenium(II), silver(I), neodymium(III) and lanthanum(III), and 1 mixed metal complex of ruthenium(II) and europium(III). The most common structural type for these complexes is mononuclear, $[M(HL^{18})_2(X)_m]^{x+}$, with the metal ion coordinated by two neutral bidentate 2-(pyrazol-3-yl)pyridine derived-ligands and the remaining positions occupied by solvent or anion molecules (Fig. 7A). The second most common structural type is mononuclear tris-(2-(pyrazol-3-yl)pyridine) complexes, $[M(HL^{18})_3]^{2+}$ (Fig. 7B). Lastly, a handful of dinuclear and polynuclear complexes have been obtained, in which each metal centre is coordinated to either one or two neutral 2-(pyrazol-3-yl)pyridine derived-ligands and the remaining positions occupied by one or two bridging ligands and/or solvent or anion molecules (Fig. 7C).

For the pyrazine analogue of HL^{18}, namely 2-(pyrazol-1-yl)pyrazine, only 6 structurally characterized transition metal complexes were found. All 6 are mononuclear. One is a square planar platinum(II) complex (Fig. 7A), one is a bis(bidentate) iron(II) complex (Fig. 7A), three are tris(bidentate) LS-iron(II) complexes (Fig. 7B), and finally one is an organometallic iridium(III) complex (Fig. 7D).

When deprotonation of the 2-(pyrazol-3-yl)pyridine derived-ligands occurs (at *N*1), discrete and polymeric multinuclear complexes can be synthesized. At least 59 such complexes have been structurally characterized. There are 29 complexes of copper(II), 7 of copper(I), 5 of cadmium(II), 2 of silver(I), 1 of each of thallium(I), lead(II), palladium(II), iron(II), iron(III), nickel(II) and zinc(II). In addition there is 1 dinuclear complex of rhodium(II), 1 dinuclear complex where the cation comprises a dinuclear complex of rhodium(III) and the anion comprises a dinuclear complex of rhodium(II), 3 dinuclear heterometallic complexes of palladium(II)-iridium(0), 1 dinuclear heterometallic complex of lead(II)-iridium(III), and 1 of iridium(0)-rhodium(II). These deprotonated ligands coordinate to the metal centre as a bidentate ligand through the pyridine and *pyrazolate* rings and in addition to this have the ability to bridge another metal centre through the deprotonated *N*1 atom of the pyrazolate ring. Dinuclear complexes result in cases where the second metal centre is coordinated to a second 2-(pyrazol-3-yl)pyridine derived-ligand and at the same time this second ligand is coordinated to the first metal centre, with the remaining positions occupied by solvent, anion molecules or other terminal ligands (Fig. 8A). In contrast, if the second ligand strand is coordinated to a different (third) metal centre then multimetallic complexes result. These multinuclear systems can be either discrete, forming cyclic structures, or polymeric (Fig. 8B).

A special case of 2-(pyrazol-3-yl)pyridine-derived ligands is the substitution of the proton at *N*1 by a picolyl group, generating terdentate ligands, L^{19} (Fig. 3), that on complexation feature adjacent 5- and 6-membered chelate rings. Coordination with iron(II)

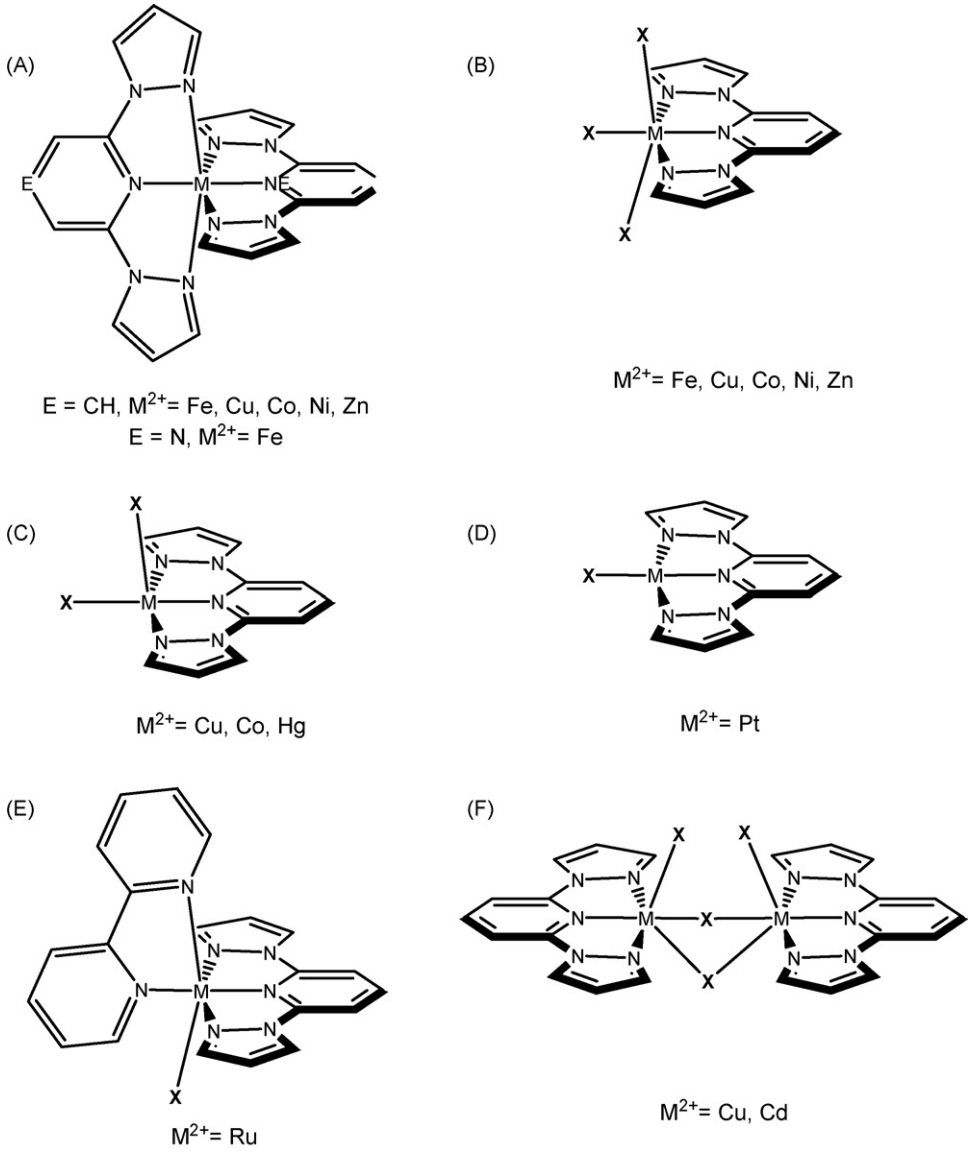

Fig. 4. A selection of the key structural types observed for coordination complexes of 2,6-bis(pyrazol-1-yl)pyridine/pyrazine derived-ligands L^1–L^{14}. X = solvent, halogen, pseudo-halogen.

salts produces a mononuclear SCO-active complex (see Section 3.2.2). Only 8 complexes of L^{19} have been structurally characterized according to the CSD (version 5.30). There is 1 dinuclear complex of copper(II), 2 dinuclear and 2 mononuclear complexes of nickel(II), and 1 mononuclear complex of each of zinc(II), cobalt(II) and manganese(II). The most common structural type for these complexes is two terdentate ligands coordinated to one six coordinate metal centre, $[M^{II}(L^{19})_2]^{2+}$ (Fig. 9A). The next most common structural type is one terdentate ligand coordinated to the metal centre with the remaining positions occupied by solvent or anion molecules, $[M^{II}(L^{19})/X)_m]^{x+}$ (Fig. 9A and C). The final structural type is a dinuclear system in which each metal centre is coordinated to one terminal 2-(pyrazol-3-yl)pyridine-derived ligand and to two 2-(pyrazol-3-yl)pyridine bridging ligands (Fig. 9D and E). A special analogue of this ligand is L^{20} (Fig. 3) where the pyridine moiety attached to the 3-position of the pyrazole ring has been replaced by a pyrazine unit. Some of the resulting iron(II) complexes are SCO-active and these will be analysed in Section 3.2.2.

For the pyrazine analogue ligand L^{20}, there are 5 structurally characterized iron(II) complexes. All 5 are iron(II) complexes of the type $[Fe^{II}(L^{20})_2]X$ (X = BF_4, or ClO_4, Fig. 9A), and 2 of them are SCO-active (see Section 3.2.2). There are no structurally characterized complexes of L^{20} with any other transition metal ions.

The final class of ligands being considered in this review is produced by the introduction of two pyridine rings, at the 3-*and* 5- positions of the pyrazole ring, resulting in a bis-bidentate ligand capable of forming dinuclear iron(II) SCO-active systems by deprotonation of the NH of the pyrazole moiety $(L^{21})^-$ (Fig. 3). That is, this type of ligand typically coordinates to two metal centres, bridging them. The remaining coordination sites can be occupied either by another ligand strand (resulting in double bridging of the 2 metal ions by the pyrazolate moieties) or by terminal or other bridging ligands. According to the CSD there are 53 structurally characterized metal complexes of these 3,5-bis(2′-pyridyl)pyrazole ligands. Of these complexes, 21 are dinuclear ruthenium(II), 1 is dinuclear ruthenium(III), 6 are dinuclear iron(II) (of which 4 are SCO-active, see Section 3.3.1), 3 are dinuclear copper(II), 1 is tetranuclear copper(II), two are dinuclear zinc(II), 1 is dinuclear cobalt(II), 1 is tetranuclear cobalt(II), 1 is mononuclear silver(I), 1 is polymeric silver(I), 1 is tetranuclear silver(I), 1 is mononuclear platinum(I), and there is 1 of each of the following mixed-metal complexes: iron(II)-chromium(III), chromium(III)-dysprosium(III),

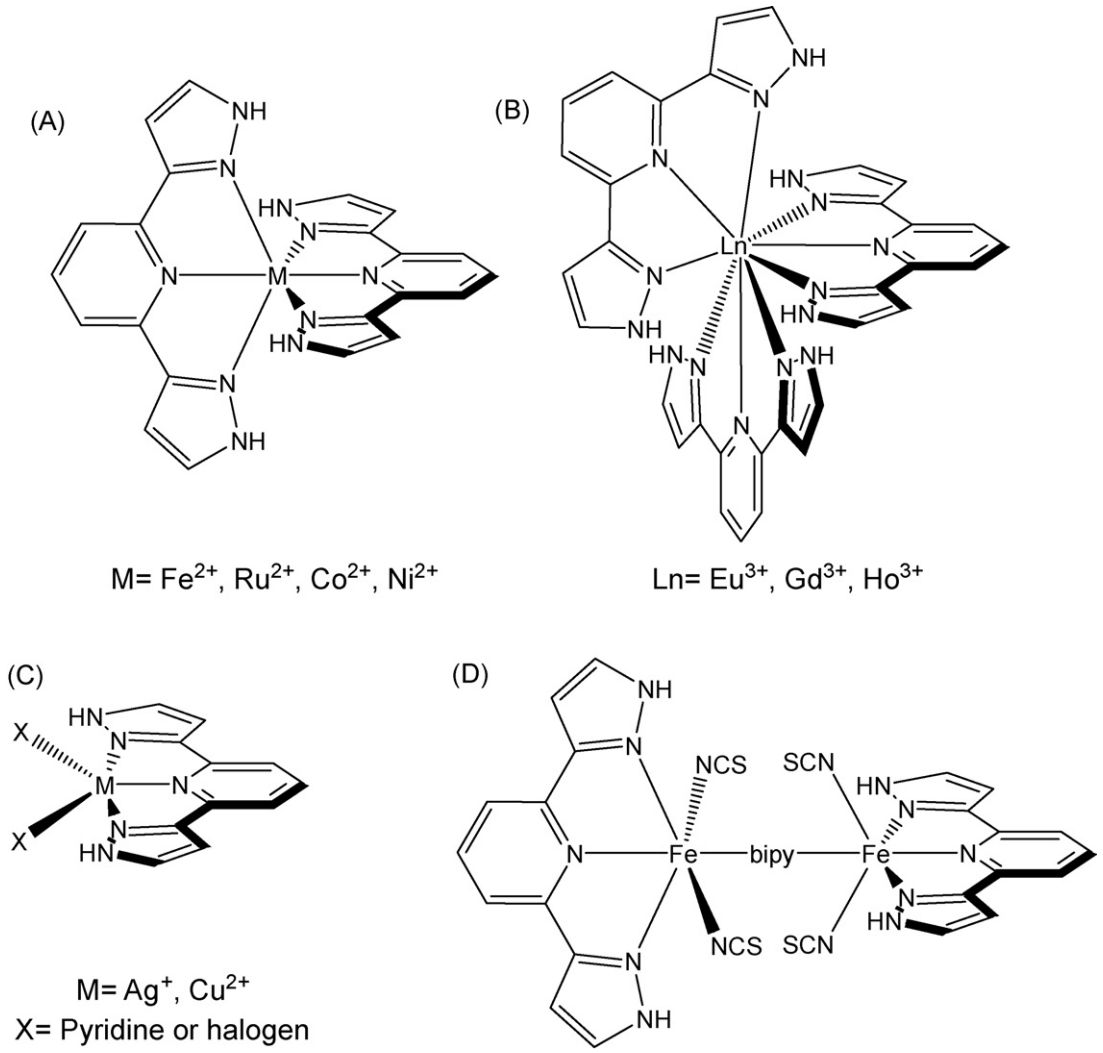

Fig. 5. A selection of the key structural types observed for coordination complexes of 2,6-bis(pyrazol-3-yl)pyridine derived-ligands (H_2L^{15}). Substitutents at the 3- and/or 4-position of the pyrazole ring are not shown for the sake of clarity.

chromium(III)-gadolinium(III), chromium(III)-neodymium(III), chromium(III)-samarium(III), chromium(III)-yttrium(III), chromium(III)-cerium(III), chromium(III)-europium(III), chromium(III)-erbium(III). All of these complexes contain the deprotonated form of the ligand. The most common structural type for these complexes is a *dinuclear* system, $[M_2(L^{21})_2(X)_4]^{x+}$, in which two 3,5-bis(2′-pyridyl)*pyrazolate* ligands are coordinated, in an equatorial fashion, with the central pyrazolate moieties bridging the two metal ions and also binding via the terminal pyridine rings; the apical positions are occupied by anion or solvent molecules (Fig. 10). There are no examples of structurally characterized complexes of the pyrazine analogue for this system.

3. Acyclic ligands and iron(II) SCO-active complexes

3.1. Terdentate ligands

3.1.1. 2,6-Bis(pyrazol-1-yl)pyridine/pyrazine family

The synthesis and chemistry of the 2,6-bis(pyrazol-1-yl)pyridine/pyrazine (1-bpp, here referred to as L^1–L^{14}, Fig. 3) and 2,6-bis(pyrazol-3-yl)pyridine (3-bpp, here referred to as H_2L^{15}, Fig. 3) ligand families is well known [8]. As mentioned above, the 2,6-bis(pyrazol-1-yl)pyridine/pyrazine ligands are related to the classic terpyridine (terpy) system and, like terpy, they typically coordinate to transition metal ions in a meridional (mer) terdentate manner and usually form very stable complexes. Although they are structurally similar terdentate ligands, something which can be demonstrated by comparison of the mean *trans*-N–Fe–N angles in these families of complexes (terpy 177(6)° vs 1-bpp 174(7)° vs 3-bpp 176(4)°; CSD 5.30, Vista V.2.1), the coordination chemistry is different due to the different basicity, σ-donor and π-acceptor/donor capacities of pyridine/pyrazine vs pyrazole nitrogen atoms [25]. Some of the resulting iron(II) complexes are SCO-active [8], and these are the topic of discussion in this section. A comprehensive review by Halcrow, of iron(II) SCO-active complexes of the the ligand families 3-bpp, 1-bpp and pyrazine analogues of the latter, was published while this manuscript was in preparation so the reader is referred to that paper for additional details [9].

In all twenty of the complexes analysed in this section, each iron(II) centre coordinates to two, almost perpendicular, terdentate 2,6-bis(pyrazol-1-yl)pyridine derived ligands in a *N*-blocked neutral monodentate binding mode (Fig. 2), resulting in an N_6 distorted octahedral coordination sphere (Fig. 4A). Two angles can be used to help describe the distortions in the resulting complex (Fig. 11): ϕ is defined as the angle formed between the two *trans*-pyridine units, and θ is the angle formed between the mean planes through the two sets of ligands (in the case of an ideal octahedron $\phi = 180°$ and

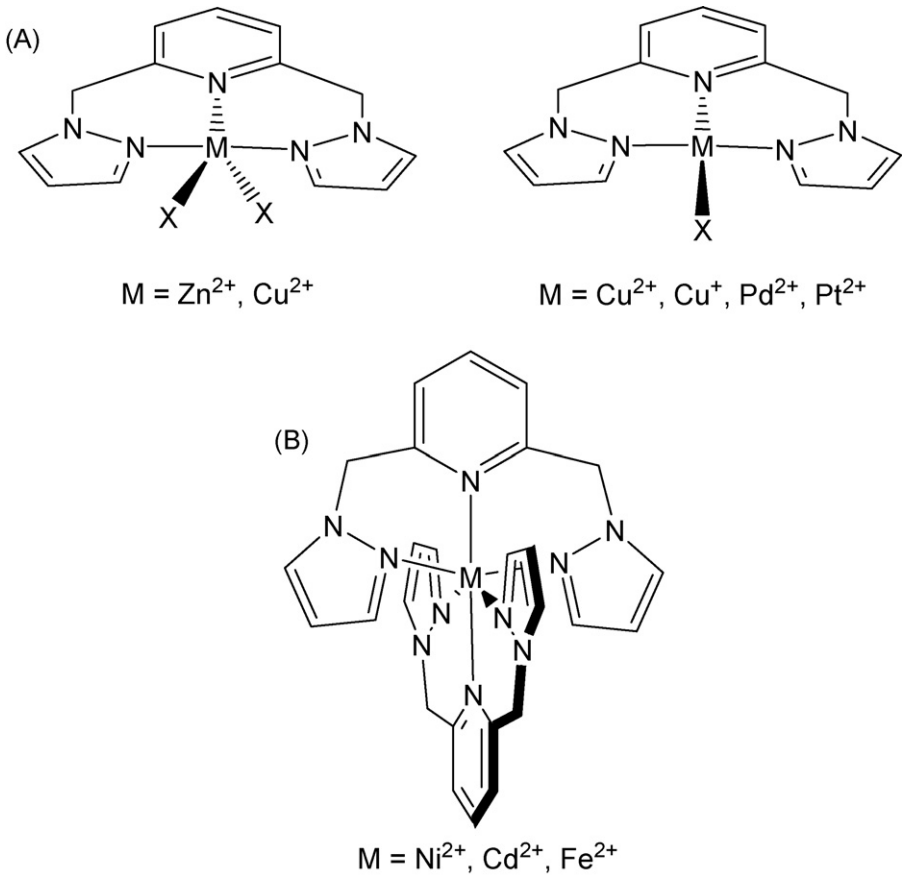

Fig. 6. A selection of the key structural types observed for coordination complexes of 2,6-bis(1-pyrazolylmethyl)pyridine derived-ligands (L^{16}). Substitutents at the 3-, 4- and/or 5-position of the pyrazole ring are not shown for the sake of clarity.

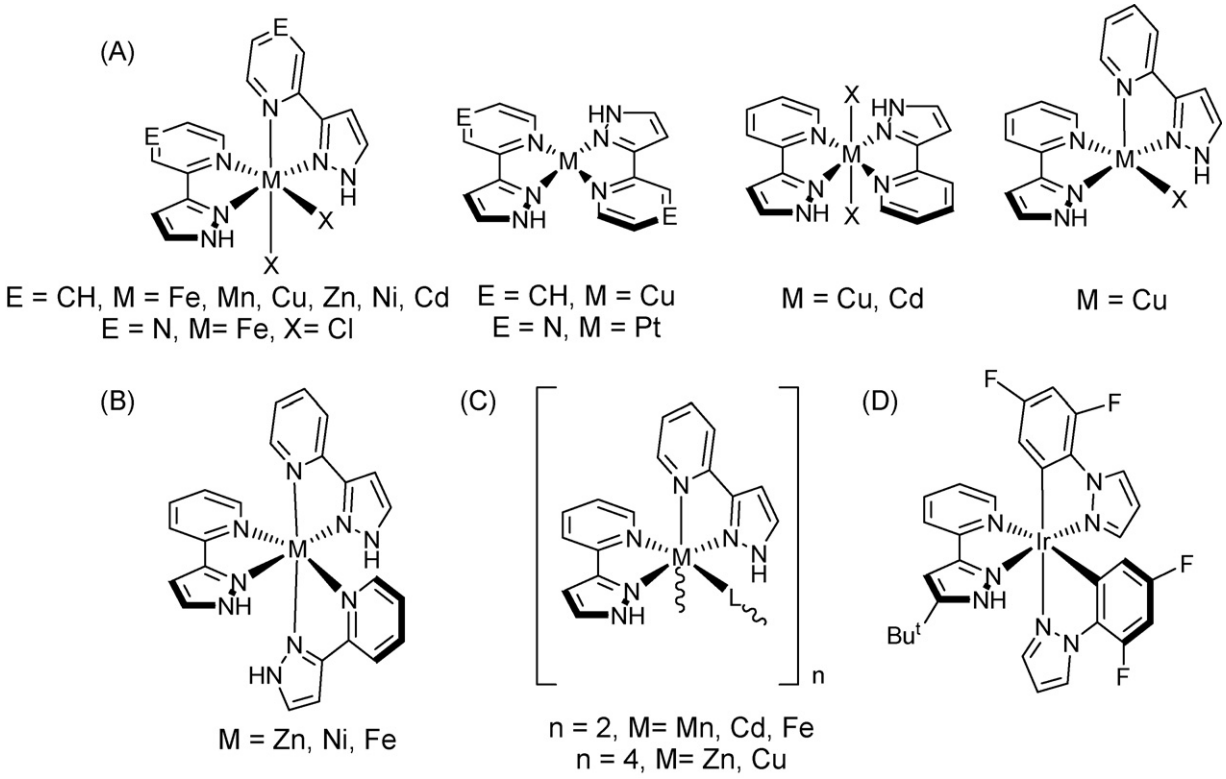

Fig. 7. A selection of the key structural types observed for coordination complexes of the ligand 2-(pyrazol-3-yl)pyridine/pyrazine (HL^{18} and pyrazine analogue) in acid media, substituents at the 3 and/or 5 positions of the pyrazole ring are omitted for the sake of clarity. X = Anion or solvent molecules.

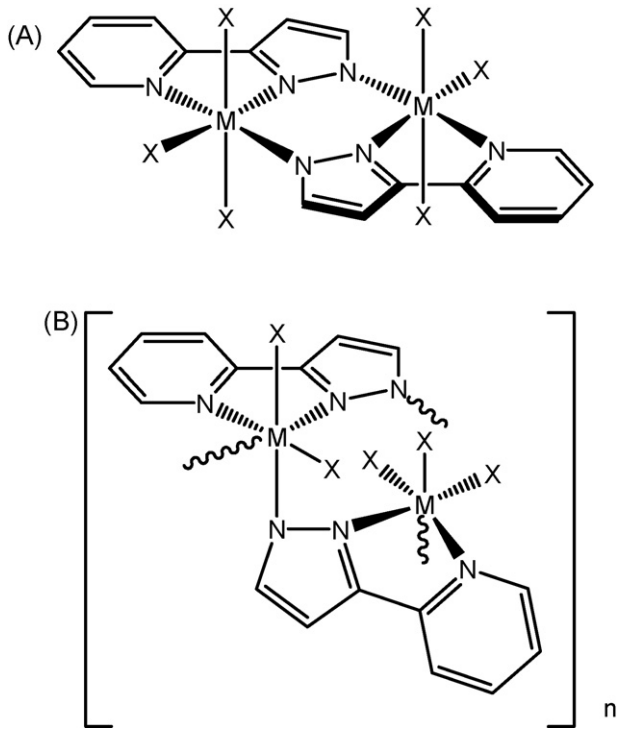

Fig. 8. A selection of the key structural types observed for coordination complexes of the ligand 2-(pyrazol-3-yl)pyridine, $(L^{18})^-$, in basic media. X = Anion or solvent molecules.

$\theta = 90^\circ$) [26]. Consideration of these angles is very important when trying to explain the magnetic properties of the iron(II) complexes and such an analysis is presented below.

Solvent-free $[Fe(L^1)_2][BF_4]_2$ (**1**), was synthesized in air, in acetone at room temperature by reacting one equivalent of $Fe(BF_4)_2{\cdot}6H_2O$ with two equivalents of L^1 (Fig. 3), before concentrating the solution to precipitate **1** as a mustard yellow solid. Recrystallization from acetonitrile-diethyl ether affords a polycrystalline material.

Bridgeman, Halcrow et al. [26,27] clearly demonstrated that **1**, obtained as stated above, undergoes an abrupt and complete spin transition (ST) on cooling. The ST of this polycrystalline sample of **1** is centred at $T_{1/2}$ = 261 K and it exhibits a small hysteresis loop ($\Delta T_{1/2}$ = 3 K). At high temperatures $\chi_M T$ = 3.6–3.7 $cm^3\,K\,mol^{-1}$, consistent with the presence of iron(II) in the high spin state (HS) whereas upon cooling this drops to $\leq$0.3 $cm^3\,K\,mol^{-1}$, consistent with the presence of the low spin state (LS).

This complex crystallizes, from acetonitrile-diethylether, in the monoclinic $P2_1$ space group. No magnetic data was reported for these single crystals, but X-ray datasets acquired at both 240 and 290 K (Fig. 12) showed that the asymmetric unit comprises the complex cation and two tetrafluoroborate anions, and the local symmetry of the cation is D_{2d}, at both temperatures. During cooling through the ST no phase transition was detected, but the crystallographic *c* axis and cell volume decreased slightly, by 3.3% and 2.6% respectively, while the *b* axis and β increased slightly, by 0.7% and 2.5% respectively.

The short Fe–N bond lengths (1.893(3)–1.981(4) Å) observed in the crystal structure determined at 240 K clearly indicate that complex **1** is in the LS state (Fig. 12). Both of the BF_4 anions are disordered by rotation about a B–F bond. In contrast, the longer Fe–N bond lengths, 2.127(2)–2.193(2) Å [27]), observed in the crystal structure determined at 290 K show that it is in the HS state. At this temperature all the fluorine atoms in both BF_4 anions are badly disordered.

^{1}H NMR studies carried out in CD_3CN, CD_3NO_2 and $CO(CD_3)_2$, on the microcrystalline powder precipitated from the reaction mixture, showed that **1** is stable in solution. Evans method magnetic susceptibility studies in 99:1 $CO(CD_3)_2$:$Si(CH_3)_4$, in the range 325–185 K, showed a complete ST occurred, centred at 248 K, slightly lower than the solid state transition temperature ($T_{1/2}$ = 261 K [26]). Many research groups [28–34] have investigated thermal spin transitions of iron(II) complexes in solution by following the change in magnetic susceptibility by ^{1}H NMR spectroscopy using the Evans method [35] or by determining the HS mole fraction by measuring the difference of the resonance shifts during the ST as recently reported by Weber and Walker [34]. This requires that the SCO system should be stable in solution, otherwise solvolysis, ligand and anion-exchange reactions could occur complicating the analysis of the results [36]. Usually the $T_{1/2}$ values obtained from measurements in the solid state (e.g. from SQUID magnetometer data) are different (bigger or smaller) from those obtained from measurements in solution (e.g. from Evans NMR data). This is not unexpected, as instead of interacting with neighboring complexes in the solid state, in solution the complex interacts with the solvent, resulting in a somewhat different ligand-field being experienced by the iron(II) centre. In addition, due to the elimination of all of the inter-complex interactions that existed in the crystal lattice (eg. anion–π, π–π and hydrogen bond interactions), in virtually all of the cases of mononuclear iron(II) complexes the ST-curves calculated from solution measurements are gradual, even when the ST in the solid state was abrupt.

Complex **1** undergoes the LIESST effect in the 80–85 K temperature range [37,38]. A single crystal was held at 30 K for 30 min while being irradiated with a He-Ne laser (λ = 632.8 nm, 15 mW), before X-ray crystal structure data was collected. This revealed that the iron(II) centre was trapped in the light induced metastable HS state: the average Fe-N bond length is 2.165(2) Å and the unit cell volume increased by 2.3% from that observed for the LS state. In contrast to the structure at higher temperature (of the thermally stable HS state) the tetrafluoroborate anions in the metastable HS state are ordered.

Interestingly, dark-brown crystals grown by diethyl ether vapour diffusion into a $MeNO_2$ solution at 240 K (below the transition temperature) provided the solvate, **1** $2.9CH_3NO_2{\cdot}0.25H_2O$. An X-ray crystallographic study on **1** $2.9CH_3NO_2{\cdot}0.25H_2O$ at 150 K shows that this complex crystallizes in the $P2_12_12_1$ space group and there are *two* crystallographically independent cations in the asymmetric unit. The Fe–N bond lengths show that both iron(II) centres are in the LS state (1.902(3)–1.991(3) and 1.899(3)–1.977(3) Å [26]), but one of the molecules has an almost perfect D_{2d} symmetry while in the other molecule the pyrazole moieties in *trans*-positions coordinate asymmetrically (one of the Fe–$N_{pyrazole}$ bonds is 0.040 Å longer than the other one). Intriguingly, this solvated version of **1** exhibited the same $T_{1/2}$ as the solvent-free complex **1**. This is a most surprising finding, as it is well known that solvent molecules within the crystal lattice can facilitate cooperativity between the iron centres by means of hydrogen bonding or π–π interactions, or indeed simply by modifying the general packing interactions, thereby modifying the magnetic properties of the compound. In the present case the authors explained the magnetic behaviour as presumably being dominated by the electrostatic interactions between the iron centres.

In order to explore new systems, Halcrow and co-workers synthesized the complex $[Fe(L^1)_2][Co(C_2B_9H_{11})_2]_2$ (**2**) [39], in refluxing $MeNO_2$ in air by reacting two equivalents of L^1 and two equivalents of $FeCl_2{\cdot}4H_2O$ with an excess of $Ag[Co(C_2B_9H_{11})_2]$. Diethyl ether vapour diffusion into this $MeNO_2$ solution afforded air sensitive orange needles of the nitromethane solvate, $[Fe(L^1)_2][Co(C_2B_9H_{11})_2]_2{\cdot}MeNO_2$ (**2**$\cdot MeNO_2$), suitable for X-ray crystallography (see below), which were dried under vacuum to

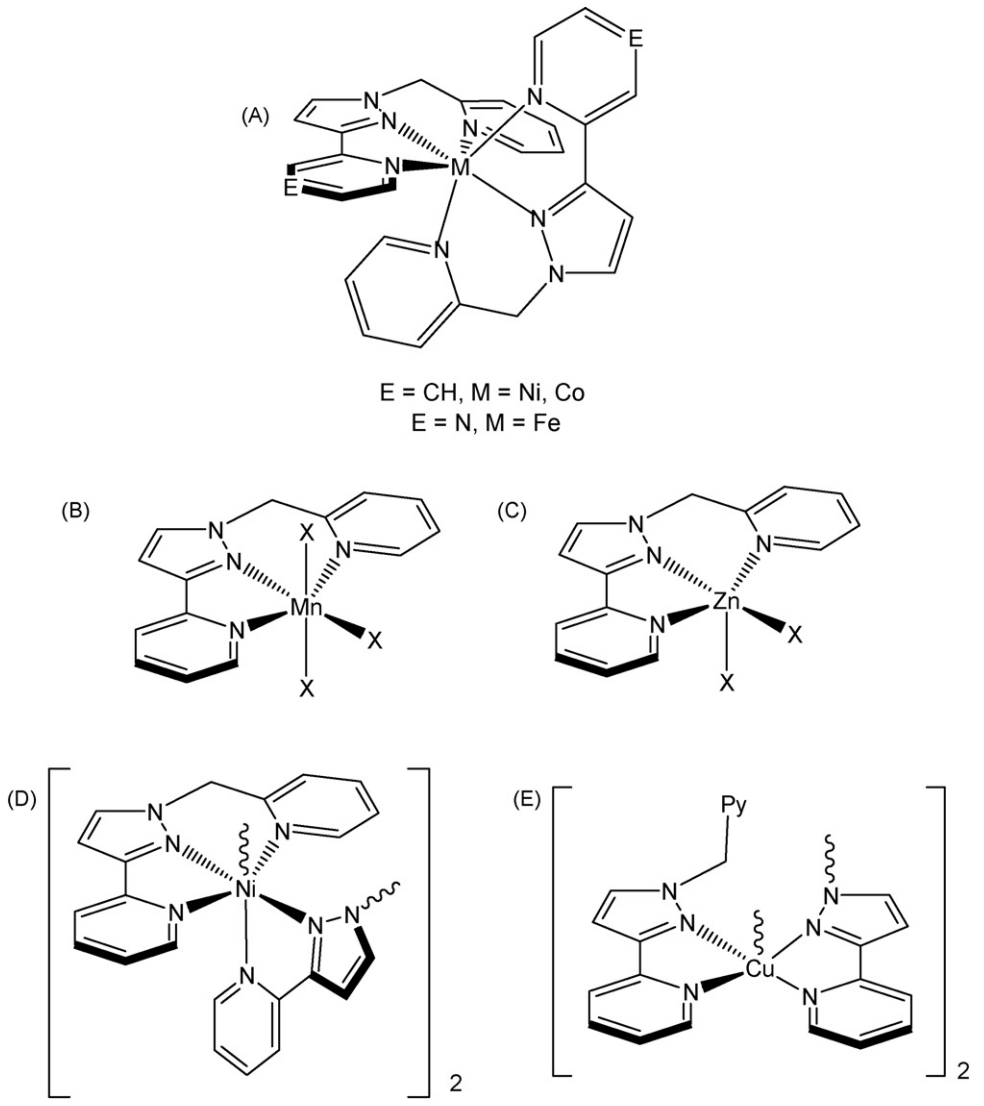

Fig. 9. A selection of the key structural types observed for coordination complexes of the ligand *N*-picolyl-2-(pyrazol-3-yl)pyridine/pyrazine (L^{19} and L^{20}). X = Anion or solvent molecules.

obtain anhydrous **2**, according to microanalysis. This anhydrous sample was used for the magnetic measurements described below.

The polycrystalline anhydrous sample of **2** undergoes a gradual and incomplete ST centred at 318 K. Magnetic measurements at 340 K showed a $\chi_M T$ value of 2.7 $cm^3\ mol^{-1}$ K, and upon cooling this value drops to 1.7 $cm^3\ mol^{-1}$ K at 220 K. While this is a significant drop in $\chi_M T$, it is not as low as the value expected for a fully populated LS state. Rather it corresponds to a spin transition where only 50% of the iron centres switch to the LS state, and the other 50% remain in the HS state. This behaviour indicates that there are two different magnetic centres present. The X-ray crystallography results corroborate this. At 150 K the asymmetric unit contains two different cations, where each iron centre is structurally different from each other. One of these cations, molecule A, is in the LS state according to Fe–N bond lengths (1.916(7)–1.996(8) Å). The other cation, molecule B, is in the HS state (Fe–N bond lengths 2.129(7) –2.231(8) Å). At 300 K the bond lengths of molecule A increased by approximately 2.25%, consistent with a mixture of HS and LS states but with the LS state still the major component; while molecule B remains in the HS state (Fe–N bond lengths 2.127(5)–2.210(4) Å). Molecule B has a 'rotation' component of Jahn–Teller distortion (ϕ = 159.6(3), θ = 87.03(9)° at 150 K) which locks the iron centre in the HS state in the range of temperatures studied. The presence of two different complexes in the asymmetric unit, one of which is locked in the HS state, explains the lack of a fully LS state, i.e. the observation of incomplete ST, for complex **2**.

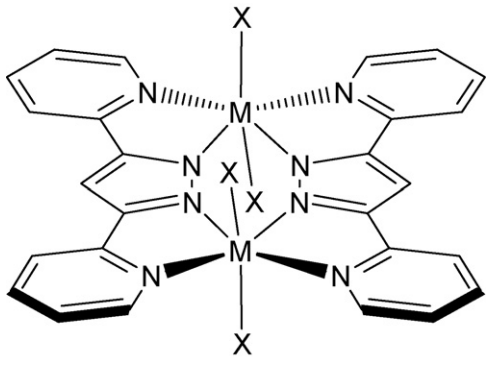

Fig. 10. The most common structural type observed for coordination complexes of the ligand 3,5-bis(2′-pyridyl)pyrazole, $(L^{21})^-$. X = Anion or solvent.

One approach to try to systematically modify the SCO parameters (transition temperature, presence or absence and the width of a hysteresis loop) is doping of the material with different ligands,

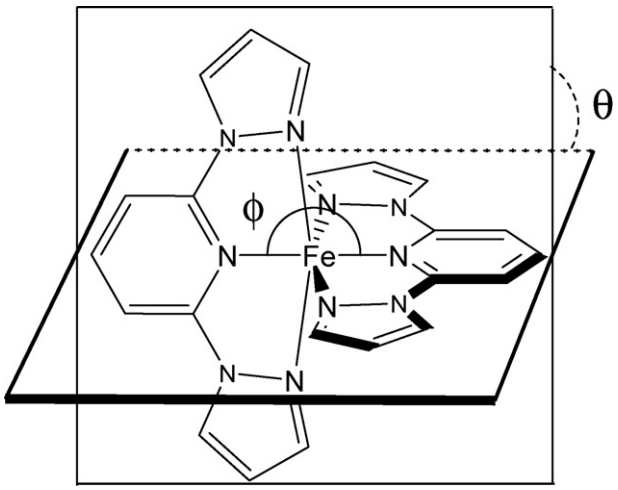

Fig. 11. Coordination sphere of the iron(II) complexes of the 2,6-bis(pyrazol-1-yl)pyridine derived ligands L^1–L^{14}, showing the angles ϕ and θ.

different metal ions or different anions. Létard and co-workers [40] used the anion doping approach to prepare four more complexes of the type $[Fe(L^1)_2][ClO_4]_x[BF_4]_{2-x}$. The $x = 2$ and $x = 0$ complexes, $[Fe(L^1)_2](ClO_4)_2$ (**3**) and $[Fe(L^1)_2](BF_4)_2$ (**1**), reported earlier, are not isostructural and have differing magnetic behaviour. As mentioned above, complex **1** shows an abrupt and complete ST at 260 K with a narrow hysteresis loop. Remarkably, complex **3**, differing from **1** only in the presence of ClO_4 anions in place of the BF_4 anions, remains HS within the 5–300 K temperature range [26,27,37].

The doped complexes prepared were $[Fe(L^1)_2][ClO_4]_{0.30}[BF_4]_{1.70}$ (**4**), $[Fe(L^1)_2][ClO_4]_{0.98}[BF_4]_{1.02}$ (**5**), $[Fe(L^1)_2][ClO_4]_{1.68}[BF_4]_{0.32}$ (**6**), and $[Fe(L^1)_2][ClO_4]_{1.89}[BF_4]_{0.11}$ (**7**). They were synthesized as solvent free crystalline materials by recrystallization of the appropriate mixture of complex **1** and complex **3** by diethyl vapour diffusion into acetone solutions, or as powders by addition of large amounts of diethyl ether to the acetone solutions. The colour of these complexes was not stated. Powder diffraction data showed that complexes **4** and **5** are isostructural with **1** and complex **7** is isostructural with **3**. When complex **6** was rapidly precipitated, by addition of diethylether, it was a mixture of both phases, however, crystalline **6**, obtained by slow vapour diffusion of diethylether, is isostructural with **3**.

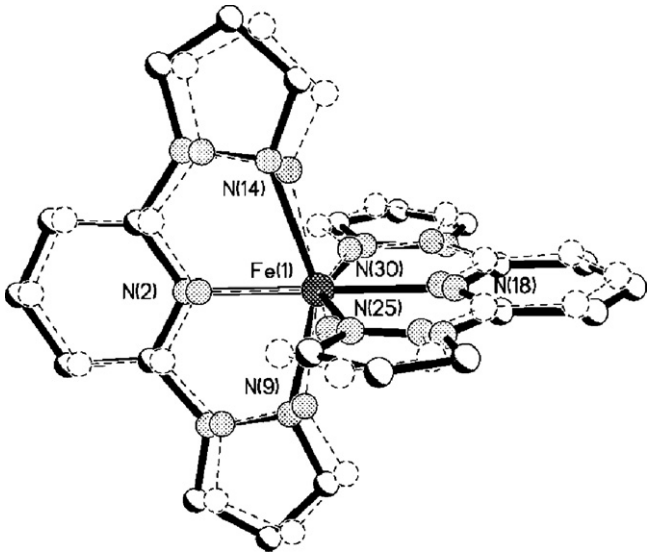

Fig. 12. Ball and stick representation of the structure of complex **1** in the HS state at 290 K (solid line) and in the LS state at 240 K (dotted line), emphasising the shorter Fe-N distances and closer to 90° *cis*-N–Fe–N angles seen in the latter. Anions omitted for the sake of clarity. This figure was generated from data obtained from the CCDC as published originally in reference [27].

Crystalline samples of complexes **1**, **4** and **5** show a complete spin transition whereas complex **7** shows only 5% ST. The *powder* sample of **6** shows 75% ST, whereas in the *crystalline* sample less than 5% of the iron(II) centres undergo ST (Fig. 13). Both samples of **6** are solvent free, so this result once again shows how critical morphology, and hence the synthetic and crystallization methods used, is in the area of SCO-active materials. Both the $T_{1/2}$ value and the width of the hysteresis loop observed for these complexes reduce with increasing percentage of ClO_4^- (Table 1).

Complexes **1**, **4** and **5** were characterized by X-ray crystallography at 300 and 150 K. From the crystallographic data the BF_4^- to ClO_4^- anion ratios within the doped complexes **4** and **5** showed some differences from those obtained from the microanalytical results (**4** X-ray 0.44:1.56 vs microanalysis 0.30:1.70; **5** X-ray 0.98:1.02 vs microanalysis 0.87:1.13). It is unclear if this discrepancy is due to variation in the anion ratios within different crystals or limitations in the X-ray refinement. However there is good agreement between the magnetic data collected from powder and crystalline samples of **1**, **4** and **5**.

The Fe–N bond lengths in complexes **1**, **4** and **5** are the same (and are consistent with the presence of the LS state at 150 K and HS state at 300 K). Nonetheless, as expected, the cell volume increases as the proportion of ClO_4^- does. For example the cell volume for complex **5** is 1.79% bigger than for complex **1**, at 150 K. This is consistent with the doping by perchlorate anions pushing the cations further apart, due to the bigger size of this anion (24% larger by volume [41]) compared to tetrafluoroborate. The *a* and *b* axis lengths in complex **5** are both longer, by 0.45% and 0.41% respectively, than in **1**, at 150 K. These axes reflect the distance between the iron centres in neighboring molecules, that interact *via* terpyridine embrace-like interactions in two dimensional (2D) layers along the *ab* plane (Fig. 14A, 2D layers 'face on', viewed down the *c* axis; Fig. 14B, same diagram but viewed down the *a* axis so 2D layers 'edge on'). For the *c* parameter the change is more dramatic, increasing by 18.20% from **1** to **5**, at 150 K. This axis reflects the distance between the above mentioned alternating terpyridine-embrace 2D-layers of molecules (Fig. 14). The perchlorate/tetrafluoroborate anions sit in between these layers, resulting in greater separation between them as the proportion of the larger anion increases. However, only a small decrease in the $T_{1/2}$ and a small increase in the hysteresis loop width are observed as the $\%ClO_4$ increases (Table 1). These results indicate that the cooperativity of the SCO in **1** and related compounds is likely transmitted in two dimensions by π–π ('terpyridine-embrace') interactions within the 2D cation layers in the crystal lattice. The authors concluded that doping complex **1** with perchlorate ions results in a decrease of ΔH and ΔS, a decrease in the strength of the face-to-face π–π interactions and a small but consistent increase in the spacing between the iron centres.

A crystal structure determination was also performed on complex **6**. As expected this complex is isostructural with **3**. However, an unusual angular Jahn–Teller distortion is present trapping the iron centre in **6** in the HS state, explaining why *crystalline* **6** undergoes only 5% thermal ST. The Fe–N bond *angles* in **3** and **6** are identical, however, as a consequence of the Jahn–Teller distortion, the bond *lengths* are longer in **6** than **3**.

Complex **1** presents the light induced excited spin state trapping effect (LIESST effect) when it is irradiated at 10 K with a green laser ($\lambda = 532$ nm), with a quantitative photoconversion to the meta-stable HS state. The T(LIESST), which is defined as the limiting temperature above which the light-induced magnetic HS information is erased in a SQUID cavity [42], for complex **1** is 81 K [43]. Complexes **4**–**6** also present a LIESST effect. Given that the

Table 1
Magnetic data for the family of doped complexes, $[Fe(L^1)_2][ClO_4]_x[BF_4]_{2-x}$.

Complex	X	$T_{1/2}\uparrow$ (K)	$T_{1/2}\downarrow$ (K)	$\Delta T_{1/2}$ (K)	T(LIESST) (K)	T(LITH)↓ (K)	T(LITH)↑ (K)
1	0	261	261	0	81	60	88
4	0.30[a]	257.5	260.7	0.6	81	68	91
5	0.98[b]	257.2	258.3	1.1	81	68	92
6	1.68	254.4	255.5	1.6	82	68	94

T(LITH)↑ and T(LITH)↓ are the temperatures where there is apparently 50% of photo-converted HS molecules in cooling and warming modes, respectively, under continuous irradiation.

[a] $X = 0.30$ from microanalysis but 0.44 by single crystal X-ray structure determination.

[b] $X = 0.98$ from microanalysis but 0.87 by single crystal X-ray structure determination.

$T_{1/2}$ values are very similar for these complexes, the empirical relationship (Eq. (1), with $T_0 = 150$ K) predicts that the T(LIESST) values should not differ significantly, as observed (Table 1) [42]. A different type of thermal hysteresis loop is observed when the temperature is varied while the sample is being irradiated with a laser light to promote the conversion to the metastable HS-state, known as light-induced thermal hysteresis T(LITH) [44]. The T(LITH) parameters for complex **1** are also presented in Table 1.

$$T(\text{LIESST}) = T_0 - 0.3T_{1/2} \quad (1)$$

With the aim of increasing the cooperativity in the SCO transition, Halcrow and co-workers [45] introduced a hydroxymethyl group in the 4-position of the pyridine group of L^1, resulting in the ligand 2,6-bis(pyrazolyl-1-yl)-4-hydroxymethylpyridine (L^2, Fig. 3). The method of synthesis of the complex $[Fe(L^2)_2](BF_4)_2$ (**8**) was not detailed in the original paper, but the perchlorate analogue, $[Fe(L^2)_2](ClO_4)_2$ (**9**), was synthesized in air in acetone at room temperature by reacting 2 equivalents of L^2 with 1 equivalent of $Fe(ClO_4)_2{\cdot}6H_2O$. The resulting yellow solution was filtered and the filtrate concentrated to 1/3 of its initial volume and stored overnight at −30 °C, resulting in the precipitation of solvent-free **9** as a mustard yellow microcrystalline solid, which was used for the magnetic studies (see below).

Solvent-free single crystals of complexes **8** and **9**, suitable for X-ray crystallography, were grown by diethyl ether vapour diffusion into $MeNO_2$ solutions of the complexes [45,46]. The resulting crystalline sample of complex **8** undergoes an abrupt ST upon cooling with $T_{1/2} = 271$ K and a small hysteresis loop ($\Delta T_{1/2} < 2$ K). It crystallizes in the monoclinic *Cc* space group. There is no phase transition during the ST, but the colour changes from dark yellow to brown. The asymmetric unit comprises one complex cation $[Fe(L^2)_2]^{2+}$ and two BF_4^- anions. At 300 K the hydroxymethyl groups of the ligands are disordered, but at 30 K this disorder is eliminated. At both temperatures the hydroxymethyl groups form hydrogen bonds with the fluorine atoms of the anions. However, this does not result in a three-dimensional network, consistent with the observation of a narrow hysteresis loop. As expected, the higher temperature crystal structure (300 K) shows an iron centre in the HS state (average Fe–N distance 2.143 Å), whereas the data collected at 30 K shows the iron centre in the LS state (average Fe–N bond length 1.962 Å).

A single crystal of complex **8** was irradiated at 30 K on the X-ray diffractometer with red laser light (λ = 632.8 nm, 25 mW) for 10 min. Determination of the unit cell parameters showed an increase in unit cell volume and the colour of the single crystal changed from brown to dark yellow. Both observations suggest photoconversion to the metastable HS state. This was demonstrated by acquiring the crystallographic data set and showing longer Fe–N bond lengths (average Fe–N 2.161 Å), characteristic of iron(II) in the HS state [45]. In a more in depth photomagnetic study the T(LIESST) was determined to be 70 K (Fig. 15 [46]).

Upon cooling a crystalline sample of complex **9** it undergoes an abrupt and complete ST with $T_{1/2} = 284$ K (Fig. 15), so the authors aim, of increasing the cooperativity by incorporating a hydroxymethyl substituent in the ligand, was achieved, as was seen for complex **8** too. However a wide hysteresis loop was not observed in the ST-curve of either **8** or **9**. Complex **9** is isostructural with **8**. It crystallizes, by diethyl ether vapour diffusion into a $MeNO_2$ solution, in the monoclinic *Cc* space group. The asymmetric unit comprises the complex cation and two ClO_4^- anions. As in **8**, the hydroxymethyl groups in **9** are disordered at higher temperatures (340 K) but not at 120 K. The quality of the crystal degrades upon cooling, possibly due to the ST taking place around RT ($T_{1/2} = 284$ K with a small hysteresis loop), which is the same temperature as the complex is crystallized at. Hence anisotropic refinement was only possible for the structure collected at high temperature. At 340 K the Fe–N bond lengths are consistent with an iron(II) centre in HS state (average Fe–N 2.153(8) Å). Upon cooling to 120 K a decrease in the Fe–N bond length is registered confirming the ST from HS to LS state (average Fe–N 1.97 Å).

As for complex **8**, complex **9** shows photomagnetic behaviour. Irradiation of a single crystal in the LS state, at 30 K, with a red laser light (λ = 632.8 nm, 25 mW) results in a change in colour from brown to yellow and an increase in unit cell volume. It was not

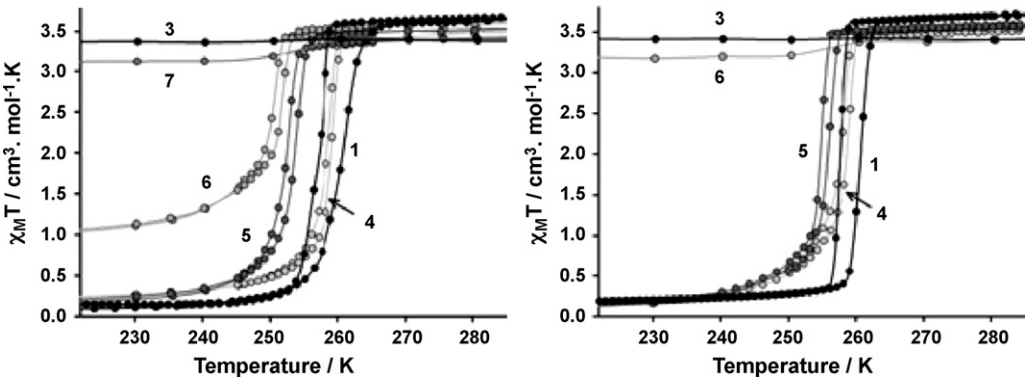

Fig. 13. Spin transition curves for complexes **1**–**7**. Crystalline materials (left) and powder samples (right). From reference [40]. Reproduced and modified by permission of The Royal Society of Chemistry.

possible to carry out an anisotropic refinement of the resulting X-ray dataset, but the results are good enough to differentiate between the LS and metastable HS states, with an average Fe–N bond distance of 2.15 Å confirming conversion to the latter. Moreover, the photoconversion is quantitative, with T(LIESST) = 284 K, T(LITH)↓ = 48 K and T(LITH)↑ = 65 K (Fig. 15) [46].

Complex $[Fe(L^3)_2](ClO_4)_2$ (**10**) (L^3 = 2,6-bis(4-methylpyrazol-1-yl)pyridine, Fig. 3) was synthesized by the same method as **9**. VT-magnetic measurements of polycrystalline samples, obtained by concentrating a nitromethane solution of **10**, show an abrupt ST at 233 K with a small hysteresis loop ($\Delta T_{1/2}$ = 3 K). At RT the $\chi_M T$ value, 2.8 cm^{-3} K mol^{-1}, is consistent with the presence of a mixture of *ca.* 80:20 HS:LS.

Single crystals suitable for X-ray crystallography were obtained by diethyl ether vapour diffusion into a $MeNO_2$ solution of **10**. It crystallizes in the tetragonal $P\text{-}42_1c$ space group with the iron atom on a −4 centre. The asymmetric unit consists of a quarter of the cation and one half of the anion. At 250 K the anion is disordered and the average Fe–N bond distance (2.149 Å) indicates that the iron centre is in the HS state. Upon cooling to 30 K a change in the

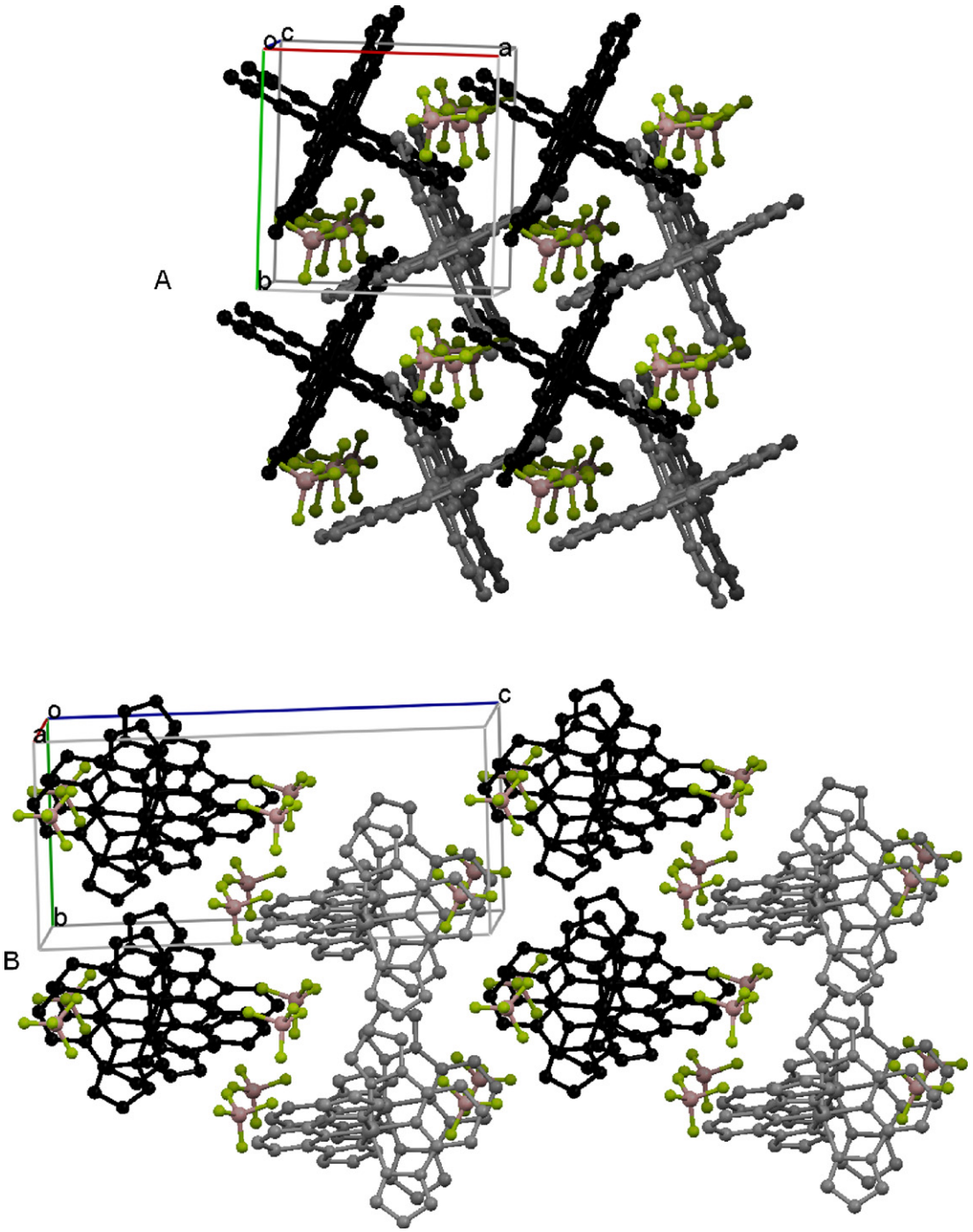

Fig. 14. (A) Crystal packing in complex **5** showing the 2D layers of terpyridine-embraced complexes that alternate (alternation highlighted as black and grey 2D layers) perpendicular to the *c* axis (viewing direction). (B) The same crystal packing diagram but viewed down the a axis so that the 2D layers are edge on and it is possible to observe the ClO_4^-/BF_4^- anions sitting in between these alternating black and gray 2D layers. This figure was generated from data obtained from the CCDC as published originally in reference [40].

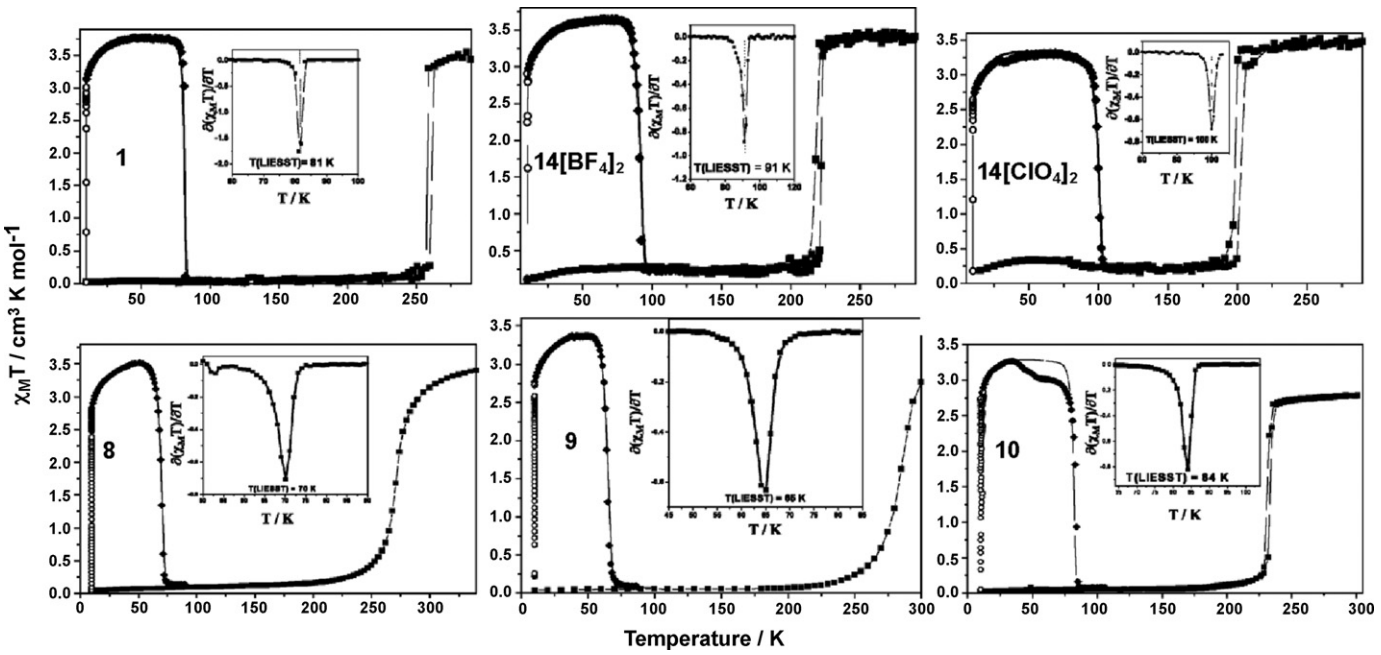

Fig. 15. Temperature dependence of $\chi_M T$ for complexes **1**, **8**-**10**, **14**$[BF_4]_2$ and **14**$[ClO_4]_2$. ■ = Thermal spin transition curves collected without irradiation; ○ = Irradiation of the samples at 10 K; ♦ = *T*(LIESST) measurement, data recorded in warming mode with the red laser ((λ = 632.8 nm, 25 mW) turned off after irradiation at 30 K for 1 h. The solid line through the *T*(LIESST) measurement shows the fit generated from the deduced experimental thermodynamic parameters. The insets show the derivative of the $d\chi_M T/dT$ curves, whose minimum corresponds to *T*(LIESST). From reference [46]. Reproduced by permission of The Royal Society of Chemistry.

crystallographic phase, to the orthorhombic $P2_12_12_1$ space group, is observed. The asymmetric unit now comprises one cation and two anions (which are completely ordered). In agreement with the magnetic data, the average Fe–N bond distance at 30 K (1.947 Å) shows that the iron(II) centre is in the LS state. Irradiation of the LS state single crystal at 30 K with red laser light (λ = 632.8 nm, 25 mW) produces a change in the colour of the crystal from dark yellow-brown (LS) to yellow (metastable HS). However the crystal decomposed, preventing the determination of the unit cell parameters for this metastable HS form of the complex [46].

The conditions for the synthesis of complexes $[Fe(L^4)_2](BF_4)_2$ (**11**) and $[Fe(L^5)_2](BF_4)_2$ (**12**) (L^4 = 2,6-bis(4-chloropyrazolyl-1-yl)-pyridine and L^5 = 2,6-bis(4-bromopyrazolyl-1-yl)-pyridine, Fig. 3) were not stated in the original publication. They only mention that both samples were isolated as microcrystalline solids [47]. Complexes **11** and **12** both undergo complete and abrupt ST upon cooling with $T_{1/2}$ = 202, $\Delta T_{1/2}$ = 3 and $T_{1/2}$ = 253, $\Delta T_{1/2}$ = 2 K, respectively [47].

Both **11** and **12** crystallized (no experimental conditions were stated for the crystallization of either of these complexes) in the tetragonal space group $P\text{-}42_1c$ at 300 K with an asymmetric unit comprising of quarter of the complex cation (the iron atom lies on a S_4 axis) and half of one anion (it is disordered across a C_2 axis). Complex **11** changes colour from yellow to brown upon cooling, and crystallographic studies at 220 and 202 K demonstrated that the ST is accompanied by a phase transition to the monoclinic $P2_1$ space group, where the asymmetric unit comprises the entire complex cation and two (ordered) anions.

The crystal structure determined at 300 K for complex **11** shows the average Fe–N bond distance is 2.162 Å, typical for an iron(II) centre in the HS state, meanwhile at 220 K the average Fe–N bond length decreased to 1.944 Å, confirming the ST to the LS state. Likewise, the data set collected on complex **12** at 300 K showed the iron centre is in the HS state (average Fe–N bond length 2.157 Å), and while the single crystal of **12** decomposed below the ST temperature, determination of the unit cell parameters showed that it too underwent a phase transition to the $P2_1$ space group [47].

Halcrow and co-workers [48] introduced a pyrazine moiety into the L^1 motif, resulting in ligands L^6–L^9 (Fig. 3). A family of complexes of these pyrazine-derived ligands was synthesized in air in acetone at room temperature, by reacting one equivalent of FeX_2 (X = BF_4^- or ClO_4^-) with two equivalents of the selected ligand L^n (*n* = 6–9, Fig. 3). In all cases the solution was stirred for 15 min, and then concentrated to 1/3 of its initial volume, causing a yellow powder to start to precipitate. The mixture was cooled to maximise the precipitation, before the yellow powder was collected and washed with cold methanol and diethyl ether. The powders were recrystallized from a methanol-diethyl ether mixture (no further details were provided), resulting in microcrystalline materials (used for the magnetic measurements, see below) with microanalyses that correspond to the solvent-free materials, $[Fe(L^n)_2][X]_2$, when *n* = 6, **13**$[BF_4]_2$ and **13**$[ClO_4]_2$; *n* = 7, **14**$[BF_4]_2$ and **14**$[ClO_4]_2$; *n* = 9, **16**$[BF_4]_2$ and **16**$[ClO_4]_2$. The complexes of the ligand with the bulkiest substituent (mesitylenyl) analysed as the monohydrates, $[Fe(L^8)_2][BF_4]_2{\cdot}H_2O$ and $[Fe(L^8)_2][ClO_4]_2{\cdot}H_2O$, **15**$[BF_4]_2{\cdot}H_2O$ and **15**$[ClO_4]_2{\cdot}H_2O$, respectively, are LS at room temperature so they are not discussed further here.

The microcrystalline samples of complexes **13**$[BF_4]_2$ and **13**$[ClO_4]_2$ exhibit abrupt ST upon cooling, with $T_{1/2}$ of 223 and 206 K, and hysteresis loop widths of 3 and 5 K, respectively. These results were confirmed by DSC experiments. No crystal structure could be obtained for these solvent-free materials. However orange-yellow crystals, suitable for X-ray crystallography, of the solvate **13**$[BF_4]_2{\cdot}3MeNO_2$ were obtained by the vapour diffusion of diethyl ether into a nitromethane solution of **13**$[BF_4]_2$. This solvate presents an abrupt ST at 198 K with a concomitant change of colour to dark brown. The X-ray data were acquired at 150 and 300 K, confirming that the complex is in the pure HS and LS states, respectively (Fe–N bond lengths 2.114(3)–2.191(3) Å at 300 K and 1.891(3)–1.982(3) Å at 150 K [48]). At both temperatures badly disordered solvent and anion molecules are present: the differences between the disorder models at the two temperatures are slight, so it is not possible to determine whether the abruptness of the ST is mediated by changes in the disorder regime.

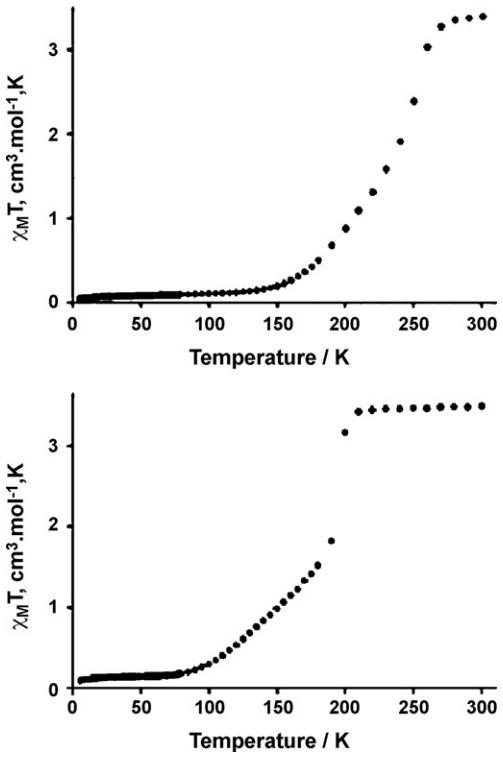

Fig. 16. ST curves for solvent-free microcrystalline samples of complexes **14**$[BF_4]_2$ (top) and **14**$[ClO_4]_2$ (bottom). From reference [49]. Reproduced and modified by permission of The Royal Society of Chemistry.

The microcrystalline samples of complexes, recrystallized from methanol-diethyl ether (see above), **14**$[BF_4]_2$ and **14**$[ClO_4]_2$ undergo ST upon cooling, but the shapes of the ST curves for the two complexes are very different. Complex **14**$[BF_4]_2$ undergoes a very gradual transition centred at 235 K whereas **14**$[ClO_4]_2$ undergoes a two step transition (Fig. 16). The first step, at 196 K, is abrupt and the second step, centred at 133 K, is more gradual; the intersection of the curves for each of these steps occurs when half of the molecules are in the LS state. In a later paper [49] the same authors were able to crystallise both complexes, and in light of the structural data obtained gave an explanation of the very different magnetic behaviour observed on changing from tetrafluoroborate to perchlorate anions. However, although it is mentioned that the crystals were obtained by diethyl ether vapour diffusion into solutions of the complex the solvent was not specified. It is likely that, as above, the solvent was methanol, but it is unfortunate that this was not stated as, as seen above, magnetic behaviour is often critically dependent on morphology, and hence the solvents used (regardless of whether they are present in the product or not).

Both **14**$[BF_4]_2$ and **14**$[ClO_4]_2$ crystallise solvent-free in the tetragonal space group $I\bar{4}$. Upon cooling the single crystals changed colour from yellow to brown indicative of a ST from HS to LS. The ST is not accompanied by a phase transition. The iron centres have a distorted octahedral coordination sphere formed by two sets of the tridentate ligand L^7. The iron atom and the two chlorine, or two boron, atoms of the anions lie on an S_4 axis in complexes **14**$[ClO_4]_2$ and **14**$[BF_4]_2$, respectively. In both cases the asymmetric unit therefore comprises a quarter of the cation and a quarter of each anion. The crystal structures determined at 30 K show the iron(II) centres are LS (average Fe–N for **14**$[BF_4]_2$ is 1.973 Å, for **14**$[ClO_4]_2$ 1.988 Å). At 240 K the crystal structure determination on **14**$[BF_4]_2$ shows a ~50% mixture of HS and LS (average Fe–N 2.057 Å). At 180 K the crystal structure determination on **14**$[ClO_4]_2$ shows a ~0.3 ratio of HS to LS (average Fe–N 2.047 Å). In contrast, at 290 K the iron centres in both complexes are in the pure HS state (average Fe–N for **14**$[BF_4]_2$ 2.164 Å, for **14**$[ClO_4]_2$ 2.176 Å).

In the crystal structures of **14**$[BF_4]_2$ and **14**$[ClO_4]_2$ collected at low temperatures the anions are ordered. However, at higher temperatures, 290 K, one of the anions, BF_4^- or ClO_4^- respectively, is disordered. There are no π–π interactions within the crystal lattice of either **14**$[BF_4]_2$ or **14**$[ClO_4]_2$, but there are weak H_2C–H···anion hydrogen bonding interactions. In the case of **14**$[BF_4]_2$, at 290 K the methyl group of the substituted pyrazole moiety of L^7 interacts with one ordered and one disordered BF_4^- (C···F distances 3.38(2) and 3.529(6) Å, respectively). Likewise, in **14**$[ClO_4]_2$ at 290 K there are three interactions between the methyl substituent and the anions, two with the disordered and one with the ordered ClO_4^- (C···O distances 3.35(2) and 3.49(4) Å to the disordered anion and 3.40(9) Å to the ordered anion). While at 240 and 180 K for **14**$[BF_4]_2$ and **14**$[ClO_4]_2$ respectively, there is only one weak hydrogen bond between the anion and the methyl group (C···F distance 3.489(8) and C···O 3.403(5) respectively). This diminution in the number of interactions between the metal centres results in decreased cooperativity, explaining the unusual shapes in the spin transition curves (an abrupt ST at higher temperatures while at lower temperatures the ST became more gradual, see below).

A detailed VT single crystal X-ray diffraction study was carried out for both systems, between 360 and 30 K for **14**$[BF_4]_2$ and 290 and 30 K for **14**$[ClO_4]_2$. In both cases the length of the *a* axis and the unit cell volume follow the same behaviour as the magnetic data when the temperature is lowered, that is a relatively abrupt transition occurs between 270 and 240 for **14**$[BF_4]_2$ and between 210 and 190 K for **14**$[ClO_4]_2$ (Fig. 17). After this the change in these crystallographic parameters with temperature is gradual. Totally different behaviour is seen for the *c* axis length; it increases sharply at the beginning of the ST to LS, matching the abrupt change in magnetic moment, until 50% of the spin state conversion has occurred, after which it gradually decreases. These changes in *c* are not reflected in the structure of the cations. The only change to the cations during the increase in the *c* axis length on cooling is the expected shortening of the Fe–N bond lengths due to the ST. However, for both complexes, the temperature where the slope of the ST curve changes matches that at which ordering of the anions occurs. This anion order–disorder transition changes the distance between the iron centres, with the onset of disorder upon warming pushing them apart. The sharp increase in *c* axis length is the result of the loss of all but one of the CH···anion hydrogen bonding interactions (one CH_3···F and CH_3···O interaction, respectively, remain) which reduces the cooperativity between the iron centres, and this is reflected in the more gradual part of the ST curve.

The lower basicity and higher π-acceptor ability of pyrazine over pyridine leads to the expectation that the pyrazine should better stabilise the LS state. Consistent with this, both Goodwin [50] and Britosvek [51] and their co-workers have found for iron(II) complexes of pyridine- vs pyrazine- based ligands that the pyrazine containing ligand systems better stabilised the LS state. In contrast, in these pyrazole-containing ligands the overall effect of changing the pyridine ring to a pyrazine ring is not so clearcut. For example, $T_{1/2}$ for the pyridine-based complex **1** is 261 K whereas it drops to 223 K for the analogous pyrazine-based complex **13**. This shows that the *pyrazine* analogue better *stabilizes the HS state* for this system. In another example taken from this survey, for the two pyrazine-based complexes [**14**$[BF_4]_2$ ($T_{1/2}$ = 235 K) and **14**$[ClO_4]_2$ ($T_{1/2}$ = 196 and 133 K; two step ST) the first $T_{1/2}$ is higher than it is in the pyridine analogues $[Fe(L)_2][BF_4]_2$·4MeCN and $[Fe(L)_2][ClO_4]_2$·2{$(CH_3)_2O$}, both of which have $T_{1/2}$ of approximately 175 K (L = 3,5-bis(3′-methylpyrazol-1′-yl)pyridine). This appears at first glance to be consistent with better stabilization of the LS state by the pyrazine-based system. However, it is important

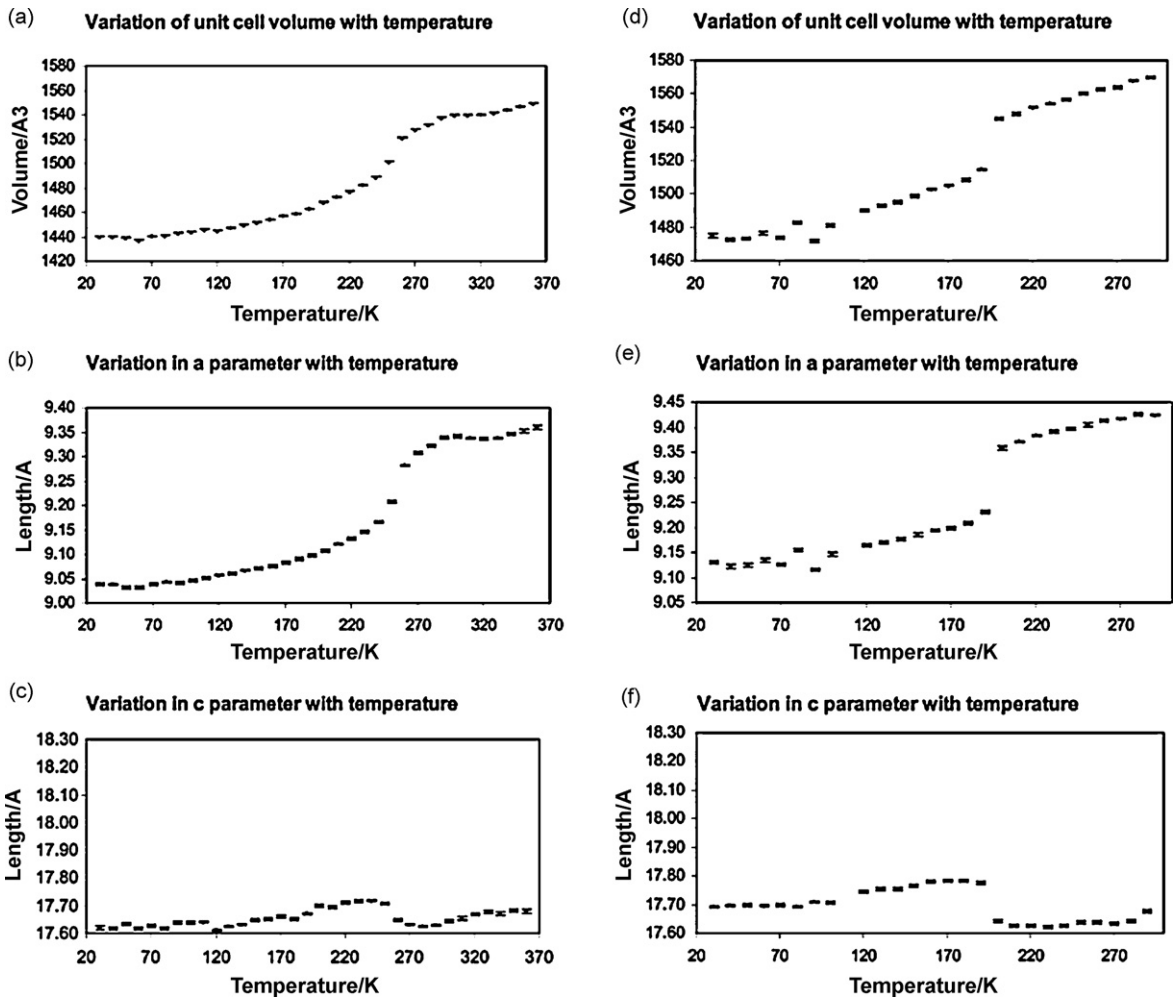

Fig. 17. VT single crystal X-ray diffraction study showing the changes in the volume, *a* and *c* cell parameters for complexes **14**$[BF_4]_2$ (a–c) and **14**$[ClO_4]_2$ (d–f). From reference [49]. Reproduced by permission of The Royal Society of Chemistry.

to note that there are differences in solvent content which make such a comparison not completely valid. Differences in counter ion and/or solvent content also plague other potential comparisons of pyrazole-pyridine vs pyrazole-pyrazine systems (see later, Section 3.2.2).

Although the pyrazine-based ligands L^n (n = 6–9) were synthesized with the aim of linking the complexes, and hence facilitating cooperativity, by forming hydrogen bonding networks via the available nitrogen atom 'out the back' of the pyrazine ring, this did not occur. That nitrogen atom is not involved in any hydrogen bonding in the iron(II) complexes structurally characterized to date.

Complexes **13**$[BF_4]_2$ and **13**$[ClO_4]_2$ present photomagnetic behaviour [38]. When the cooled sample (10 K) was irradiated with a light source of 532 nm, $\chi_M T$ increased, consistent with the formation of the metastable HS state. The photoconversion was quantitative within 1 h of irradiation. The T(LIESST) values were estimated to be 91 and 100 K for **13**$(BF_4)_2$ and **13**$(ClO_4)_2$ respectively. The shapes of the T(LIESST) curves are in all cases abrupt, as are the thermal spin transition curves, suggesting the existence of cooperative effects in the photoinduced phenomenon and thermal ST. Moreover, hysteresis loops (named Light Induced Thermal Hysteresis, LITH) were found in magnetic measurements in which these two samples were constantly irradiated, with width values of 11 K for **13**$(BF_4)_2$ and 31 K for **14**$(ClO_4)_2$. These results confirm that some cooperativity is present in the photo-induced HS state.

As the introduction of a pyrazine ring failed to facilitate the desired hydrogen bonding between the complexes to better promote supramolecular interactions between the mononuclear complexes, and hence promote the observation of abrupt ST and hysteresis loops, Ruben and co-workers [52] instead modified the structure of the ligand L^1 by functionalization of the 4 position of the pyridine ring with another pyridine moiety (L^{10}, Fig. 3). The complex $[Fe(L^{10}H^+)(L^{10})](ClO_4)_3{\cdot}MeOH$ (**16**) was synthesized by reacting one equivalent of $Fe(ClO_4)_2$ with two equivalents of L^{10} in a CH_2Cl_2-MeOH (2:1) mixture at room temperature, precipitating a red solid identified as **16** (the authors did not specify whether the synthesis was done under a N_2 atmosphere or in air).

The red single crystals used for both the X-ray crystallography and magnetic measurements were obtained by slow evaporation of a methanolic solution of the complex and were characterized as $[Fe(L^{10}H^+)(L^{10})](ClO_4)_3{\cdot}MeOH$ by microanalysis. Interestingly, without the addition of acid, one of the ligands coordinated to the iron(II) centre has been protonated at the uncoordinated 4′-pyridyl group, allowing the formation of a hydrogen-bonded polymer in which the protonated pyridine acts as hydrogen bond donor and the un-protonated pyridine of a neighboring molecule acts as the hydrogen bond acceptor (Fig. 18). The crystal structure determination at 180 K shows an iron(II) centre in a LS state, with a distorted octahedral geometry (Fe–N bond lengths 1.883(5)–1.968(6) Å). The methanol in the crystal structure is involved in very weak CH_3-OH···π interactions (distance between uncoordinated pyridine centroid and O of 4.12 Å). Magnetic susceptibility measurements showed the presence of ST with a small hysteresis loop ($T_{1/2}\uparrow$ = 287 and $T_{1/2}\downarrow$ = 285 K). This small hysteresis loop shows the existence

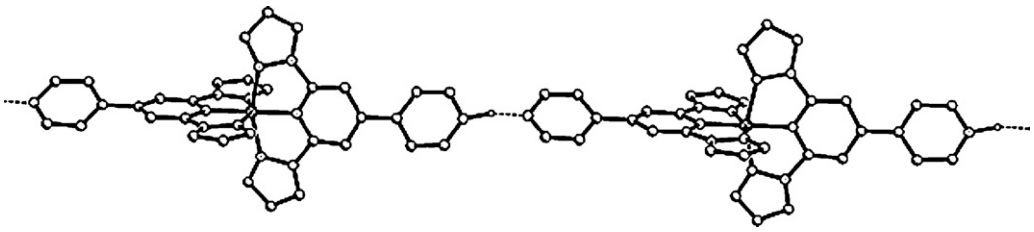

Fig. 18. Hydrogen bonding between individual complexes of **16** leads to a supramolecular, 1D, chain. Hydrogen atoms, except the NH proton in the pyridinium moiety, and anions are omitted for the sake of clarity. This figure was generated from data obtained from the CCDC as published originally in reference [52].

of cooperativity within the crystal lattice. The cooperativity could be a result of the presence of the hydrogen bonding or of the very weak methanol–π interaction, or both, in the crystal lattice. The $T_{1/2}$ of complex **16** is 26 K higher than the unsubstituted parent ligand iron(II) complex **1** [27]. The ST was also studied by VT ^{57}Fe Mössbauer spectroscopy (Table 2) which showed an increase in the % LS upon cooling, and corresponding reduction of % HS, as well as the presence of a ferric impurity.

Following the same approach, the ligand 4′-(4‴-cyanophenyl)-1,2′:6′1″-bispyrazolylpyridine (L^{11}, Fig. 3) was synthesized. Ruben and co-workers synthesized [53] the complexes $[Fe(L^{11})_2](ClO_4)_2{\cdot}2CH_3CN$ (**17**), and $[Fe(L^{11})_2](BF_4)_2{\cdot}2CH_3CN$ (**18a** and **18b**) by reacting 2.2 equivalents of L^{11} and one equivalent of $Fe(ClO_4)_2{\cdot}6H_2O$ or $Fe(BF_4)_2{\cdot}6H_2O$, respectively, in refluxing acetonitrile for 6 h under a N_2 atmosphere. Addition of diisopropyl ether under N_2 to the cooled solutions allowed the isolation of orange-yellow powders. Crystals suitable for X-ray crystallography were grown by slow diisopropyl ether diffusion into acetonitrile solutions of the complexes. Complex **18** crystallized as orange (**18a**) and red (**18b**) polymorphs, the orange polymorph being the major product. The crystalline samples obtained by diisopropyl ether vapour diffusion were used in the magnetic measurements.

Complex **17** crystallizes in the monoclinic *P*2/*c* space group. The asymmetric unit comprises the dication, two perchlorate anions, one of which is disordered, and two acetonitrile molecules. At 150 K the Fe–N bond lengths show that the complex is in the LS state (1.921(9)–1.992(3) Å). As expected for a SCO-active complex, the unit cell volume increases upon heating, with values of 4278, 4305, 4374 and 4403 Å^3 at 150, 200, 250 and 300 K respectively. Despite monitoring the cell volume on heating, the authors only reported the full X-ray crystal structure determination for complex **17** at 150 K (LS state).

Polymorphs **18a** and **18b** crystallise in monoclinic *P*2/*c* and orthorhombic $Pna2_1$ space groups respectively. Again the asymmetric units comprise the dication, two anions, and two CH_3CN molecules. The acetonitrile molecules occupy different positions in the lattice in the two polymorphs. In the case of **18a** they sandwich the dication, forming a moderate NC-$CH_3{\cdots}\pi$ interaction between the CH group of one of the acetonitrile molecules and one of the pyrazole rings of L^{11} (C···centroid distance of 3.679 Å) and a H_3C–CN···π interaction between the second acetonitrile molecule and the central pyridine ring of a different L^{11} ligand strand in the same complex cation (N···centroid distance of 3.128 Å). In polymorph **18b** moderate C–H···NC–CH_3 interactions are present between the nitrogen of one of the acetonitrile molecules and (a) a hydrogen atom of the pyridine ring (C···N is 3.389(5) Å), (b) the hydrogen atom at the 5-position of the pyrazole ring (C···N is 3.315(6) Å) and (c) the α–H of the 4-cyanophenyl group (C···N is 3.632(6) Å) of the same ligand strand. The other acetonitrile molecule does not interact with the complex cation at all. In both polymorphs the Fe–N bond lengths at 180 K are consistent with the presence of a mixture of LS and HS states, in which the LS state predominates (**18a** 1.943(2)–2.017(2); **18b** 1.883(3)–1.962(3) Å).

Table 2
Mössbauer data for complex **16** at different temperatures.

T (K)	Spin state	δ_{iso} (mm s^{-1})	ΔE_Q (mm s^{-1})	AR (%)
300	LS	0.33(1)	0.67(2)	58
	HS	0.947(4)	1.403(9)	35
	I	0.37(5)	0.9(1)	7
275	LS	0.33(1)	0.64(1)	76
	HS	0.94(2)	1.40(2)	17
	I	0.44(4)	1.1(1)	7
259	LS	0.33(1)	0.63(3)	83
	HS	0.91(7)	1.5(2)	11
	I	0.48(5)	0.9(2)	6
52	LS	0.373(2)	0.608(2)	93
	I	0.49(3)	0.98(6)	7

I = impurity, δ_{iso} = isomer shift relative to α-Fe, ΔE_Q = quadrupole splitting, AR = area ratio of the components A_{HS}/A_{tot}. Statistical standard deviations are in parentheses.

The magnetic susceptibilities for **17** and **18a** were measured in the range 380–4.5 K, in both warming and cooling modes. The 300–100 K portion of this study is shown in Fig. 19. The authors did not specify why the magnetic measurements were started at such a high temperature, 380 K, but presumably they wanted to facilitate the desolvation of these complexes (see below). Unfortunately, because of the low yield of red polymorph **18b**, no magnetic studies were done on that polymorph.

During the first cycle the magnetic susceptibility $\chi_M T$ of complex **17** at 380 K is *ca.* 3.36 emu K mol^{-1} which is close to that expected for an iron(II) centre in the HS state. Upon cooling a relatively abrupt two-step ST occurs (Fig. 18). The first step is centred at ∼200 K while the second step is centred at ∼150 K. At 125 K, $\chi_M T$ is ca. 0.09 emu K mol^{-1} which is indicative of an iron(II) centre in the LS state. Upon heating there is now a gradual *one step* ST, centred at 196K. A broad hysteresis loop is observed ($\Delta T_{1/2}$ = 34 K and $T_{1/2}\downarrow$ = 162 and $T_{1/2}\uparrow$ = 196 K).

For orange polymorph **18a** the first cycle shows upon cooling a relatively abrupt and two step ST, the first step is centred at centred at ∼180 K, while the second step is centred at ∼150 K. In warming mode the two-step transition is maintained but the transition temperatures shifted to lower temperatures with a hysteresis loop characterized by $\Delta T_{1/2}$ = 6 K (Fig. 19). At 380 K $\chi_M T$ is *ca.* 3.63 emu K mol^{-1}, which corresponds to an iron(II) centre in the HS state, whereas at 130 K it has dropped to 0.03 emu K mol^{-1}, consistent with complete ST to the LS state. The authors proposed that the discrepancy between the magnetic and structural data at T = 180 K is due to the presence of two different SCO-active centres in the bulk sample of the crystals, possibly due to a partial de-solvation of the material before magnetic measurements could be obtained. This would explain the two step ST curve.

Three further cooling and warming cycles were done on **17** and **18a**. This revealed a dependence of the magnetic properties on the extent of the de-solvation of the samples, for both complexes. Upon losing some solvent molecules there is an increase in $T_{1/2}$ and a decrease in $\Delta T_{1/2}$; indeed hysteresis is completely lost in the

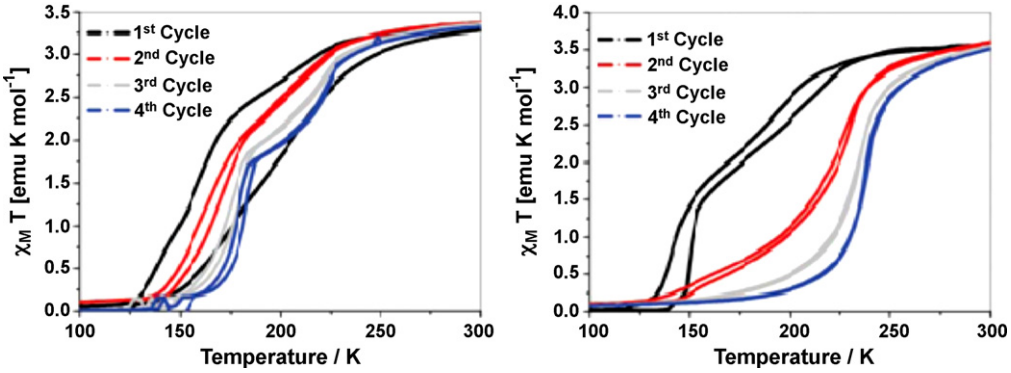

Fig. 19. Spin transition curves for complex **17** (left) and **18a** (right). From reference [53]. Reproduced and modified by permission of The Royal Society of Chemistry.

case of complex **18a** (Table 3). The abruptness of the ST curve also changes with further cycles, albeit in different ways for each complex. For complex **17** the curve became more abrupt during the subsequent cycles, whereas for complex **18a** initially the ST curve became smoother and less abrupt during the 2nd and 3rd cycles, but in the 4th cycle it became abrupt and single step, with $T_{1/2}$ = 236 K. For both complexes no further change was observed after the 4th cycle suggesting that complete removal of the solvent molecules had occurred by then.

Powder X-ray diffraction (XRD) studies of complexes **17** and **18a** were carried out at 293 K, before and after the SQUID studies (heating and cooling cycles). In the case of complex **17** the XRD pattern of a freshly prepared single crystal compared to the XRD pattern of the same sample after the first cooling cycle (from 293 to 150 K) showed the same diffraction pattern, demonstrating that there is no phase change during the thermal ST. However the powdered samples of complex **17** showed a different XRD pattern to that of the crystalline material. The authors explained this as being due to solvent loss during the XRD measurement at room temperature. Comparison of the XRD powder pattern acquired at room temperature (293 K) and that calculated from the X-ray crystal structure acquired at 180 K, showed totally different diffraction patterns, for both complexes **17** and **18a**. This is consistent with a phase transition and with the two-step ST observed for these complexes. Moreover, for both complexes **17** and **18a**, the XRD patterns for the 1st and 4th thermally cycled SQUID samples were completely different. This demonstrates that the differences in the magnetic properties during the thermal cycles are due to the loss of acetonitrile molecules from the crystal lattice, producing changes in the crystal packing.

The loss of solvent is also consistent with the FTIR spectra of these samples before and after the SQUID study. Before the SQUID study, the low and high frequency bands [54] characteristic of the lattice acetonitrile molecules are clearly observed for both **17** (2251 and 2291 cm^{-1}) and **18a** (2254 and 2292 cm^{-1}). In contrast, after the 4th heating-cooling cycle in the SQUID, none of these bands were present. This is further evidence that solvent loss occurs during the SQUID study. No TGA, DSC or microanalysis data were obtained to confirm this.

Ruben and co-workers [55] also synthesized the ligands L^{12-14} (Fig. 3) in order to study the effect of substituents at the 4-position of the pyridine moiety on the SCO properties of the respective iron(II) complexes. The complexes, $[Fe(L^n)_2](ClO_4)_2{\cdot}mCH_3CN$ (**19** n = 12, m = 0; **20** n = 13, m = 0; **21** n = 14, m = 2), were synthesized by reacting a solution of two equivalents of the corresponding ligand and one equivalent of $Fe(ClO_4)_2{\cdot}6H_2O$ in acetonitrile at 80 °C for about 5 h under N_2. After filtration, the complexes were obtained by diffusing diisopropyl ether (not stated whether as a vapour or liquid) into the respective filtrate, under N_2. Complexes **19** and **20** crystallise as brown crystalline materials and complex **21** as a dark red crystalline material. These crystalline samples were used for the magnetic measurements described below.

VT-magnetic susceptibility measurements in the 380–4.5 K range of temperature, show that complex **19** undergoes an abrupt and complete ST upon cooling. The ST is centred at 333 K. Complex **19** crystallizes in the *Pbcn* space group as brown crystals. The asymmetric unit comprises the cation and two perchlorate anions. At 180 K the average Fe–N bond length is 1.943 Å, characteristic of the LS state, which is in agreement with the magnetic measurements.

Complex **20** undergoes a complete but gradual ST, with $T_{1/2}$ = 281 K. X-ray crystallography at 180 K showed that complex **20** crystallizes in the *Pcca* space group as brown crystals. Again there are no solvent molecules present. The asymmetric unit is comprised by one dication and two perchlorate anions. The hydroxyl group at the back of the ligand does not interact with any other group. The average Fe–N bond length is 1.947 Å indicative of the LS state.

Magnetic susceptibility studies on complex **21** showed that it undergoes a more interesting ST upon cooling than complex **20** does. From 380 to 300 K the value of χT of 3.03 emu K mol^{-1} is constant and is in agreement with the presence of the HS state. The ST occurs between 300 and 125 K as a gradual and incomplete transition. The χT value of 1.76 emu K mol^{-1} at 140 K indicates that only half of the iron(II) centres are in the LS state. From 120 to 5 K a significant *increase* of the χT value occurs. The authors explained this behaviour as being a consequence of ferromagnetic coupling between the remaining HS complexes. X-ray crystal structures were determined on two different crystals at 180 and 298 K. At both temperatures complex **21** is in the *C*2/*c* space group and the asymmetric unit comprises one dication, two perchlorate anions and two acetonitrile solvent molecules. At 298 K the average Fe–N bond length is 2.158 Å, consistent with iron(II) in the HS state. At 180 K the average Fe–N bond length is 2.088 Å, consistent with an admixture of the LS and HS states, which is in agreement with the magnetic measurements.

Table 3
Transition temperature values ($T_{1/2}$) and hysteresis loop widths ($\Delta T_{1/2}$) for complexes **17** and **18a** in function of the heating and cooling cycle.

	Complex **17**				Complex **18a**			
Cycle	1	2	3	4	1	2	3	4
$T_{1/2}$ (K)	179	173	181	185	166	221	231	236
$\Delta T_{1/2}$ (K)	34	4	4	3	6	2	0	0

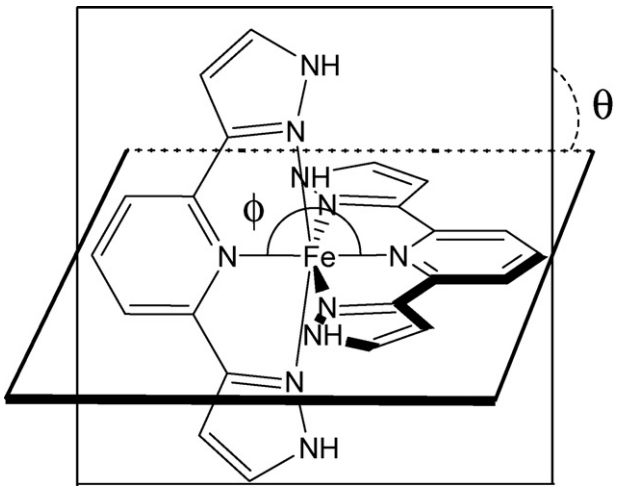

Fig. 20. Coordination sphere of the iron(II) complexes of the 2,6-bis(pyrazol-3-yl)pyridine ligand, H_2L^{15}, showing the angles ϕ and θ.

3.1.2. 2,6-Bis(pyrazol-3-yl)pyridine family

Nine of the ten complexes described in this section are mononuclear, $[Fe^{II}(H_2L^{15})_2]X_2{\cdot}n$(solvent), with the iron centre coordinated to two almost perpendicular, neutral, H_2L^{15} (Fig. 3) ligands, each of which is coordinated in a meridional fashion (Fig. 5A). In contrast, one complex, **30**·MeOH, is a *dinuclear* complex in which only *one* H_2L^{15} ligand is bound per metal centre (Fig. 5D). None of the 10 complexes described in this section contain a deprotonated H_2L^{15} ligand. Indeed, to date, there are no structurally characterized examples of any first row transition metal ion coordinated to a deprotonated H_2L^{15} ligand.

In the family of *mononuclear* SCO-active complexes $[Fe^{II}(H_2L^{15})_2]X_2{\cdot}n$(solvent) each ligand is bonded to iron(II) through the nitrogen atom of the central pyridine and through the imine nitrogen atom of the two pyrazole rings (*N2*). To date there are no examples in the literature of an SCO-active iron(II) complex of a *substituted* H_2L^{15} (probably due to synthetic issues rather than a lack of interest). Rather, studies have concentrated on the effect of the anion and solvent molecules on the SCO-properties of the $[Fe^{II}(H_2L^{15})_2]^{2+}$ dication.

Ligand H_2L^{15} is the $C_{pyrzole}$–$C_{pyridine}$ analogue of L^1 (Fig. 3). As in the case of L^1, the complexes of H_2L^{15} have an angular Jahn–Teller distortion which is described by the angles φ and θ (Fig. 20). Once the neutral ligand H_2L^{15} is coordinated to the iron(II) centre, the uncoordinated NH (*N1*) of the pyrazole ring is often involved in hydrogen bonding interactions with water or solvent molecules and/or anions. In most of the cases when the NH is hydrogen bonded to water molecules the LS state is stabilised; the authors suggest that this is due to concomitant strengthening of the Fe–$N_{pyrazole}$ σ-bond (see below). There are no examples of deprotonation and coordination of the NH group to a metal centre. In the solid state the cross shaped dication generally packs in layers where the pyridine and pyrazole rings interact via edge-to-face and face-to-face π and C-H···π interactions.

The first SCO-active complex of iron(II) and ligand H_2L^{15} reported in the literature was complex $[Fe(H_2L^{15})_2](BF_4)_2{\cdot}2H_2O$ (**22**·2H_2O) [56]. This complex was synthesized by Sugiyarto and Goodwin by reacting one equivalent of $Fe(BF_4)_2{\cdot}6H_2O$ and two equivalents of H_2L^{15} in hot ethanol under nitrogen. Upon cooling, the addition of a small amount of diethyl ether to the solution produced **22**·2H_2O as a red-brown microcrystalline solid. This material was dehydrated by heating it at 110 °C in a N_2 atmosphere, yielding a bright yellow solid, **22**. VT-magnetic measurements on a 30% ^{57}Fe enriched sample of **22** showed that it undergoes an abrupt and complete ST with a 10 K wide hysteresis loop ($T_{1/2}\uparrow$ = 180 and $T_{1/2\downarrow}$ = 170 K) [56,57]. In contrast, the dihydrate, **22**·2H_2O, undergoes a relatively gradual ST with a much higher $T_{1/2}$ of approximately 300 K. These values, obtained from magnetic measurements, correlate well with the results obtained from VT ^{57}Fe Mössbauer spectroscopy. For **22** the ^{57}Fe Mössbauer spectrum at 295 K showed only a doublet characteristic of the HS state (ΔE_Q = 2.40 and δ_{iso} = 1.01 mm s^{-1}) while at 77 K (after slow cooling) only one doublet characteristic of the LS state was observed (ΔE_Q = 0.68 and δ_{iso} = 0.37 mm s^{-1}). When the sample was rapidly cooled a fraction of the HS state was trapped in that state so two doublets were observed, for the trapped HS state (ΔE_Q = 3.01 and δ_{iso} = 1.13 mm s^{-1}) and the LS state (ΔE_Q = 0.67 and δ_{iso} = 0.37 mm s^{-1}).

Dehydration of **22**·2H_2O to **22** causes a change in phase, as seen by X-ray powder diffraction (no single crystals were obtained for either of these forms). The big difference in the magnetic properties of **22**·2H_2O and **22** was explained as likely resulting from differences in the hydrogen bond interactions. In **22**·2H_2O the NH group of the pyrazole ring is likely hydrogen bonded to the water molecules. The authors suggest that this increases the electron density at the imine nitrogen, making the $N_{pyrazole}$–Fe σ-bond stronger thus favouring the LS state (increasing the $T_{1/2}$). When these water molecules are removed it is suggested that the NH group instead hydrogen bonds to the BF_4 anions, perhaps connecting the dications together, improving the communication between iron centres and leading to the observation of abrupt ST with hysteresis [57].

In a later publication these authors were able to crystallise complex **22** as the *trihydrate* (**22**·3H_2O), from an acetone solution containing few drops of water, although no magnetic data were reported for this particular crystalline solvate. Complex **22**·3H_2O crystallizes in the *C*2/*c* space group. The asymmetric unit comprises one dication, two tetrafluoroborate anions and three molecules of water. One of the tetrafluoroborate ions is ordered while the other one is disordered over two positions with occupancies 0.57:0.43. The uncoordinated NH of the pyrazole ring is involved in hydrogen bonding. The disorder in the second BF_4^- ion leads to two hydrogen bonding scenarios: either (a) one ligand strand in the dication is hydrogen bonded to two water molecules and the other ligand strand is hydrogen bonded to two BF_4^- anions, or (b) both ligand strands are hydrogen bonded to one water molecule and one BF_4^- anion. At room temperature, the average Fe–N bond length, 1.95 Å, is indicative of the LS state, which is in agreement with the magnetic data reported for the dihydrate [58].

Goodwin and co-workers [58] synthesized complex $[Fe(H_2L^{15})_2]I_2{\cdot}4H_2O$ (**23**·4H_2O) under a N_2 atmosphere by reacting two equivalents of H_2L^{15} in warm ethanol and one equivalent of $FeCl_2{\cdot}4H_2O$ in warm water, followed by addition of a warm aqueous solution of sodium or ammonium iodide. On cooling, **23**·4H_2O crystallized as a red-brown solid. It was filtered off, washed with water and recrystallized from hot water. Dehydration of this complex was achieved by heating the sample at 110 °C under a N_2 atmosphere resulting in **23** as a yellow solid.

The sample of crystalline **23**·4H_2O was predominantly LS (1.04 BM) at room temperature. The magnetic moment decreases further, to 0.67 BM on cooling to 176 K. Somewhat surprisingly, the Mössbauer spectrum of **23**·4H_2O at room temperature showed only one asymmetric doublet characteristic of LS iron(II) (ΔE_Q = 0.71 and δ_{iso} = 0.34 mm s^{-1}). The authors suggested that the asymmetry in the spectrum could be due to the presence of a small amount of the HS state (although there was no evidence of the HS state doublet in the Mössbauer spectrum) or possibly orientation effects.

In contrast to **23**·4H_2O, the very hygroscopic anhydrous salt, **23**, is in the HS state from room temperature to 206 K. Below this temperature an abrupt ST occurs, with the system being fully LS at

195 K. A hysteresis loop of 2 K is present ($T_{1/2}\downarrow$ = 200 K, $T_{1/2}\uparrow$ = 202 K) [58].

Crystals of **23**·4H_2O suitable for X-ray crystallography were grown from an aqueous solution containing a few drops of acetone. This complex crystallizes in the *P*-1 space group. The asymmetric unit comprises one dication, two iodide ions and three molecules of water. At room temperature the average Fe–N bond length is 1.95 Å, consistent with LS iron(II). Both of the ligand strands in the dication are hydrogen bonded to one water molecule and one iodide anion. Interestingly the water molecules are involved in a complex hydrogen bonding network that runs along the *a b* plane (Fig. 21). This network is formed by one central water molecule that interacts with one external water molecule and one external iodide ion, these external groups interact at the same time with an identical neighboring repeat unit. The network forms channels in which the dications are accommodated [58].

Goodwin and co-workers [59] also synthesized the complex $[Fe(H_2L^{15})_2](SCN)_2{\cdot}2H_2O$ (**24**·2H_2O), under a nitrogen atmosphere by reacting a hot ethanolic solution of one equivalent of H_2L^{15} and a hot aqueous solution of two equivalents of $FeCl_2{\cdot}4H_2O$, followed by an aqueous solution of ammonium thiocyanate. After the solution was cooled down the deep-red crystals that formed were filtered off and washed with cold water, resulting in bright orange-yellow polycrystalline material after drying, **24**·2H_2O. This material was used in the magnetic measurements described below. Subsequent recrystallization from nitromethane afforded crystals of **24**·2H_2O suitable for X-ray crystallography.

VT-magnetic measurements showed that the polycrystalline sample of complex **24**·2H_2O undergoes a *two-step*, abrupt and complete ST upon cooling. In both steps a hysteresis loop was found (first step $T_{1/2}\uparrow$ = 256, $T_{1/2\downarrow}$ = 247 K, $\Delta T_{1/2}$ = 9 K; second step $T_{1/2}\uparrow$ = 219, $T_{1/2\downarrow}$ = 193 K, $\Delta T_{1/2}$ = 24 K). Interestingly the ST is time-dependent in the vicinity of the transition temperatures [59]. The ST was also characterized by ^{57}Fe Mössbauer spectroscopy. Surprisingly at 298 K the presence of both HS and LS states was detected, with HS the major component (doublet with ΔE_Q = 2.11 and δ_{iso} = 0.96 mm s^{-1}). This inconsistency between the magnetic and Mössbauer data was not explained. At 78 K, as expected, only one doublet is detected and it corresponds to the LS state (ΔE_Q = 0.71 and δ_{iso} = 0.34 mm s^{-1}) [59].

A crystal structure determination on **24**·2H_2O (*P*-1 space group) at room temperature showed that the average Fe–N distance is 2.16 Å, consistent with the presence of the HS state. The pyrazole and pyridine rings are involved in face to face and edge to face π interactions. The water molecules are hydrogen bonded to the thiocyanate counter anions that lie in channels formed by the dications. Each anion and water molecule is hydrogen bonded to two different cations through the NH of the pyrazole ring, thus providing links between the individual complexes, enhancing cooperativity and leading to the observed abrupt ST with hysteresis [59].

Further investigation [60] of this system revealed even more interesting magnetic behaviour. When a freshly prepared sample was thermally cycled once, the magnetic data matched perfectly with the *two step* ST (and parameters) noted above, but when this already cycled sample was cycled again a totally different ST curve was obtained. In this case a *one step*, abrupt and complete ST, with hysteresis, was obtained ($T_{1/2}\uparrow$ = 231 K, $T_{1/2\downarrow}$ = 233 K, $\Delta T_{1/2}$ = 2 K). Further, when this doubly cycled sample was kept in a closed sample holder for at least one day, subsequent magnetic measurements revealed the same *two step* ST curve as for the freshly prepared sample (Fig. 22). A second cycle on this sample showed that the ST curve again changes to a single step. This behaviour is totally reproducible and is certainly remarkable.

To try to explain these intriguing results the authors used a range of techniques including VT ^{57}Fe Mössbauer spectroscopy studies, differential scanning calorimetry (DSC) and thermogravimetric analysis (TGA). These studies provided data consistent with the magnetic data. From the results obtained the authors were able to show that the two-step ST sample is in the more stable thermodynamic state and is favoured due to the hydrogen bonding interactions present. Variable temperature X-ray, synchrotron powder diffraction and soft X-ray studies showed that during the thermal cycling the hydrogen bonding interactions are broken, leading to changes of orientation and position of NCS^- anions and water molecules, resulting in a crystallographic phase transition. Overall, the authors found that the change from two-step to one-step behaviour is temperature induced, and the change back from one-step to two-step is time dependent [61].

The complex $[Fe(H_2L^{15})_2](SeCN)_2$ (**25**) was also synthesized by Goodwin and co-workers [59]. In the same manner as for **24**·2H_2O but using potassium selenocyanate. The microcrystalline material

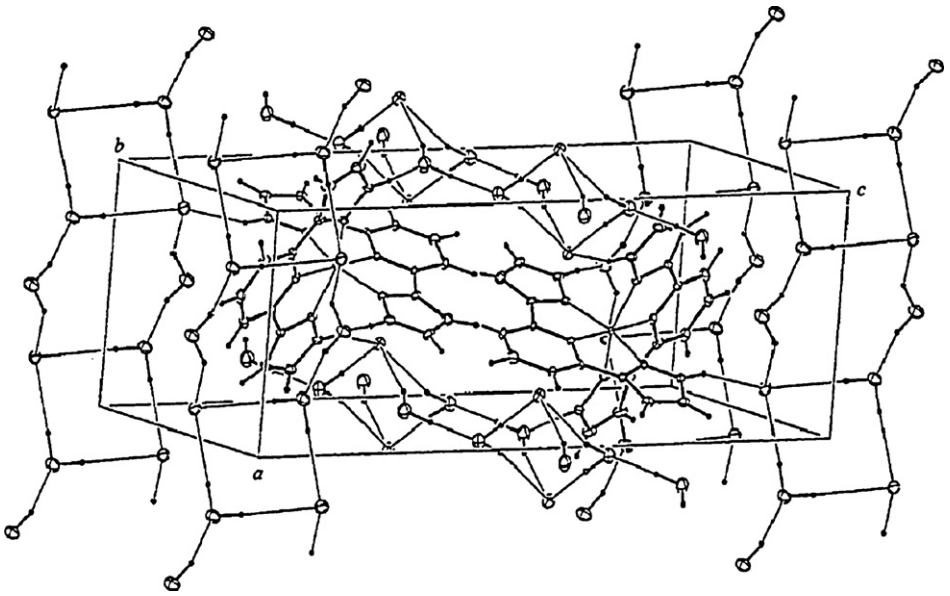

Fig. 21. Packing diagram of complex **23**·4H_2O showing the hydrogen bonding network running parallel to the *a b* plane. From reference [58]. Reproduced by permission of The Australian Journal of Chemistry.

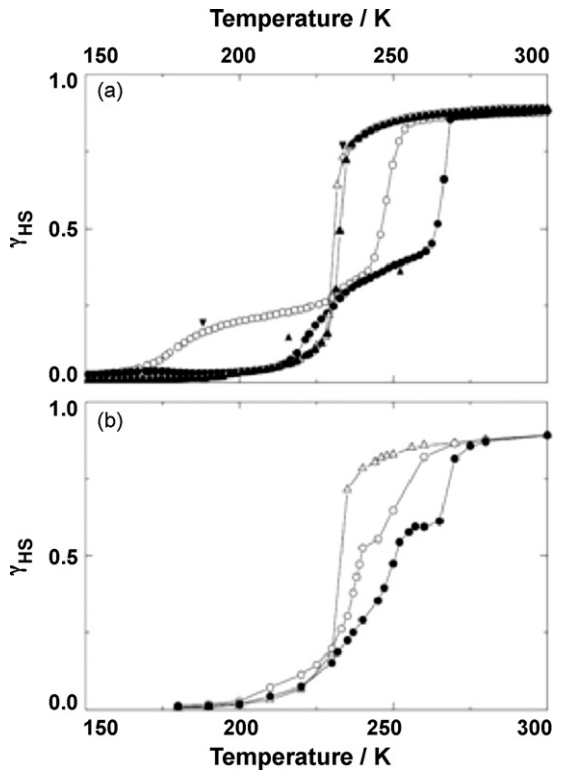

Fig. 22. ST curve for the complex **24**·2H$_2$O from (a) magnetic measurements, (b) ^{57}Fe Mössbauer spectroscopy studies. Fresh sample: cooling (○), heating (●). Cycled sample: cooling (△), heating (▲). From reference [60]. Copyright Wiley–VCH Verlag GmbH & Co. KGaA. Reproduced and modified with permission.

obtained after cooling the hot ethanolic solution was used for the magnetic measurements. Orange-yellow crystals of **25** suitable for X-ray crystallography were obtained from a nitromethane solution.

On cooling, complex **25** undergoes a complete and abrupt ST, centred at 231 K with a very small hysteresis loop ($\Delta T_{1/2} \leq 1$ K). This was corroborated by ^{57}Fe Mössbauer spectroscopy studies. Surprisingly, at 298 K two doublets are observed, the major one being HS (HS $\Delta E_Q = 2.14$ and $\delta_{iso} = 0.95$ mm s^{-1}; LS $\Delta E_Q = 0.70$ and $\delta_{iso} = 0.36$ mm s^{-1}), once again this inconsistency between the magnetic and Mössbauer results was not explained. At 78 K only one doublet is present and it corresponds to the LS state ($\Delta E_Q = 0.74$ and $\delta_{iso} = 0.43$ mm s^{-1}).

A single crystal X-ray structure determination carried out at room temperature shows that complex **25** is in the HS state (average Fe–N 2.17 Å). As expected, extensive face to face and edge to face π interactions (terpyridine embrace interactions) between the pyridine and pyrazole rings are present (Fig. 23). Again the dications are packed in layers, forming channels that host the anions. The NH of the pyrazole rings are hydrogen bonded to the Se and N atoms of the SeCN$^-$, leading to bridging between adjacent dications, forming a two dimensional array that runs parallel to the *ab* plane (Fig. 23A). Overall these intermolecular interactions lead to cooperativity between the dications and hence to the observed abrupt ST, albeit without hysteresis in this case [59].

Goodwin and co-workers [62,63] synthesized the complex [Fe(H$_2$L^{15})$_2$](CF$_3$SO$_3$)$_2$·3H$_2$O (**26**·3H$_2$O) enriched in ^{57}Fe to 30%, by reacting two equivalents of the ligand and one equivalent of FeCl$_2$·4H$_2$O in water under a N$_2$ atmosphere. After heating the mixture until a deep-red brown solution was obtained, it was filtered and a concentrated aqueous solution of LiCF$_3$SO$_3$ was added to the filtrate while it was hot. On cooling deep red-brown crystals of **26**·3H$_2$O were obtained. When **26**·3H$_2$O is heated at 60–70 °C under N$_2$ a bright yellow solid is obtained and was characterized as

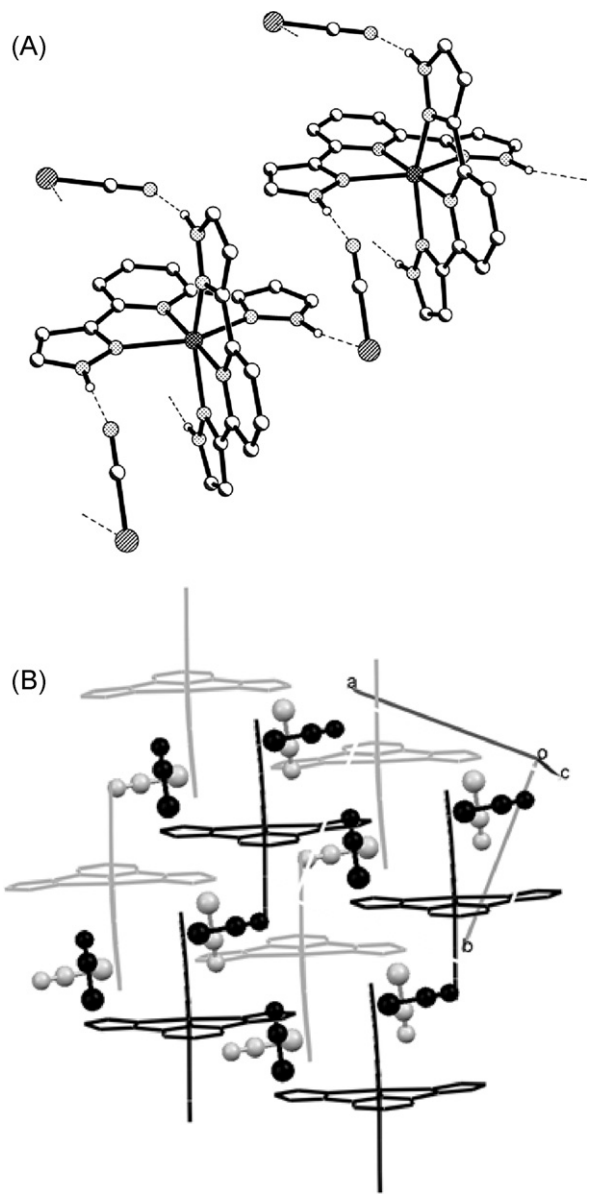

Fig. 23. (A) Ball and stick representation of complex **25** showing the hydrogen bond interactions between the NH of the pyrazole moieties and the SeCN$^-$ anions bridging the complex cations forming a 2D sheet. (B) Perspective view of the packing of complex **25** down the *c* axis, highlighting the layers of 2D hydrogen bonded sheets (one layer black, next layer grey) as well as the terpyridine embrace interactions between complex cations within a layer. This figure was generated from data obtained from the CCDC as published originally in reference [59].

the monohydrate, **26**·H$_2$O. This yellow and stable sample, **26**·H$_2$O, was used for the magnetic measurements (see below).

Crystals of **26**·3H$_2$O suitable for X-ray crystallography were obtained from an acetone solution containing some drops of water. This complex crystallizes in the *P*-1 space group. At room temperature the average Fe–N distance is 1.946 Å, typical of iron(II) in the LS state [62]. As is common in this family of complexes, the uncoordinated NH of the pyrazole ring is hydrogen bonded with water molecules and the oxygen atom of the anions. The authors suggest that these interactions increase the electron density at the imine-like nitrogen of the pyrazole ring making the ligand a stronger σ-donor and stabilising the LS state.

The 30% ^{57}Fe enriched sample of complex **26**·H$_2$O presented an almost complete and very abrupt single step ST upon cooling, with $T_{1/2}\downarrow = 147$ K (Fig. 24). Intriguingly, in the warming mode there are

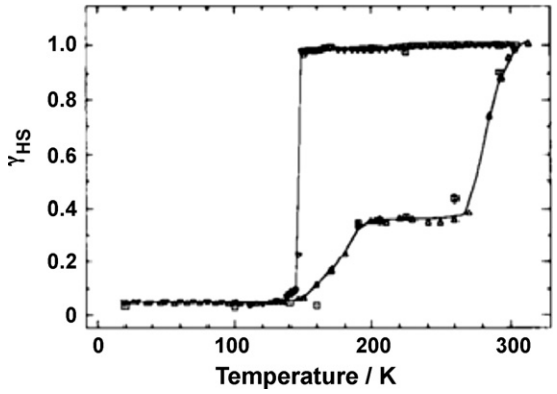

Fig. 24. Spin transition curve for complex **26**·H_2O derived from magnetic susceptibility (▽ for decreasing temperatures and △ for increasing temperatures) and Mossbauer investigations (o). From reference [63]. Copyright Wiley-VCH Verlag GmbH & Co. KGaA. Reproduced and modified with permission.

two steps. The first step has $T_{1/2}\uparrow \approx 150$ K and the second step has $T_{1/2}\uparrow \approx 285$ K. That is, the ST curve is very asymmetric and exhibits a very wide hysteresis loop (Fig. 24). VT ^{57}Fe Mössbauer spectroscopy studies are in agreement with these results (Fig. 25). The spectrum recorded at 292 K showed one doublet characteristic of iron(II) in the HS state ($\Delta E_Q = 2.28$ and $\delta_{iso} = 0.87$ mm s^{-1}). Upon cooling the intensity of this doublet decreases and a new doublet characteristic of the iron(II) LS state appears ($\Delta E_Q = 0.69$ and $\delta_{iso} = 0.29$ mm s^{-1}). The hysteresis loop, and the asymmetry of it, were detected by Mössbauer spectroscopy as well as by the magnetic measurements [63].

When this sample was held at 20 K and irradiated with a green laser light a quantitative photoconversion to the metastable HS state was achieved (LIESST effect). When this photoconverted sample was irradiated with a red light the sample was switched back to the LS state. Moreover when the sample is quench cooled thermal spin trapping of the HS state occurs [63].

Goodwin and co-workers [64] synthesized the mixed valent complex $[Fe^{II}(H_2L^{15})_2][Fe^{III}(CN)_5(NO)]$ (**27**) with the aim of increasing the cooperativity between the iron(II) centres by introducing a complex anion capable of forming hydrogen bonding interactions with it. It was synthesized under N_2 in warm water by reacting two equivalents of H_2L^{15} and one equivalent of $FeCl_2{\cdot}4H_2O$, followed by the addition of an excess of sodium nitroprusside dihydrate in a warm aqueous solution, resulting in the precipitation of **27** as a bright yellow microcrystalline solid. This precipitate was used in the magnetic measurements. Crystals suitable for X-ray crystallography were obtained by slow liquid-liquid diffusion of a freshly prepared aqueous solution of $[Fe(H_2L^{15})_2]Cl_2$ layered over an aqueous solution of the complex anion.

VT magnetic measurements on the microcrystalline sample of **27** revealed an abrupt and complete ST upon cooling and a narrow hysteresis loop ($T_{1/2}\downarrow = 184$ K, $T_{1/2}\uparrow = 181$ K and $\Delta T_{1/2} = 3$ K) [64]. This small hysteresis loop shows that there is cooperativity between the iron centres due to a three dimensional hydrogen bonding network (see below). VT ^{57}Fe Mössbauer spectroscopy

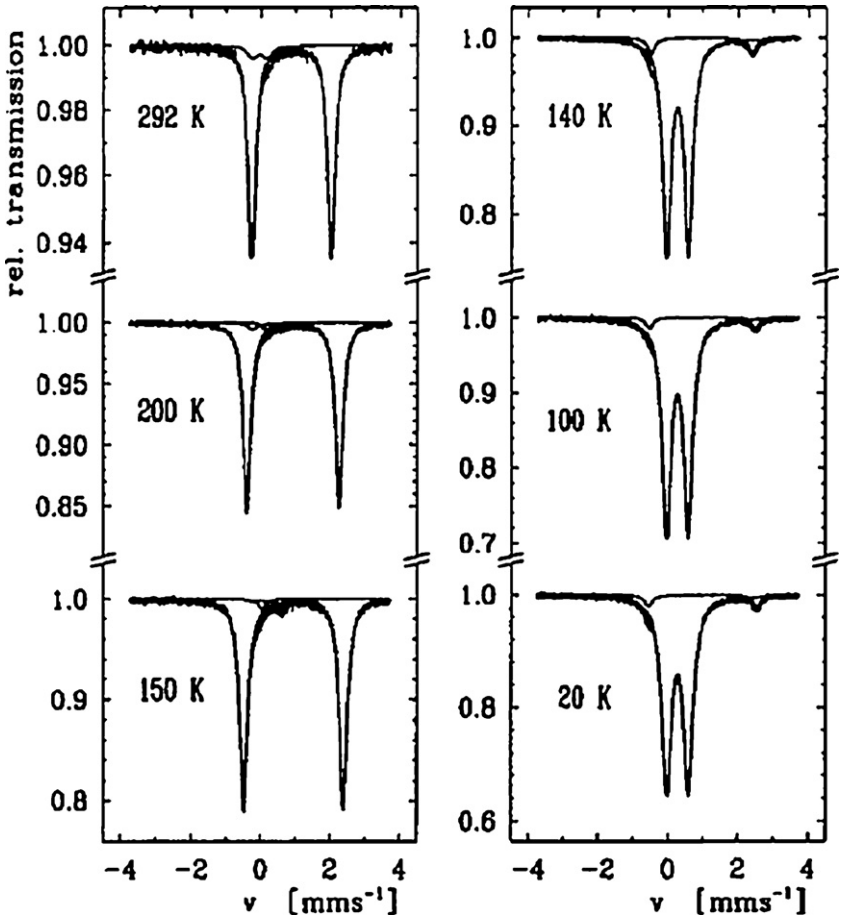

Fig. 25. VT-Mössbauer studies of complex **26**·H_2O recorded in the cooling direction. At 292 K the spectrum is dominated by an iron(II) HS doublet. Between 150 and 140 K it is possible to observe the coexistence of the HS and LS states. At temperatures below 140 K a residual HS fraction of *ca.* 5% is observed. From reference [63]. Copyright Wiley–VCH Verlag GmbH & Co. KGaA. Reproduced with permission.

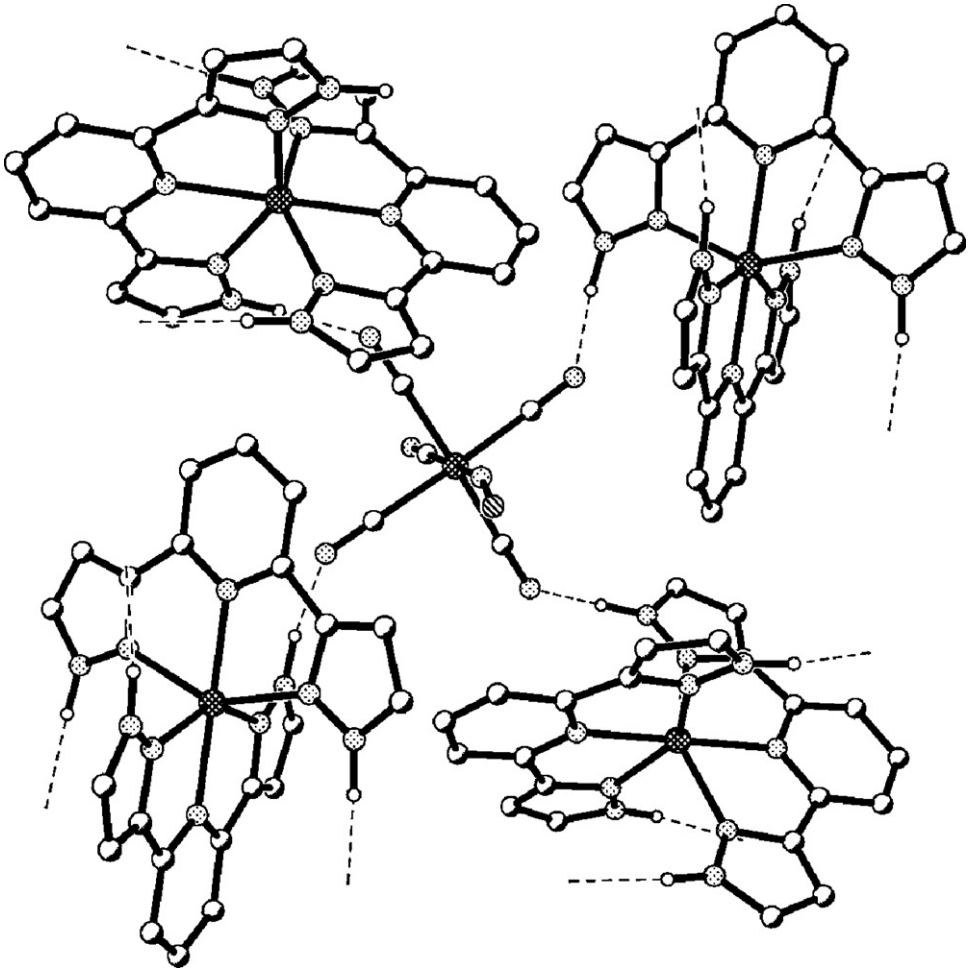

Fig. 26. Ball and stick representation of complex **27** showing the hydrogen bond interactions (dotted black lines) between the uncoordinated NH group of a ligand strand and an equatorial CN group of the nitroprusside anion (100 K). This figure was generated from data obtained from the CCDC as published originally in reference [64].

studies on a 100% ^{57}Fe enriched complex cation and 50% ^{57}Fe enriched complex anion sample showed that at 298 K the complex cation is in the HS state (ΔE_Q = 2.09, δ_{iso} = 0.96 mm s^{-1}), while at 80 K it is in the LS state (ΔE_Q = 0.65, δ_{iso} = 0.42 mm s^{-1}).[64] A resonance for the complex anion, characteristic of iron(III) in the LS state and similar to other nitroprusside anions reported in the literature (298 K, ΔE_Q = 1.84, δ_{iso} = −0.28 mm s^{-1}; 80 K, ΔE_Q = 1.90, δ_{iso} = −0.22 mm s^{-1}), was also observed at both temperatures. In the low temperature spectrum, the lines corresponding to the cation are broadened suggesting the presence of two doublets with identical isomer shift but slightly different quadrupole splitting. This can be explained by the existence of two slightly different iron cations at low temperature. This hypothesis was proven by the X-ray crystal structure determinations carried out at 294 and 100 K. The space group at 294 K is tetragonal *P*4/*ncc*. During the ST a phase change occurs to orthorhombic *Pnca*. At 100 K, two crystallographically independent iron centres exist whereas at 294 K there is only one. At 294 K the average Fe-N distance is 2.174 Å which clearly indicates the iron(II) is in the HS state, whereas at 100 K it is 1.958 and 1.959 Å (for the two independent cations) which is typical of the LS state. As expected, the structural details of the nitroprusside anion are practically identical at both temperatures.

A remarkable hydrogen bonding network is present in this system: each cation is hydrogen bonded to four anions and *vice versa* (Fig. 26). The four equatorial CN groups of the anion are interacting with the four uncoordinated NH pyrazole groups on the cation. At 294 K the apical groups in the nitroprusside anion are aligned along the four-fold axis; while at 100 K the NC–Fe–NO axis is tilted away from the four-fold axis. As for the other complexes in this family, in addition to the hydrogen bond interactions there are also face to face and edge to face interactions between the central pyridine and the pyrazole ring of neighboring molecules [64].

The mixed metal complex $[Fe^{II}(H_2L^{15})_2][Cr^{III}(bpy)(ox)_2]_2{\cdot}2H_2O$ (**28**·2H$_2$O, bpy = 2,2′-bipyridine and ox = oxalate dianion) was synthesized, by Coronado and co-workers, in another attempt to obtain SCO-active systems that present high cooperativity between the iron(II) centres [65]. It was prepared by reacting two equivalents of H_2L^{15} and one equivalent of $Fe(SO_4)_2{\cdot}7H_2O$ in methanol at room temperature, followed by adding this solution to a suspension of two equivalents of $Ba[Cr(bpy)(ox)_2]_2{\cdot}3H_2O$ in water. The precipitated $BaSO_4$ was removed by filtration, and the filtrate was slowly concentrated, obtaining **28**·2H$_2$O as large red single crystals. The authors did not specify whether or not the synthesis was carried out under a N_2 atmosphere or in air.

A crystal structure determination at 180 K showed that complex **28**·2H$_2$O crystallizes in the *P*-1 space group. There are two crystallographically independent $[Fe^{II}(H_2L^{15})_2]^{2+}$ dications. In one of these dications, Fe1–A, the Fe–N distances are in the range 2.146(2)–2.210(2) Å, corresponding to the HS state, while in the other, Fe1–B, the range is 1.921(2)–1.976(2) Å, typical of the LS state. The complex cation that contains Fe1–A is the hydrogen bond donor in 4 hydrogen bonding interactions: the four uncoordinated NH of the pyrazole rings per dication interact with three complex anions and one water molecule. The other complex cation, that con-

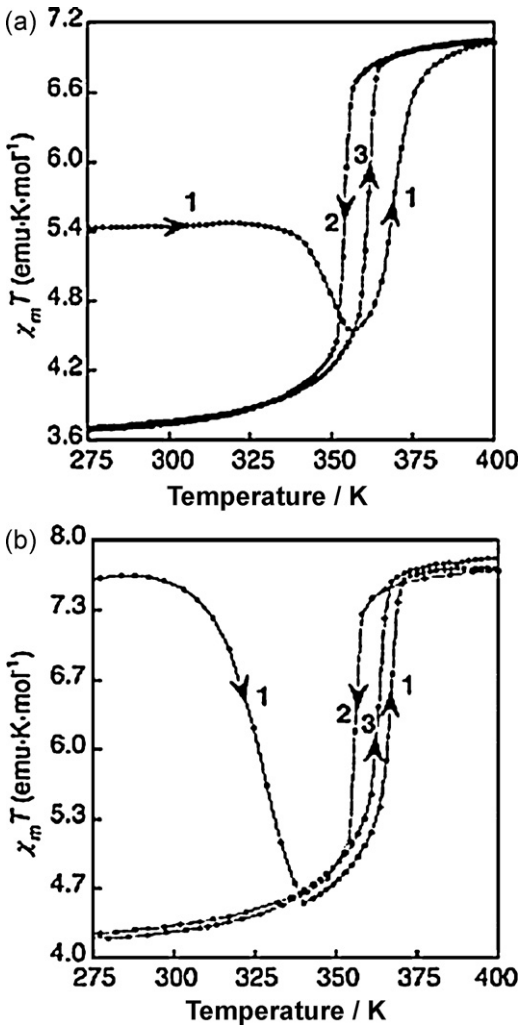

Fig. 27. ST curve for **28**·2H_2O (a) and **28′**·2H_2O (b). Curve 1: first heating. Curves 2 and 3: subsequent temperature cycles (cooling and heating, respectively). Reprinted and modified with permission from Reference [66]. Copyright 2007 American Chemical Society.

tains Fe1–B, interacts with four complex anions, which are better hydrogen bond acceptors than water. The authors propose that this results in an increase in the electron density at *N*1 of the pyrazole ring (non-coordinated nitrogen), which makes the pyrazole moieties better σ-donors and hence better able to stabilise the LS state (than the complex cation that contains Fe1–A which interacts with only three complex anions, and one water molecule) [65]. Overall, layers of the complex cations alternate with layers of the complex anions. Within these individual layers hydrogen bonding with water molecules interconnects the cations or anions respectively. The complex cations also make π–π interactions with neighboring molecules, forming terpyridine embraced dimers but not 2D chains or 3D networks. The complex anions also form such π–π interactions, but in this case it occurs between the bipyridine rings of neighboring molecules, resulting in stacks that run parallel to the *b* axis.

The magnetic susceptibility (5.5 emu K mol^{-1}) of the crystalline sample of **28**·2H_2O from 50 K to room temperature is consistent with the presence of a 1:1 mixture of HS:LS iron(II) complexes, along with two Cr^{3+} ions per molecule of iron(II) complex (Fig. 27).

Surprisingly, at temperatures above 320 K the susceptibility *decreases*, reaching a *minimum* of ~4.5 emu K mol^{-1} at 356 K, before rising again, to a maximum of 7 emu K mol^{-1} at 400 K, consistent with all of the iron(II) centres having been converted to the HS state. Coming back down from 400 K, i.e. in the cooling mode, a complete and abrupt ST is observed with $T_{1/2}\downarrow$ = 353 K, to a susceptibility of about 3.7 emu K mol^{-1} at 275 K, consistent with fully LS iron(II) along with two Cr^{3+} per Fe^{2+}. When this already cycled sample is heated up to 400 K a complete and abrupt ST is observed with $T_{1/2}\uparrow$ = 369 K. Further cycles showed no return to the initial ST behaviour (curve 1, Fig. 27). Rather, curves 2 and 3 were reproducible (Fig. 27). TGA studies showed that in the 300–380 K temperature range both molecules of water per complex are lost. This readily explains the difference in the magnetic properties of the freshly prepared and previously heated samples. Clearly the unusual decrease in the magnetic susceptibility seen on heating the freshly prepared sample from room temperature to 356 K is simply due to solvent loss at these elevated temperatures.

The resulting anhydrous sample can be rehydrated within a few minutes under a flow of humid air, forming **28′**·2H_2O, which interestingly has different magnetic behaviour (Fig. 27) to the freshly prepared sample of **28**·2H_2O [65]. The magnetic susceptibility of the rehydrated sample, **28′**·2H_2O, in the 50 K to room temperature range is in agreement with *all* of the iron(II) centres being in the HS state (7.5 emu K mol^{-1}). Again the unusual decrease of the magnetic moment is observed as the temperature is increased from room temperature to approximately 340 K. However it is clear that this is simply due to the dehydration of the material. Once it is solvent free, the ST curve follows the same shape as the dehydrated sample (Fig. 27).

The initial difference in the behaviour was explained by an X-ray crystallographic study at 180 K on a crystal that was dehydrated then rehydrated. That is on **28′**·2H_2O. This study showed that there is only one crystallographically independent iron(II) centre in **28′**·2H_2O (not 2 as there was in **28**·2H_2O, see above). The range of Fe–N distances, 2.145(3)–2.204(3) Å, is in agreement with the iron(II) centres being in the HS state. As expected the complex cation is hydrogen bonded to three complex anions and one water molecule.

Interestingly, anhydrous **28** can instead be resolvated with MeOH by flowing nitrogen gas saturated with dry methanol vapour over it, generating **28′**·MeOH [65]. TGA studies showed that only one molecule of MeOH per iron(II) is incorporated in the crystal lattice (the authors did not report microanalysis results for this resolvated material **28′**·MeOH). Not surprisingly, the magnetic properties of **28′**·MeOH are different from **28′**·2H_2O. A constant value of χT = 4.8 emu K mol^{-1} is seen from low temperature to room temperature, indicating that 33% of the iron centres are in the LS state. At 330 K a maximum is reached, then on further heating desolvation occurs, causing a slight decrease in susceptibility before the magnetic susceptibility increases abruptly (from their published figure this occurs at about $T_{1/2} \approx 360$ K by eye), to a value consistent with the presence of fully HS iron(II). After this the dehydrated material follows the same ST curve as seen for **28** (Fig. 28) [65].

In a further variation on the above Fe^{2+}:2Cr^{3+} mixed metal complex these authors [66] synthesized a complex with a different heterocycle bound to Cr^{3+}. Two differently solvated versions of $[Fe^{II}(H_2L^{15})_2][Cr^{III}(phen)(ox)_2]_2$·*solvents* (**29**·*solvents*) were prepared following the same procedure for the synthesis of **28**·2H_2O, but using two equivalents of Ba[Cr(phen)$(ox)_2]_2$·3H_2O as a starting material. After slow evaporation of the filtrate over a couple of days the kinetic product **29**·5.5H_2O·2.5MeOH was obtained as orange needles. The resulting mother liquor was left standing for 3 weeks affording the thermodynamic product $[Fe(H_2L^{15})_2][Cr(phen)(ox)_2]_2$·0.5$H_2O$·0.5MeOH (**29**·0.5$H_2O$·0.5MeOH) as red prisms.

A crystal structure determination of the red prisms of **29**·0.5H_2O·0.5MeOH at 180 K showed that the complex crystallizes in the *P*-1 space group. As for complex **28**·2H_2O there are

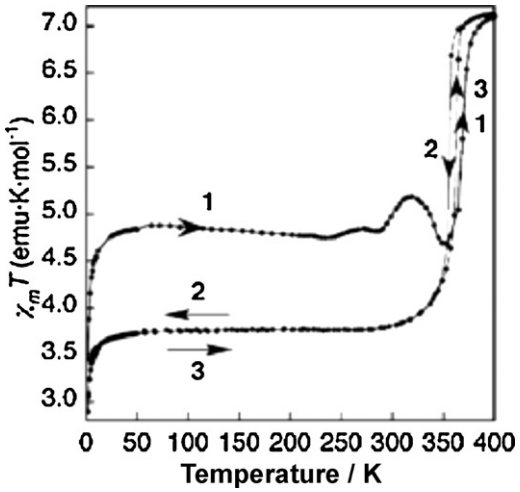

Fig. 28. ST curve for **28**′·MeOH. Curve 1: First heating. Curves 2 and 3: Subsequent temperature cycles (cooling and heating, respectively). Reprinted and modified with permission from Reference [66]. Copyright 2007 American Chemical Society.

two crystallographically independent iron(II) centres, and again one, Fe1–A, is in the HS state (Fe–N 2.159(2)–2.229(2) Å) and the other, Fe1–B, is in the LS state (Fe–N 1.924(2)–1.985(2) Å). The HS complex cation is hydrogen bonded to three complex anions and one water molecule, while the LS state complex cation is hydrogen bonded to four complex anions. The crystal packing is also very similar to **28**·2H_2O, with alternating layers of cations and anions. In the cation layer, one pyrazole ring of the complex cation interacts with a pyrazole ring of a neighboring cation via a π–π interaction, forming terpyridine-embraced dimers. The complex anions also feature π–π interactions, but in this case they occur between the phenanthroline ligands.

Red complex **29**·0.5H_2O·0.5MeOH undergoes a dehydration–rehydration process but, unlike the rehydration of **28**, rehydration of the anhydrous material (i.e. **29**) stabilizes the LS state. This was confirmed by an X-ray dataset acquired at 180 K on the rehydrated complex, that only contains half molecule of water per iron centre (**29**′·0.5H_2O), which showed Fe–N bond lengths ranging from 1.914(6) to 2.013(7) Å. The rehydrated crystal of **29**′·0.5H_2O remain in the *P*-1 space group, with cell parameters very similar to **29**·0.5H_2O·0.5MeOH, but the *a* parameter and the cell volume are halved, and there is only one crystallographically independent iron(II) centre and two crystallographically independent complex anions. Each complex cation is hydrogen bonded to four complex anions, and one of these anions is weakly interacting with one water molecule. But, unlike in **28**′·2H_2O, here the ligands surrounding the iron(II) centre stack strongly through π–π interactions forming chains along the *a* axis. These interactions may well help to stabilize the iron(II) centres in the LS state [66].

An X-ray crystal structure determination on the orange needles of **29**·5.5H_2O·2.5MeOH at 180 K showed that this complex crystallizes in the $P2_1/a$ space group. There is only one iron(II) in the asymmetric unit and it is in the HS state (Fe–N 2.145(7)–2.212(7) Å). Surprisingly, the HS complex cation is hydrogen bonded to four complex anions, interactions which appear in other complexes to have stabilised the LS state. The fact that the complex is not LS in this case was tentatively explained by the authors as being a result of one *N*H being hydrogen bonded to a Cr-bonded oxygen of the oxalate unit, which is a poorer hydrogen bond acceptor than the terminal oxygen atoms. Another possible explanation given by the authors is that the stabilization of the HS state may be due to the lack of strong π–π interactions in this system [66].

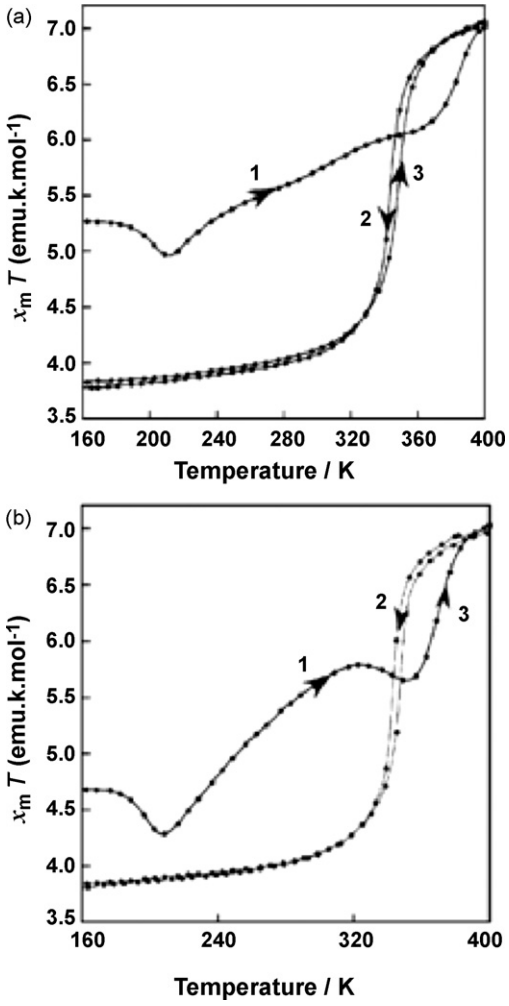

Fig. 29. Temperature dependence of χT for **29**·0.5H_2O·0.5MeOH (a) and **29**′·0.5H_2O (b). Curve 1: first heating. Curves 2 and 3: subsequent temperature cycles (cooling and heating, respectively). Reprinted and modified with permission from Reference [66]. Copyright 2007 American Chemical Society.

VT magnetic studies showed that red complex **29**·0.5H_2O·0.5MeOH has a constant χT value of 5.27 emu K mol^{-1} from low temperature to 180 K (Fig. 29). This value is consistent with the structural data, with both indicating that 50% of the iron(II) centres are in the HS state. Further heating showed a slight decrease of the magnetic moment, to a minimum of 4.9 emu K mol^{-1}, due to dehydration of this material (i.e. to **29**). Then a gradual increase is observed until 370 K where an abrupt and complete transition to the HS state is observed. At 400 K the χT value of 7 emu K mol^{-1} indicates that all iron(II) centres are in the HS state. This dehydrated material, **29**, showed an abrupt and complete ST with a narrow hysteresis loop ($T_{1/2}\downarrow$ = 343 K, $T_{1/2}\uparrow$ = 348 K, Fig. 29).

As expected, the rehydrated sample (**29**′·0.5H_2O, rehydrated as for **28**′·2H_2O) has different magnetic behaviour (Fig. 29). From low temperature to 180 K a constant χT value of 4.7 emu K mol^{-1} is observed. This value corresponds to 28% of HS iron(II) centres, which is inconsistent with the structural data at 180 K as that showed the iron(II) centre was in the LS state. On heating above 180 K the χT value drops to a minimum, of 4.3 emu K mol^{-1}, before an increase is seen with further heating. A maximum is reached at 320 K, followed by a decrease in the 320–350 K temperature range, where dehydration of the sample takes place (forming **29**). Finally, on further heating the behaviour is the same as mentioned above for the dehydrated material **29** ($T_{1/2}\downarrow$ = 343 K and $T_{1/2}\uparrow$ = 348 K) [66].

Rosa and co-workers [67] synthesized the *dinuclear* complex $[Fe^{II}_2(H_2L^{15})_2(\mu\text{-bpy})(SCN)_4]\cdot 2MeOH$ (**30**·2MeOH) by reacting 1 equivalent of $[Fe(MeOH)_4(SCN)_2]$ (made in situ from the reaction of 1 equivalent of $Fe(SO_4)_2\cdot 6H_2O$ with 2 equivalents of KSCN in methanol) with 1 equivalent of H_2L^{15} at room temperature under a N_2 atmosphere. The resulting red solution was added *via* cannula to a solution of 1 equivalent of 4-4′-bipyridine in dichloromethane. After stirring for 1 hour a red solid, **30**·2MeOH, deposited and was filtered. This solid was used for the magnetic measurements (see below).

Red crystals of **30**·2MeOH, suitable for X-ray crystallography, were obtained by layering a freshly prepared solution of $[Fe(H_2L^{15})(MeOH)(SCN)_2]$ in methanol over a 4,4′-bipyridine solution in dichloromethane, under an argon atmosphere. Acquisition of the X-ray dataset at 293 K showed that this dinuclear complex crystallizes in the $P2_1/n$ space group, with half of the molecule in the asymmetric unit. The iron atoms are related by a centre of inversion that lies in the middle of the bridging 4,4′-bipyridine, i.e. are crystallographically identical (Fig. 5D). Each iron atom is coordinated to the central pyridine and to two pyrazole rings of the H_2L^{15} ligand, in *meridional* fashion, and, in the same plane, a nitrogen donor from the 4,4′-bipyridine fragment that bridges to the second iron. Two, *trans* coordinated, thiocyanate ligands complete the iron coordination sphere. Each of the two methanol molecules in the crystal lattice is hydrogen bonded to one of the pyrazole rings in each ligand strand of the complex cation. As usual in this family of complexes of H_2L^{15}, there are face to face $\pi\cdots\pi$ interactions between the pyrazole rings of neighboring molecules and between the central pyridine ring of the ligand and a pyrazole moiety of a neighboring molecule, forming sheets that run along the *bc* plane. There are C–H$\cdots\pi$ interactions between the H at the 5-position of the pyrazole ring and a thiocyanate anion of an adjacent molecule. Hydrogen bonding interactions are also present, between the NH of one pyrazole and a sulphur atom of a thiocyanate ion of a neighboring complex. The bond lengths and angles, 2.108(2)–2.233(2) Å and 88.52(7)–95.73(6)°, respectively, are typical of an iron(II) centre in the HS state [67].

VT magnetic susceptibility studies on the powder sample of complex **30**·2MeOH showed that it is in the [HS–HS] state at room temperature and undergoes an abrupt and incomplete SCO upon cooling (χT is 7.4 $cm^3\,K\,mol^{-1}$ at 250 K and decreases to 4.7 $cm^3\,K\,mol^{-1}$ between 120 and 70 K). The authors were unable to differentiate between a mixed state species, [HS–LS], or a 1:1 [HS–HS]:[HS–LS] mixture of species, either of which is consistent with the observed value of χT at 120–70 K [67].

Irradiation of **30**·2MeOH with the 647 nm band of a Kr^+ laser at 10 K resulted in the observation of a LIESST effect, with T(LIESST) = 72 K and almost quantitative photoconversion to the metatable HS state. This sample presents a 6 K wide LITH (Light Induced Temperature Hysteresis) [67].

In this section nine complexes of the type $[Fe^{II}(H_2L^{15})_2]X_2\cdot n$(solvent) have been presented. These complexes of the $C_{pyrazole}$–$C_{pyridine}$ connected 2,6-bis(pyrazol-3-yl)pyridine ligand (H_2L^{15}, Fig. 3) all feature $NH_{pyrazole}$ donors and hence hydrogen bonding in the lattice. This is a significant point of difference to the complexes of the $N_{pyrazole}$–$C_{pyridine}$ connected 2,6-bis(pyrazol-1-yl)pyridine/pyrazine ligands (L^1–L^{14}, Fig. 3), and in general results in greater cooperativity and hence more frequent observation of, and wider, hysteresis loops for the complexes of H_2L^{15}.

Unfortunately all of these complexes crystallized as solvates (mostly hydrates) and attempts to remove the crystallization solvent resulted in decomposition of the crystal and/or highly hygroscopic products. Therefore the effect of the change in anion on the SCO properties, in particular on $T_{1/2}$, is not clearcut. However, all of the crystal structures showed that the solvent in the crystal lattice plays a very important role in the packing (in particular hydrogen-bonding) and hence on the SCO properties. In almost all of the cases when the $NH_{pyrazole}$ group is hydrogen bonded to water molecules the $T_{1/2}$ is higher (LS state is stabilised) than when it is hydrogen bonded to anions or solvent free. For example, complex **27** is an anhydrous material with $T_{1/2}\uparrow$ = 181 and $T_{1/2}\downarrow$ = 184 K, whereas the rest of the solvated complexes have $T_{1/2}$ > 220 K.

Another key point to be taken from these studies is that when ST in a solvated complex occurs near or above room temperature, solvent loss can occur, resulting in an otherwise totally unexpected decrease in moment with increasing temperature. On the plus side these studies clearly demonstrate the tuning effect that solvent can have on ST. However, they also indicate that, in order to enhance the potential future of such SCO complexes as long lifetime nano switches or memory components operating reversibly at about room temperature, one should aim to produce solvent free SCO complexes; if nothing else achieving this should greatly simplify the study.

3.1.3. 2,6-Bis(1-pyrazolylmethyl)pyridine

A more flexible and 'longer armed' version of the terdentate ligands described in the above sections is the ligand 2,6-bis(pyrazol-1-ylmethyl)pyridine, L^{16}, and the more substituted version L^{17} (Fig. 3). In these ligands the 2- and 6- positions of the central pyridine group are bonded via a saturated and hence flexible –CH_2– linker to the *N*1 atom of the pyrazole moieties. These neutral terdentate ligands coordinate to the iron centre via the central N-pyridine donor and the two *N*2-pyrazole donors in a meridional fashion. Significantly, the resulting chelate rings are six-membered, not five-membered as was the case for L^1 to H_2L^{15} (Fig. 30).

The only SCO-active iron(II) complex reported to date is $[Fe(L^{16})_2](ClO_4)_2\cdot H_2O$ (**31**) [68,69]. It was synthesized by reacting an aqueous solution of $Fe(ClO_4)_2\cdot 6H_2O$ with a methanolic solution of L^{16} (no ratio was given) which resulted in the precipitation of a light green powder (the authors did not specify whether the synthesis was done under a N_2 atmosphere or in air) [68]. Magnetic susceptibility measurements on this powder showed a gradual and complete ST upon cooling ($T_{1/2} \approx 210$ K). The thermal HS to LS conversion was also characterized by ^{57}Fe Mössbauer spectroscopy. At 300 K only a HS state iron(II) doublet (δ_{iso} = 0.98 and ΔE_Q = 1.92 mm s^{-1}) was observed while at 80 K only a LS state doublet is seen (δ_{iso} = 0.53 and ΔE_Q = 0.39 mm s^{-1}).

Single crystals were obtained from an aqueous methanolic solution and an X-ray crystal structure determination was carried out at 135 K [70]. Complex **31** crystallizes in the $P2_1$ space group. The asymmetric unit comprises one complex cation, two perchlorate anions and one water molecule. One of the perchlorate anions is disordered over two positions. The average Fe–N bond length is 2.04 Å. This is borderline with respect to the expected range for iron(II) in the LS state, but it is significantly shorter than the average Fe–N bond length of 2.207 Å observed in the closely related but HS state complex $[Fe(L^{17})](ClO_4)_2\cdot H_2O$ (**32**, SCO inactive) [70]. The bite angles in **31** (*cis*-$N_{pyrazole}$–Fe–$N_{pyridine}$), 89.25° and 89.45°, and the average *trans*-$N_{pyrazole}$–Fe–$N_{pyrazole}$ angle, 178.65°, are far closer to the octahedral ideals (90° and 180°) than those found in the LS complexes of the 2,6-bis(pyrazol-1-yl)pyridine family (79.03–80.70°, see Section 3.1.1). This is as expected: complex **31** features more flexible 6-membered chelate rings whereas the L^1–L^{14} complexes feature less flexible and smaller, 5-membered, chelate rings. A more detailed analysis of the structure of **31** is not possible as the *cif* file is not available in the CSD.

Despite the methyl substituted analogue of L^{16}, L^{17}, also featuring the increased and more flexible bite, coordination of two L^{17} ligands to a central iron(II) results in the complex, $[Fe(L^{17})](ClO_4)_2\cdot H_2O$ **32**, being locked in the HS state, presumably due to steric repulsions.

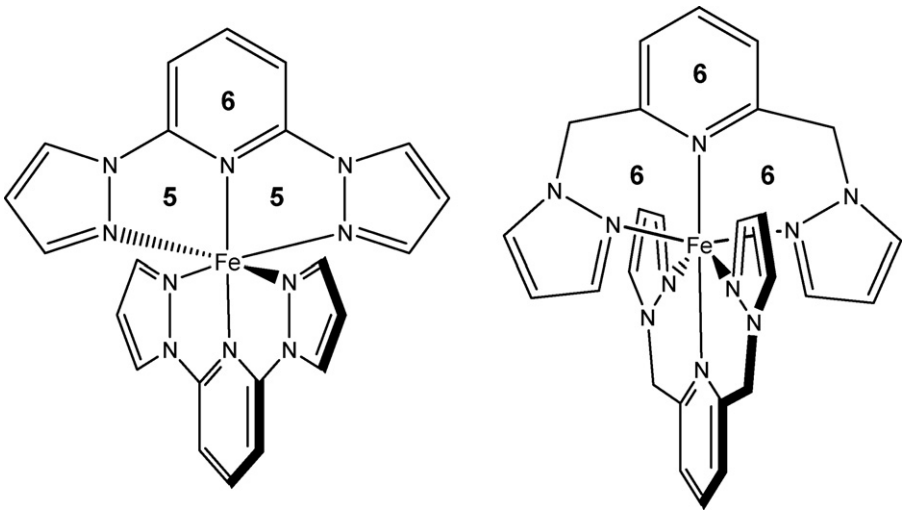

Fig. 30. Schematic representation of the structural differences that result from the different chelate ring sizes generated on complexation of L^1 (left) and L^{16} (right) to iron(II).

3.1.4. Comparisons

To date the skeleton of the ligand L^1 has been modified by substitution of the 3 or 4 or 3 and 5 positions in the pyrazole ring and/or at the 4-position of the pyridine ring and/or by replacement of the pyridine ring by a pyrazine ring.

For this family of ligands, L^1–H_2L^{15}, the exact symmetry of the complex appears to play an important role in the magnetic behaviour. When these ligands have narrow bite angles the complex adopts, in the solid state, a distorted and unusual C_2-symmetry configuration rather than the expected D_{2d} configuration (which is common for SCO-active centres). The Jahn Teller distortion can be characterized by two different angles namely a rotation of one ligand above the Fe centre ($\phi = N^{Py}$–Fe–$N^{Py} < 180^\circ$) and a twist of the plane of one of the ligands relative to the other above the N^{Py}–Fe–N^{Py} vector ($\theta < 90^\circ$) (Fig. 11). These types of distortion can be present separately or at the same time. The reader is referred to the more detailed analysis of the relation between the SCO properties of iron(II) complexes of 2,6-bis(pyrazol-1-yl)pyridine based ligands and these angles presented by Halcrow [9]. But, in summary, the HS state complexes present a large variation in the ϕ and θ angles (ϕ = 61.15-90°; θ = 154.18-180°) and a narrow bite angle (71.85-74.07°). In contrast, in the LS state complexes the bite angles are larger (79.03-80.70°) and a narrower range of values is observed for the ϕ and θ angles (ϕ = 81.32-90°; θ = 174.50-180°). The values of the ϕ and θ parameters for the HS state complexes that undergo thermal ST fall close to the range described for the LS state complexes. Analysis of the difference in these angles during a SCO event showed that there are practically no changes in the θ angle but there is a small increase in the ϕ angle [9].

When the 3 and/or 5 positions of the pyrazole ring are substituted with large substituents and/or electron withdrawing groups the resulting iron(II) complexes are commonly locked in the HS state due to high steric hindrance and electronic effects [9]. In contrast, most of the iron(II) complexes of ligands substituted at the sterically undemanding 4-position of the pyrazole ring and/or 4-position of the pyridine moiety are SCO-active. This class of versatile and readily accessed ligands has allowed families of SCO-active complexes to be prepared, and may well lead to SCO-active complexes with ST properties that have been tuned in a predictable manner by the rational design/selection of appropriate substituents at the 4-positions of the pyrazole and pyridine moieties. To date, predictable control of ST properties is rare [71].

In this system the effect of changing the central pyridine ring by a pyrazine moiety was studied as well. Intriguingly, in the one pair of truly analogous complexes, **1** ($T_{1/2}$ = 261 K) and **13** ($T_{1/2}$ = 223 K), substitution of pyridine by pyrazine led to stabilization of the HS state, not of the LS state which is expected from the decrease in basicity and increase in π-acceptor ability resulting from changing pyridine to pyrazine.

In contrast to the variations in heterocycle substituents that gave rise to the families of $N_{pyrazole}$–$C_{pyridine/pyrazine}$ connected ligands, L^1–L^{14}, in the case of the $C_{pyrazole}$–$C_{pyridine}$ connected 2,6-bis(pyrazol-3-yl)pyridine ligand H_2L^{15} (Fig. 3), no studies involving substitution of the heterocyclic ring(s) have yet been reported. Rather, a family of eight SCO-active complexes of the type $[Fe(H_2L^{15})_2]X_2 \cdot n$(solvent), with varying counter anion X and solvent content, has been reported (see Section 3.1.2). All of these complexes contain $NH_{pyrazole}$ donors and hence feature hydrogen bonding. Every complex has a unique ST curve as the shape and position strongly depends on the interactions between the uncoordinated $NH_{pyrazole}$, the counterion and/or solvent molecules within the crystal lattice, and on the presence or absence of π–π interactions. If the NH is involved in hydrogen bond interactions with water molecules the LS state is stabilised, with $T_{1/2}$ around room temperature, whereas when this hydrogen bond donor interacts with anions, such as BF_4^-, the HS state is stabilised. These hydrogen bond donor properties are the biggest difference between this ligand, H_2L^{15}, and the 2,6-bis(pyrazol-1-yl)pyridine family of ligands (L^1–L^{14}), and the resulting interactions (π–π 'terpyridine embrace' interactions are present in both systems) provide greater cooperativity between the iron centres which is reflected in larger hysteresis loops. Most of the complexes of H_2L^{15} are obtained as hydrates that upon heating lose the solvent molecules, in general producing anhydrous, hygroscopic materials, in the HS state. This dehydrate–rehydrate process changes the magnetic properties of the iron(II) complexes (from LS as the hydrate to HS when anhydrous). It has also been shown that the resolvation process can be carried out with other solvents. These properties could lead to the production of molecular (solvent) detectors. The next development for this particular class of ligands will likely be the synthesis of substituted ligands. The pyridine ring is easier to functionalise than the pyrazole ring so initially these studies are likely to target the pyridine ring.

Finally, the sole SCO-active iron(II) complex of the more flexible and 'longer armed' ligand type L^{16}, complex **31**, presents a ST at around 210 K. The combination of increased flexibility and bite angle in ligand L^{16} appears to better stabilise the LS state of iron(II) in $[Fe(L^{16})_2](ClO_4)_2 \cdot H_2O$ **31** than the less flexible, smaller bite angle

ligand L^1 does in $[Fe(L^1)_2](ClO_4)_2$ **3**, as is evidenced by **31** having a $T_{1/2} \approx 210$ K whereas **3** remains HS from 300 to 5 K. However, as noted above, this comparison is again somewhat flawed, in this case due to the fact that **31** is a monohydrate whereas **3** is solvent-free. It is also interesting to note that when the ClO_4^- counter ion in complex **3** is replaced by BF_4^- the complex becomes SCO active (another example of dependence of magnetic properties on anion choice), with a higher $T_{1/2}$ (261 K) than in complex **31** (210 K). When L^{16} is substituted at the 3- and 5-positions of one of the pyrazole rings ligand L^{17} results (Fig. 3). The resulting iron(II) complex **32** is locked in the HS state, possibly due to steric effects.

3.2. Bidentate ligands and the N-blocked analogues

3.2.1. 2-(Pyrazol-3-yl)pyridine

Three structurally characterized SCO-active iron(II) complexes of the *bidentate* ligand 2-(pyrazol-3-yl)pyridine, HL^{18} (Fig. 3), have been studied.

Goodwin and co-workers [72] synthesized the complex $[Fe(HL^{18})_3](CF_3SO_3)_2{\cdot}2H_2O$ (**33**·$2H_2O$) under nitrogen by reacting one equivalent of $FeCl_2{\cdot}4H_2O$ with three equivalents of HL^{18} in warm water, followed by the addition of ammonium triflate. A microcrystalline red-brown solid was obtained and characterized as the dihydrate, **33**·$2H_2O$. This sample was used for the magnetic analysis. A very hygroscopic anhydrous yellow salt, **33**, was obtained by heating the red-brown dihydrate under nitrogen at 80 °C for 6 h. Single crystals of **33**·$2H_2O$, suitable for X-ray crystallography, were obtained by slow evaporation of a water solution.

Magnetic measurements on the microcrystalline sample of **33**·$2H_2O$, over 99-353 K, showed that it is essentially in the LS state at room temperature, with only a very small amount of the HS state present. Further analysis by ^{57}Fe Mössbauer spectroscopy confirmed the presence of the LS state of the complex ($\Delta E_Q = 0.32$ and $\delta_{iso} = 0.39$ mm s^{-1}) at room temperature. At elevated temperatures the magnetic moment increases, suggesting an increase in the HS state population, but the transition was not complete within the experimental temperature range. As in the case of the solvated complexes of the ligand H_2L^{15}, when complex **33**·$2H_2O$ is heated above 80 °C it loses solvent molecules, complicating the analysis of the magnetic data.

In contrast, magnetic measurements on anhydrous **33**, over 99–313 K, showed that it undergoes a complete and abrupt ST from the HS to the LS state, with a hysteresis loop 12 K wide ($T_{1/2}\uparrow = 241$ and $T_{1/2}\downarrow = 229$ K). The ST was also characterized by ^{57}Fe Mössbauer spectroscopy (298 K, $\Delta E_Q = 2.31$ and $\delta_{iso} = 0.97$ mm s^{-1}; 80 K, $\Delta E_Q = 0.28$ and $\delta_{iso} = 0.44$ mm s^{-1}) [72].

Complex **33**·$2H_2O$ crystallizes in the $P2_1/c$ space group. The asymmetric unit comprises one dication, two triflate anions and two water molecules. The iron centre is coordinated to *three* bidentate HL^{18} ligands. Each ligand is coordinated through the pyridine nitrogen and the imine-like nitrogen of the pyrazole ring. The average Fe–N bond length at room temperatures is 1.97 Å, consistent with the presence of LS iron(II) [72]. As expected, the uncoordinated NH in the pyrazole ring is involved in hydrogen bonding. In two of the ligand strands the hydrogen bond is with a triflate anion, while in the third it is with a water molecule (Fig. 31). This water molecule is hydrogen bonded to the second water molecule, and the latter also hydrogen bonds with both triflate anions. The overall result of these hydrogen bond interactions is the presence of chains of hydrogen bonded complexes within the crystal lattice that run parallel to the *ac* plane. As a result, one might have anticipated a high degree of cooperativity and hence abrupt and hysteretic ST for the dihydrate, **33**·$2H_2O$, however, clearly this was not observed. Rather the desolvated sample exhibited these properties, perhaps due to tightening up of the hydrogen bonding interactions so that they more directly connect up the dications (3 NH donors present) via the triflate anions.

Murray and co-workers [73] synthesized the complex $\{[Fe(HL^{18})_2(NCSe)_2](\mu\text{-}OH_2)(H_2O)_2\}{\cdot}H_2O{\cdot}MeOH$ (**34**), under nitrogen in MeOH at room temperature, by reacting two equivalents of HL^{18} and one equivalent of $[Fe(MeOH)_4(NCSe)_2]$ (synthesized *in situ* by reacting one equivalent of $Fe(ClO_4)_2{\cdot}6H_2O$ and two equivalents of KSeCN). Addition of water followed by slow evaporation under a stream of N_2 allowed the isolation of **34** as a yellow microcrystalline solid. This was used for the magnetic measurements.

Crystals suitable for X-ray crystallography were obtained by slow evaporation of a methanol–water solvent mixture under a N_2 atmosphere as described above. Complex **34** crystallizes in the *Pbcn* space group with half of the molecule in the asymmetric unit (Fig. 32). Each iron centre is coordinated to two bidentate HL^{18} ligands (through the pyridine and the imine-like nitrogen of the pyrazole ring) and two *cis*-$NCSe^-$ anions. The two pyridine rings are *cis* to each other and each is both *trans* and *cis* to the two $NCSe^-$ anions. The two pyrazole rings are *trans* to one another, so the two NH moieties point out on opposite sides of the complex. A water molecule bridges the two crystallographically identical dications through hydrogen bond interactions with one of the two uncoordinated pyrazole NH moieties in each cation, resulting in a *pseudo*-dimer. The second pyrazole NH moiety in each cation in the *pseudo*-dimer is hydrogen bonded to a terminal water molecule. The methanol molecule is hydrogen bonded to the remaining water molecule (Fig. 32). At 298 K both of the iron centres in the pseudo-dimer are in the HS state (average Fe-N 2.098 Å) while at 123 K the average Fe-N distance decreased by 0.0635 Å indicating that approximately 25% of the iron(II) ions had undergone ST to the LS state.

VT magnetic measurements on **34** showed a very gradual and incomplete ST ($T_{1/2} \approx 125$ K) during which half of the iron centres remain in the HS state. In terms of the *pseudo*-dimer this ST occurs from the [HS-HS] to '[HS-LS]' (either localised or 1:1 mixture of [LS-LS]:[HS-HS]) state [73].

The related but *dinuclear* complex $[Fe_2(HL^{18})_2(\mu\text{-}L^{18})_2(NCSe)_2]{\cdot}2H_2O$ (**35**) was synthesized by Murray and co-workers [74] in a similar manner to **34**, but with the addition of a *base*. Specifically, to two equivalents of HL^{18} and one equivalent of freshly synthesized $Fe(NCSe)_2(MeOH)_4$ (*in situ*) [74], in methanol at room temperature, was added 3 drops of aqueous NaOH (1 M). Water (2 mL) was added before concentration of the solution under a N_2 flow resulted in red-orange crystals of **35** in 9% yield.

Magnetic susceptibility measurements of the red-orange crystalline material described above showed that complex **35** undergoes a complete and abrupt ST upon cooling, with $T_{1/2} = 225$ K. The ST was further characterized by ^{57}Fe Mössbauer spectroscopy studies. At 295 K only a doublet characteristic of HS iron(II) was present ($\delta_{iso} = 0.98(1)$ and $\Delta E_Q = 1.83(1)$ mm s^{-1}), while at 77 K the only doublet had parameters $\delta_{iso} = 0.48(1)$ and $\Delta E_Q = 0.52(1)$ mm s^{-1}, confirming conversion to the LS state [74].

Complex **35** crystallizes in the *Pbca* space group. X-ray data sets acquired at 123 and 298 K showed no phase change during the ST. The asymmetric unit consists of half of the dinuclear complex, with the other half generated by a centre of inversion that lies in the middle of the complex (Fig. 33). The unique iron(II) centre is coordinated to one terminal NCSe anion, a terminal bidentate HL^{18} ligand (through the pyridine and aromatic-like N of the pyrazole ring) and to two bridging deprotonated $(L^{18})^-$ ligands, one of which is coordinated in a bidentate mode and the other in a monodentate mode (Fig. 33). The average Fe–N bond lengths at 123 and 298 K are 2.181 and 1.995 Å, respectively, clearly consistent with the HS

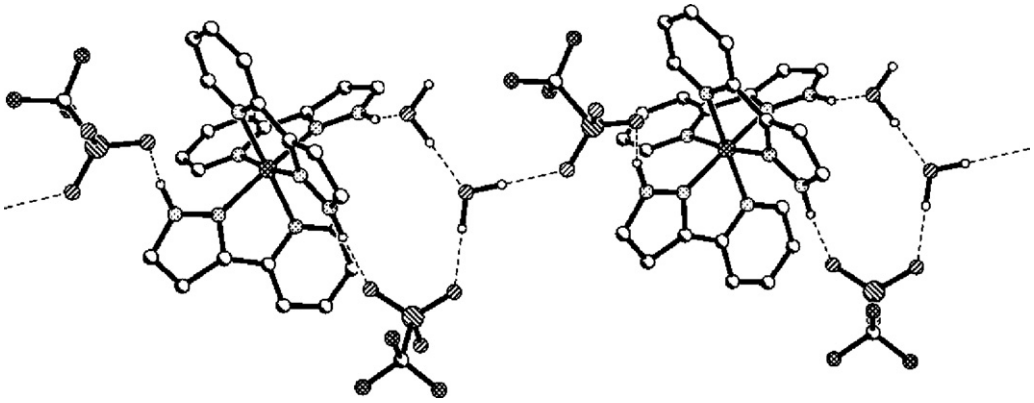

Fig. 31. Ball and stick representation of complex **32**·$2H_2O$, showing the hydrogen bonding network that runs along the *ac* plane. All hydrogen atoms, except for NH and OH, are omitted. This figure was generated from data obtained from the CCDC as published originally in reference [72].

to LS ST observed in the magnetic study [74]. The uncoordinated NH of the pyrazole ring is weakly hydrogen bonded to the terminal water molecule. There is no π–π stacking between the dinuclear molecules. This lack of strong intermolecular interactions between the complexes in the crystal lattice is in agreement with the lack of a hysteresis loop.

3.2.2. 2-(1-Picolylpyrazol-3-yl)pyridine/pyrazine family

Alkylation of the pyrazole moiety in HL^{18} by 2-chloromethylpyridine results in the terdentate, *N*-blocked, ligand L^{19} (Fig. 3). This ligand and the pyrazine analogue, L^{20}, coordinate to the iron centre in a meridional fashion but, thanks to the saturated methylene linker between $N_{pyrazole}$–$C_{pyridine}$, they are less rigid than most of the other terdentate ligands in this survey, such as 2,6-bis(pyrazol-1-yl)pyridine (L^1) or 2,6-bis(pyrazol-3-yl)pyridine (H_2L^{15}). A unique feature of these two ligands, L^{19} and L^{20}, as compared to all of the other ligands covered in this survey (Fig. 3) is the combination of five- and six-membered chelate rings they offer to a metal ion (Fig. 34). Three structurally characterized SCO-active iron(II) complexes of L^{18} and L^{19} have been reported to date.

Mukherjee and co-workers [75] synthesized the complex $[Fe(L^{19})_2](ClO_4)_2$ (**36**) by reacting two equivalents of L^{19} and one equivalent of $Fe(ClO_4)_2·6H_2O$, which was added as a solid in small portions to a methanol solution of the ligand at room temperature (the authors did not specify whether the synthesis was done under a N_2 atmosphere or in air). The resulting bright yellow solid was filtered off and dried before it was recrystallized by vapour diffusion of diethyl ether into an acetonitrile solution of the complex. The resulting sample of anhydrous **36** undergoes a very gradual and incomplete ST [75]. Attempts to obtain single crystals of this material were unsuccessful.

In a later publication, Mukherjee and co-workers [76] obtained crystals of the solvate $[Fe(L^{19})_2](ClO_4)_2·C_7H_8$ (**36**·C_7H_8) (see below). A microcrystalline sample of the toluene solvate **36**·C_7H_8 was obtained by adding toluene to an acetonitrile solution of complex **36** and placing it in the fridge overnight. The magnetic properties of this solvated sample are different from those observed for anhydrous **36** [76]. Complex **36**·C_7H_8 undergoes an abrupt and complete ST with parameters $T_{1/2}\uparrow \approx 233$, $T_{1/2}\downarrow \approx 231$ K and $\Delta T_{1/2} = 2$ K. ^{57}Fe Mössbauer spectroscopy confirmed that at 295 K the iron(II) is HS ($\delta_{iso} = 0.95(1)$ and $\Delta E_Q = 1.46(1)$ mm s^{-1}) whereas at 77 K it is LS ($\delta_{iso} = 0.46(1)$ and $\Delta E_Q = 1.28(1)$ mm s^{-1}) [76].

Crystals suitable for X-ray crystallography were obtained by recrystallization of complex **36** from an acetonitrile–toluene mixture. The structure determination on **36**·C_7H_8 showed that it

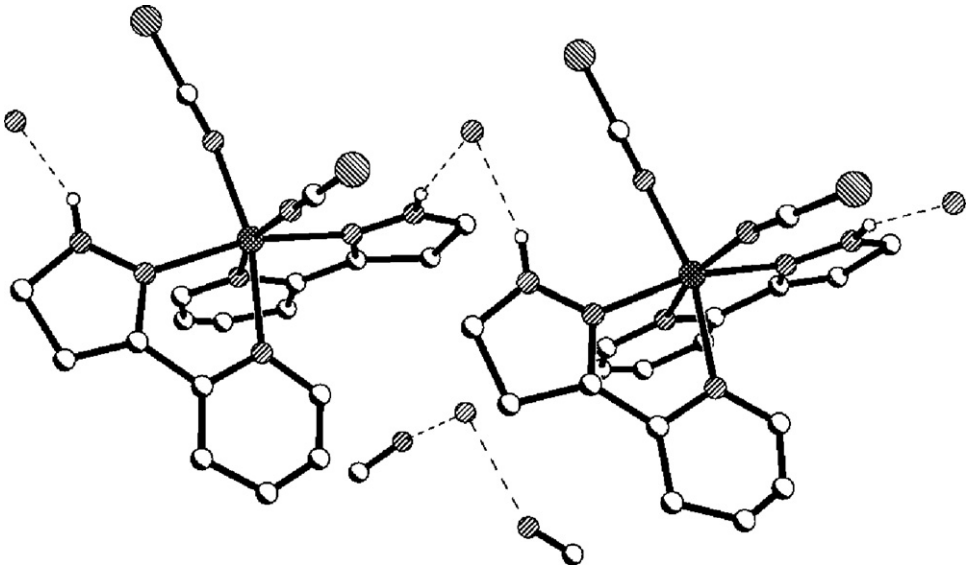

Fig. 32. Ball and stick representation of the *pseudo*-dimer formed by **34** at room temperature. The NH hydrogen atoms are shown; the OH hydrogen atoms are not as they are not present in the cif file; the CH hydrogen atoms are omitted for clarity. This figure was generated from data obtained from the CCDC as published originally in reference [73].

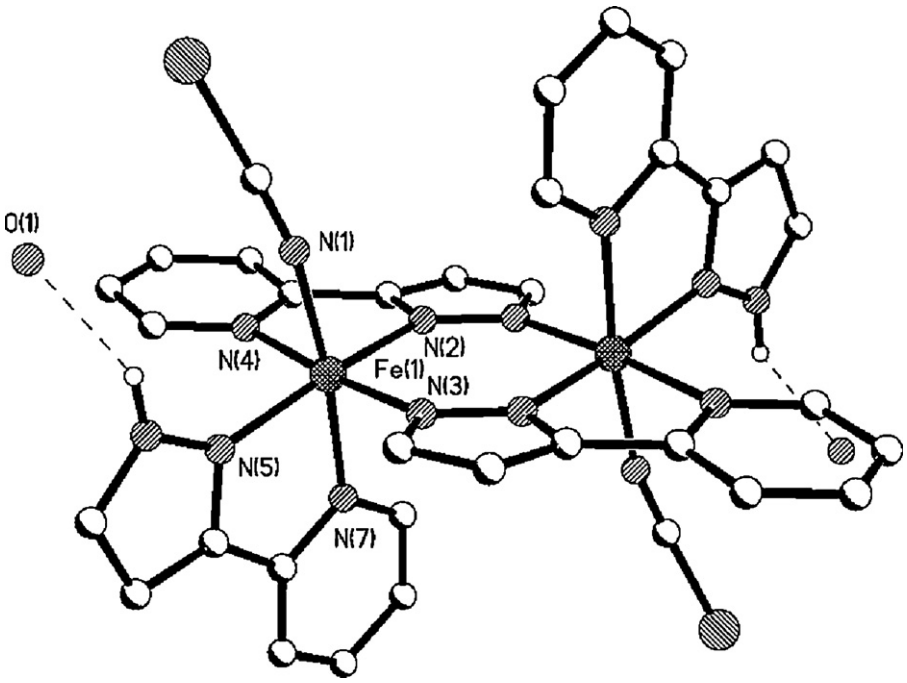

Fig. 33. Ball and stick representation of the structure of complex **35** at room temperature. The NH hydrogen atoms are shown; the OH hydrogen atoms are not as they are not present in the cif file; the CH hydrogen atoms are omitted for clarity. This figure was generated from data obtained from the CCDC as published originally in reference [74].

crystallizes in the $P2_1/n$ space group. The crystallographic data sets were acquired at 270, 240 and 120 K; no phase transition was observed during the thermal ST. The asymmetric unit comprises a cation (in which two L^{19} ligands are each coordinated in a meridional fashion), two ClO_4^- anions and one toluene molecule of solvation.

At 270 K the toluene molecule is disordered over two positions, while at 240 K only two C-atoms of the toluene molecule and all O-atoms of the perchlorate anions are disordered. Nonetheless the average Fe–N bond lengths at both 270 and 240 K are similar (2.148 and 2.142 Å respectively) and consistent with the HS state. At 270 K the *trans* angles range from 155.8(2)° to 171.2(2)° while the *cis* angles span from 74.6(2)° to 103.3(2)°.

In contrast, the structure acquired at 120 K clearly showed the iron centre to be in the LS state (average Fe–N 1.965 Å) and, as expected, the *trans* (167.8(1)–172.3(1)°) and *cis* (79.3(1)–96.2(1)°) angles are closer to 180° and 90°, respectively, than they were in the HS state structure. Careful analysis of the *cif* file obtained from the CSD, for the crystallographic data set acquired at 120 K, shows that there are π-interactions between the C–H 'edge' of the toluene molecule in the crystal lattice and the face of the pyridine ring of one complex cation (pyridine centroid to C-toluene 3.532 Å) and the C–H 'edge' of a pyridine ring of a neighboring complex cation and the face of the same toluene molecule (toluene centroid to C-pyridine 3.532 Å) as shown in Fig. 35A. The perchlorate anions are hydrogen bonded to the methylene linker of one of the ligand strands in the complex cation (Fig. 35B, CH···O 3.330(6) and 3.111(6) Å). One of the above mentioned perchlorate ions presents an anion–π interaction with the pyrazole ring in the neighboring complex cation (pyrazole centroid to O 3.152 Å). These interactions account for the abrupt and hysteretic ST in complex **36**·C_7H_8.

Murray and co-workers [77] synthesized the *pyrazine*-based complexes $[Fe(L^{20})_2](BF_4)_2$·MeOH (**37**·MeOH) and $[Fe(L^{20})_2](ClO_4)_2$·EtOH (**38**·EtOH), by reacting two equivalents of L^{20} with two equivalents of $Fe(BF_4)_2·6H_2O$ or $Fe(ClO_4)_2·6H_2O$,

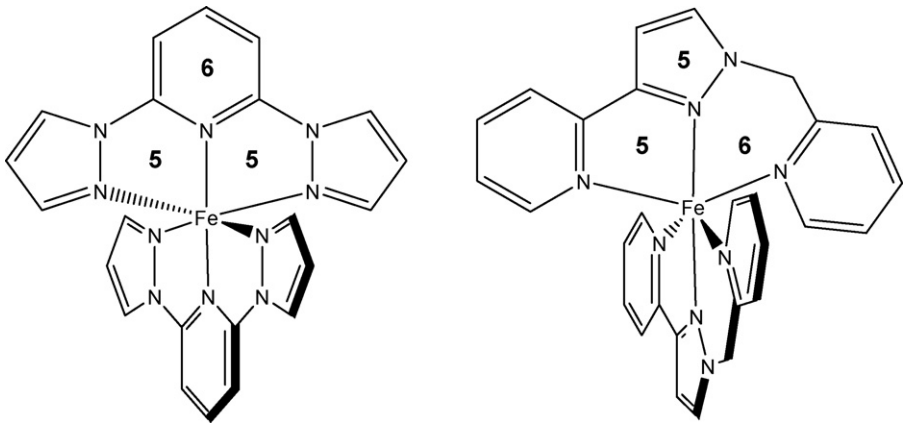

Fig. 34. Structural differences in the chelate ring size for the resulting iron(II) complexes of L^1 (left) and L^{19} (right).

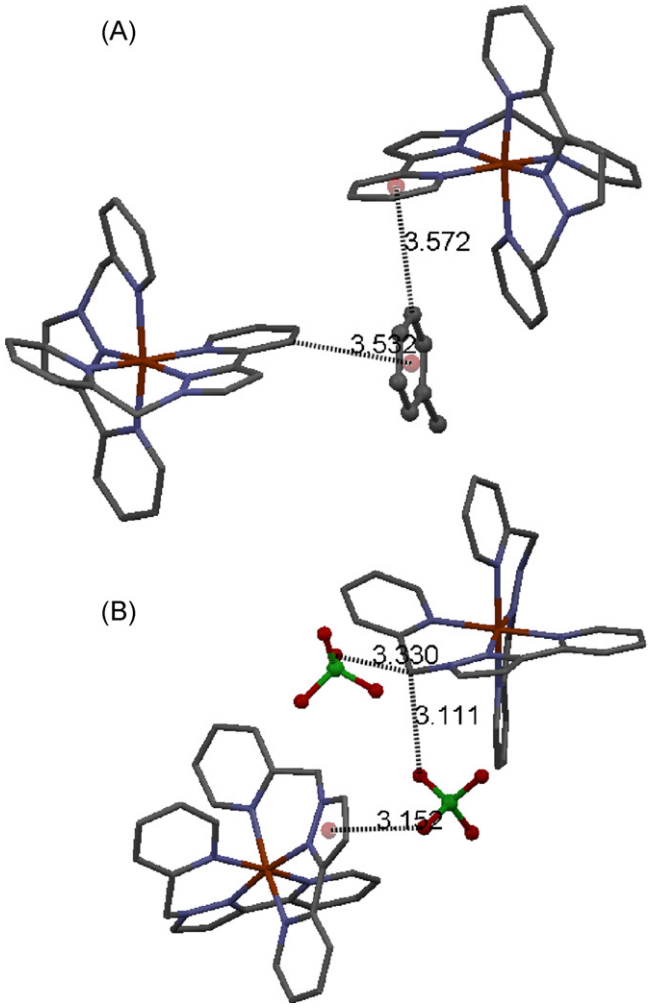

Fig. 35. Intermolecular interactions present in the crystal lattice of complex **36**·C_7H_8. The complex cations are shown in stick representation while the toluene molecule and the perchlorate anions are shown in ball and stick representation. (A) C–H face-to-face face-to-edge π interactions between the toluene solvate molecule and pyridine rings. (B) Interactions between the perchlorate anions and the methylene linker and pyrazole ring. This figure was generated from data obtained from the CCDC as published originally in reference [76].

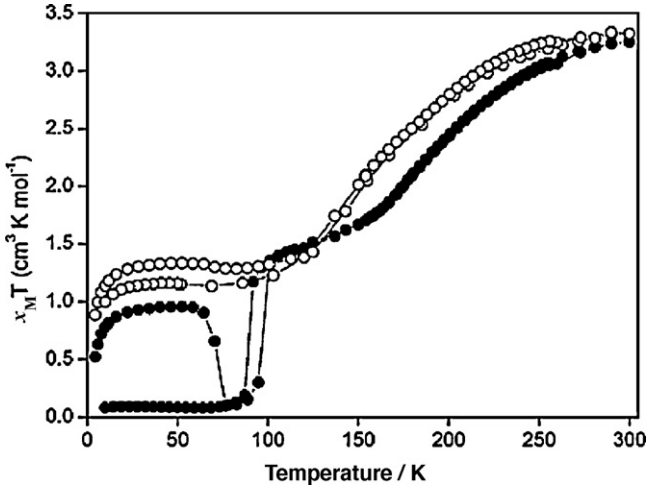

Fig. 36. Plot of $\chi_M T$ vs T for **37**·MeOH (filled circles), when cooled slowly from 300 K and then warmed slowly, and for the solvent free **37** (open circles) under slow cooling and slow warming. Thermal trapping of approximately 30% HS fraction can be seen for **37**·MeOH between 2 and 60 K when the sample is quench-cooled to 2 K, then warmed. Reprinted with permission from Reference [77]. Copyright 2007 American Chemical Society.

in methanol or ethanol respectively, at room temperature (the authors did not specify whether the synthesis was done under a N_2 atmosphere or in air). The resulting solution was subjected to diethylether vapour diffusion, affording red block crystals for complex **37**·MeOH and yellow-orange crystals for complex **38**·EtOH.

Magnetic susceptibility measurements on **37**·MeOH showed a two step ST upon cooling (Fig. 36). The first step is a gradual half SCO transition ($T_{1/2} \approx 197$ K) between 300 and 130 K. Then a plateau region is present between 125 and 105 K, in which the HS:LS states co-exist in a 1:1 ratio. With further cooling a second and abrupt ST to the fully LS form occurred with $T_{1/2} = 85$ K. Upon warming a small hysteresis loop was observed only for the lower temperature ST ($T_{1/2}\uparrow = 91$ and $T_{1/2}\downarrow = 98$ K). When this complex is quench-cooled to 4 K the magnetic measurements showed that 30% of the HS state is trapped between 10 and 65 K (Fig. 36).

The magnetic properties of the desolvated complex **37** are quite different from its methanol solvated analogue (there is no experimental detail in the original paper for the preparation of the anhydrous material). Upon cooling an incomplete and gradual ST is observed with $T_{1/2} \approx 150$ K, followed by a plateau region between 120 and 10 K, with a $\chi_M T$ value of 1.167 cm^3 mol^{-1} K consistent with a 1:1 mixture of HS:LS states In the warming mode a lower path was followed up to 100 K; after this temperature it followed the same path as it had in the cooling mode.

X-ray crystal studies on **37**·MeOH at 25 (slow cooled), 25 (quench-cooled), 123 and 293 K were carried out, showing that there is no crystallographic phase change during the ST. It crystallizes in the monoclinic *Pn* space group. At all temperatures the asymmetric unit comprises one complex molecule, in which the iron centre is coordinated to two terdentate meridional L^{20} ligands, two tetrafluoroborate anions and one methanol molecule. The average Fe–N bond lengths are in good agreement with the magnetic studies. At 25 K (slow cooled) the average Fe–N bond length is 1.983 Å distinctive of iron(II) in the LS state. For the quench-cooled state at 25 K, and at 123 K (in the plateau region), the values are 2.068 and 2.065 Å, showing a mixture of HS and LS sites. At 293 K the average Fe–N bond length is 2.165 Å, typical of HS iron(II).

Due to the presence of a combination of one five-membered and one non-planar and more flexible six-membered chelate ring the *cis* and *trans* N–Fe–N bond angles in complex **37**·MeOH are expected to be different from 90° and 180°, respectively. At 293 K the *cis* angles range from 74.45(14)° to 109.12(15)°, while the *trans* angles range from 159.18(14)° to 159.25(13)°. During the ST (upon cooling) these distorted angles become closer to the ideal octahedral values due to the steric requirements of the LS state: at 25 K slow cooled, the *cis* angles range from 78.83(13)° to 100.63(12)° and the *trans* angles from 165.58(11)° to 169.16(12)°. Furthermore, the interactions and order/disorder of the anions and solvent molecules change upon ST. At 25 K (slow cooled) all of the methanol and tetrafluoroborate anions were ordered and only one hydrogen bonding interaction was observed. In contrast, in the quench-cooled (25 K) and 123 K structures both tetrafluoroborate anions are involved in hydrogen bonding interactions. At 123 K an extra interaction exists between the disordered methanol solvent molecule and one of the BF_4^- anions that is disordered as well, therefore there are 3 possible interactions between the disordered methanol molecule and the disordered tetrafluoroborate anions. Based on these results the authors proposed that the change in the order/disorder of the anions and solvent molecules, are responsible for the hysteresis loop observed at low temperatures [77].

The uncoordinated nitrogen atom of the pyrazine ring in one ligand strand of the complex cation interacts with the π system of the pyrazine ring of a ligand strand in a neighboring molecule, which in turn interacts with the CH_2 linker (between the pyridine and pyrazole moieties) in another neighboring complex, forming 2D sheets along parallel to the *ab* plane (Fig. 37). The distance between the nitrogen atom and the pyrazine ring centroid varied during the ST.

Complex **37**·MeOH undergoes a quantitative photoconversion, by irradiation with a Kr^+ laser (λ = 532 nm) at 10 K, to the metastable HS state with ^1T(LIESST) = 49 K and ^2T(LIESST) = 70 K. As expected, ^2T(LIESST) has a sharp minimum indicative of high cooperativity and in good agreement with the magnetic properties, while ^1T(LIESST) is broad.

In contrast, complex **38**·EtOH undergoes a very gradual ST upon cooling with $T_{1/2}$ = 250 K. X-ray crystal structure analysis at 123 K showed that this complex crystallizes in the monoclinic $P2_1/n$ space group. The asymmetric unit consists of one cation (with the same coordination sphere as complex **37**·MeOH), one perchlorate anion and one ethanol solvent molecule. One of the perchlorate anions is hydrogen bonded to the ethanol molecule. The average Fe–N bond length is 1.983 Å, typical of LS iron(II). Interestingly, the spare nitrogen atom out the back of the pyrazine ring interacts in the same way as in complex **37**·MeOH, forming a 2D network, but the magnetic properties are completely different, as mentioned above. This is another clear example of how the SCO properties can be drastically changed by the nature of the counterion employed.

In principle, **38**·EtOH ($T_{1/2}$ = 250 K) is the pyrazine-based analogue of pyridine-based **36**·C_7H_8 ($T_{1/2}\uparrow \approx 233$, $T_{1/2}\downarrow \approx 231$ K and $\Delta T_{1/2}$ = 2 K), however, the latter was obtained only as the toluene solvate or solvent free (gradual incomplete ST). At first glance it appears that, as expected, replacing pyridine by pyrazine has increased the $T_{1/2}$. That is, stabilised the LS state over the HS state (see Section 3.1.1), however, it is very important to note that in this case the effect of changing pyridine for pyrazine is not easily identified, as none of the forms of these two complexes that have been reported to date are similarly solvated, and it is clear that solvation plays a critical role in ST behaviour.

3.2.3. Comparison

The ligand HL[18] can coordinate to the iron centre through the N-donor of the pyridine moiety and *N1* of the pyrazole ring. In the absence of base this ligand behaves as a neutral *bidentat*e ligand, but upon deprotonation of the NH, the pyrazolate unit of the ligand $(L^{18})^-$ is capable of bridging two metal centres. As stated in Sections 3.2.1 and 3.2.2, there are both mononuclear and dinuclear SCO active iron(II) complexes of HL[18]. It is clear that substitution of the 4-position of the pyrazole and pyridine units will allow the synthesis of new mononuclear SCO-active complexes, as in the case

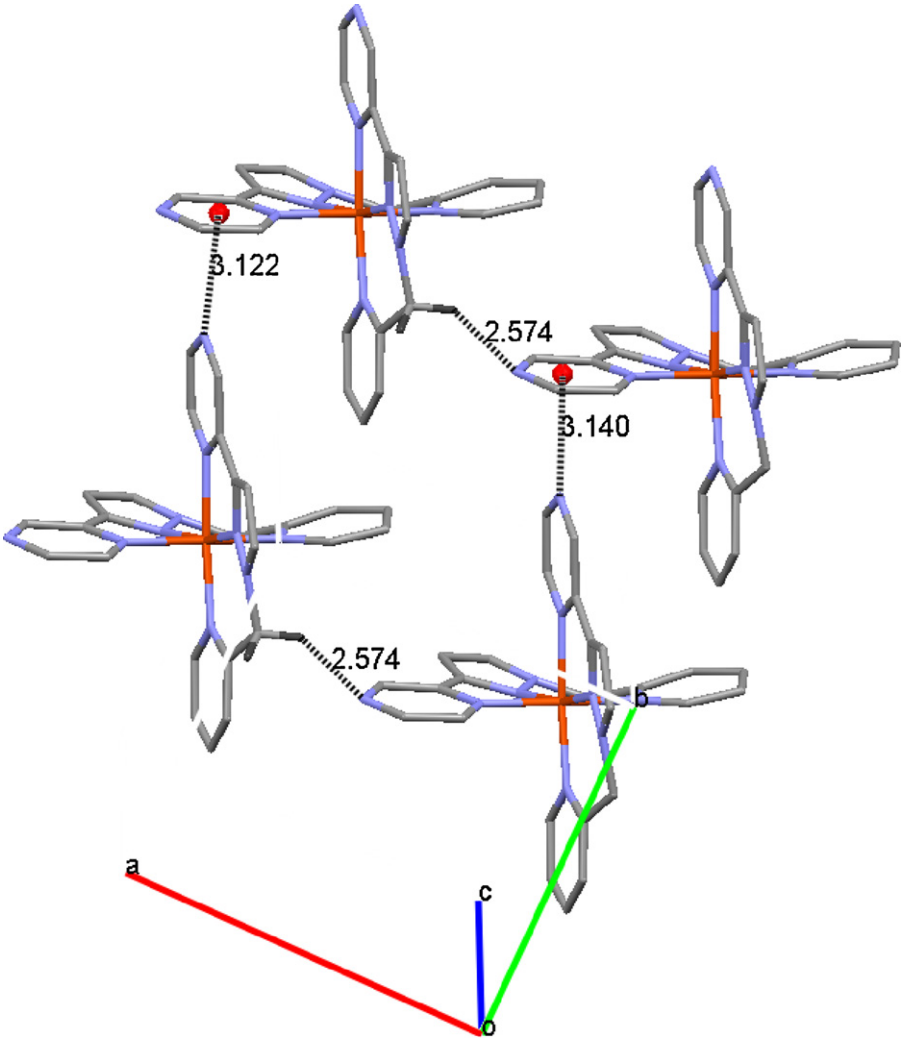

Fig. 37. Crystal packing of complex **37**·MeOH showing the π interactions between the pyrazine rings and the HC–H···π interactions between the pyrazine and the methylene linker. The solvent molecules and hydrogen atoms, except for those protons in the methylene linker that interact with the pyrazine ring, were omitted for clarity. This figure was generated from data obtained from the CCDC as published originally in reference [77].

of ligands derived from L^1 (Section 3.1.1). But depending on the ligand to metal ratio and the presence or absence of a base the synthesis of dinuclear (or polynuclear) systems can be achieved. These are of interest as they would allow the effect that the interactions between the metal centres, via the pyrazolate bridge, has on the SCO properties to be probed.

The mononuclear complexes of the neutral HL^{18} ligand have very interesting, solvent dependent SCO, due to the NH in the pyrazole ring being capable of hydrogen bonding to solvent or anion molecules. Structurally characterized SCO active complexes of this system are less abundant than in the case of the complexes of the analogous *terdentate* ligand H_2L^{15} (see Section 3.1.2), and therefore generalizations regarding the impact of these hydrogen bond properties are not so clearcut.

Dinuclear complexes of $(L^{18})^-$ are interesting with regard to probing the effect of the potentially high cooperativity between the pyrazolate bridged iron(II) centres. To date there is only one example of a structurally characterized dinuclear complex (**35**), which suggests that it may be difficult to prepare and isolate such dinuclear complexes, probably due to the formation of different products such as monometallic and polymetallic (discrete and polymeric) systems.

Another feature of the NH (*N*1) of the pyrazolate ring is that can be readily alkylated. Alkylation with a picolyl group results in the more flexible ligand L^{19} which can be seen as a hybrid of L^1 and L^{16}. The resulting iron(II) complex contains two different chelate rings, 5 and 6 membered rings (Fig. 34). This results in a ligand that confers a lower ligand field towards iron(II), and therefore stabilizes the HS state, than the related ligand of the family 2,6-bis(pyrazol-1-yl)pyridine, L^1, as seen by the value of transition temperature of complex **36**·C_7H_8 of $T_{1/2}\uparrow \approx 233$, $T_{1/2}\downarrow \approx 231$ K compared to the transition temperature complex **1**, $T = 261$ K. However, the nature of the solvent content in these two systems is different so this comparison is not completely valid. This ligand, as seen above, acts as a *terdentate* ligand. Substitution of the pyrazole and/or pyridine rings could afford further interesting SCO-active complexes, thanks to the combination of 5- and 6-membered chelate rings in the resulting iron(II) complexes.

Another approach to preparing SCO active complexes with high cooperativity is the introduction of a pyrazine ring within the ligand scaffold, as was done in the case of L^{20}. In principle, this pyrazine ring should facilitate the synthesis of multidimensional networks and/or stronger interactions with crystallization solvent molecules or anions. When ligand L^{19} is modified by replacing the pyridine ring directly attached to the pyrazole ring by a pyrazine ring, L^{20}, the SCO properties are modified and in this case an increase in the width of the hysteresis loop was achieved.

3.3. Bis-bidentate ligands

3.3.1. 3,5-Bis(pyrid-2-yl)pyrazole

In all the complexes analysed in this section, the *deprotonated bis-bidentate* $(L^{21})^-$ ligand coordinates to the iron(II) centre in a 2:2 ratio forming *dinuclear* "sandwich" complexes, where each iron centre is coordinated to two ligands through the pyridine ring and to one nitrogen of the pyrazolate anion that is bridging a second iron centre coordinated in the same manner. The two ligands strands occupy the equatorial positions and the apical positions are occupied by one substituted pyridine and one NCE^- anion (E = S, Se, BH_3).

The first SCO-active iron(II) complexes of 3,5-bis(pyrid-2-yl)pyrazolate, $(L^{21})^-$, described in the literature are the complexes *trans*-$[Fe_2(\mu\text{-}L^{21})_2(NCS)_2(Py)_2]$ (**39**) and *trans*-$[Fe_2(\mu\text{-}L^{21})_2(NCS)_2(3\text{-Br-Py})_2]$ (**40**) reported by Kaizaki and co-workers [78]. Only complex **39** was structurally characterized so it is the only complex analysed in this section. Complex **39** was synthesized by reacting one equivalent of $[(n\text{-}Bu)_4N^+][L^{21}]$ and one equivalent of $[Fe(SCN)_2(Py)_4]$ [79] in pyridine under nitrogen at room temperature affording a yellow powder characterized as anhydrous **39**. Attempts to crystallise this material were not successful [80]. A powder sample of complex **39** underwent a temperature induced single step [HS–HS] to [LS–LS] transition with $T_{1/2} = 129$ K [71]. Interestingly, in a later publication Murray and co-workers [81] reported that *trans*-$[Fe_2(\mu\text{-}L^{21})_2(NCS)_2(Py)]\cdot H_2O$ (**39**·H_2O), isolated according to the method of Kaizaki and co-workers [80] as a powder, undergoes ST at the same $T_{1/2}$ of 129 K, suggesting that the complex reported for the first time by Kaizaki was actually the monohydrate and not the solvent-free complex.

However, the crystalline anhydrous complex *trans*-$[Fe_2(\mu\text{-}L^{21})_2(NCS)_2(Py)]$ (**39**) obtained by the H-tube method (slow diffusion of reagents together) is in the [HS–HS] state over the entire temperature range studied by magnetic susceptibility and X-ray crystallography studies. Crystals suitable for X-ray crystallography were grown by H-tube methods and X-ray crystallographic datasets were acquired at 200, 123 and 90 K. These showed no difference in the bond lengths and angles around the iron(II) centre in this anhydrous *pseudo*-polymorph, confirming the lack of SCO activity, which is a very surprising finding because commonly crystalline materials undergo more abrupt ST, and present hysteresis, but in this case the bulk powder hydrate sample is the SCO active form.

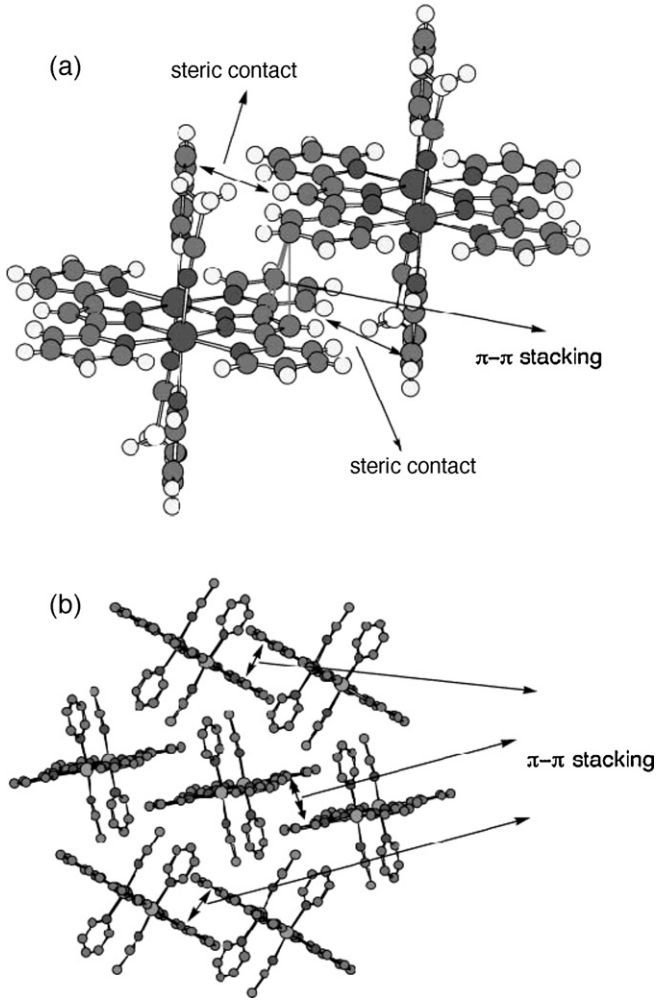

Fig. 38. Crystal lattice of complex **41** showing the π–π stacking and steric contact between neighboring complexes at 296 K. From reference [80]. Reproduced by permission of The Royal Society of Chemistry.

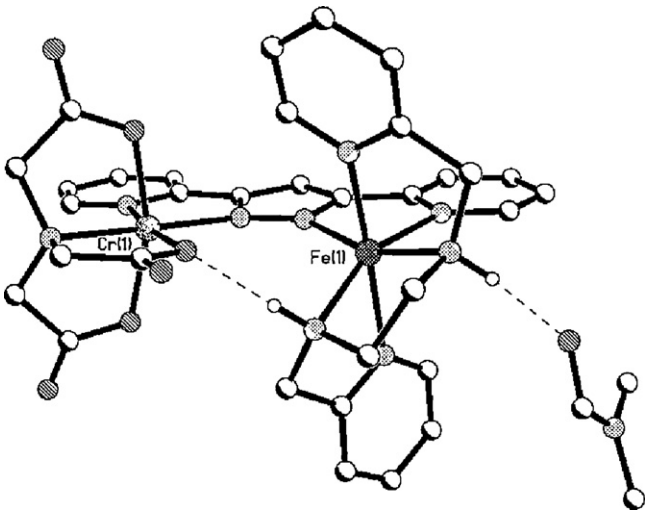

Fig. 39. Ball and stick representation of complex **43**·H_2O·3DMF showing the inter and intra-molecular hydrogen bonding interactions. The BF_4^- anion, two DMF, one water solvent molecules and the protons (except for the hydrogen bonded-H) are omitted for the sake of clarity. This figure was generated from data obtained from the CCDC as published originally in reference [83].

The complex *trans*-[$Fe_2(\mu\text{-}L^{21})_2(NCBH_3)_2(Py)_2$] (**41**) was synthesized, by Kaizaki and co-workers [80], in a similar way as complex **39** but using [$Fe(BH_3CN)_2(Py)_4$] as a starting material (synthesized as for the SCN^- analogue [79] but using $NaNCBH_3$ and $FeCl_2{\cdot}4H_2O$ as starting materials), and it was isolated as a yellow powder. This powder sample undergoes a complete and abrupt ST centred at 205 K according to magnetic susceptibility measurements. ^{57}Fe Mössbauer spectroscopy showed that at 77 K the iron(II) is LS (δ_{iso} = 0.485 and ΔE_Q = 0.565 mm s^{-1}) while at 275 K it is HS (δ_{iso} = 0.979 and ΔE_Q = 1.701 mm s^{-1}), confirming the ST.

Crystals of complex **41** suitable for X-ray were obtained from layering a methanolic solution of [$Fe(BH_3CN)_2(Py)_4$] and pyridine over a methanolic solution containing HL^{21} and $(n\text{-}Bu)_4NOH$. There is no crystal phase change during the ST. Complex **41** crystallizes in the $P2_1/n$ space group. The asymmetric unit contains half of the molecule; the complete molecule is generated by a centre of inversion. The only crystallographically independent iron(II) centre is coordinated to two $(L^{21})^-$ ligands (through one pyridine and one of the nitrogen atoms of the pyrazolate unit) which form a square plane of donors. The apical coordination sites are occupied by one pyridine molecule and one $NCBH_3$ anion (which are therefore *trans* to one another). The data set collected at 100 K shows an average Fe–N bond length of 2.00 Å, which is at the upper limit for the [LS–LS] state. At 296 K the average Fe–N distance of 2.172 Å clearly indicates that the complex is in the [HS–HS] state at higher

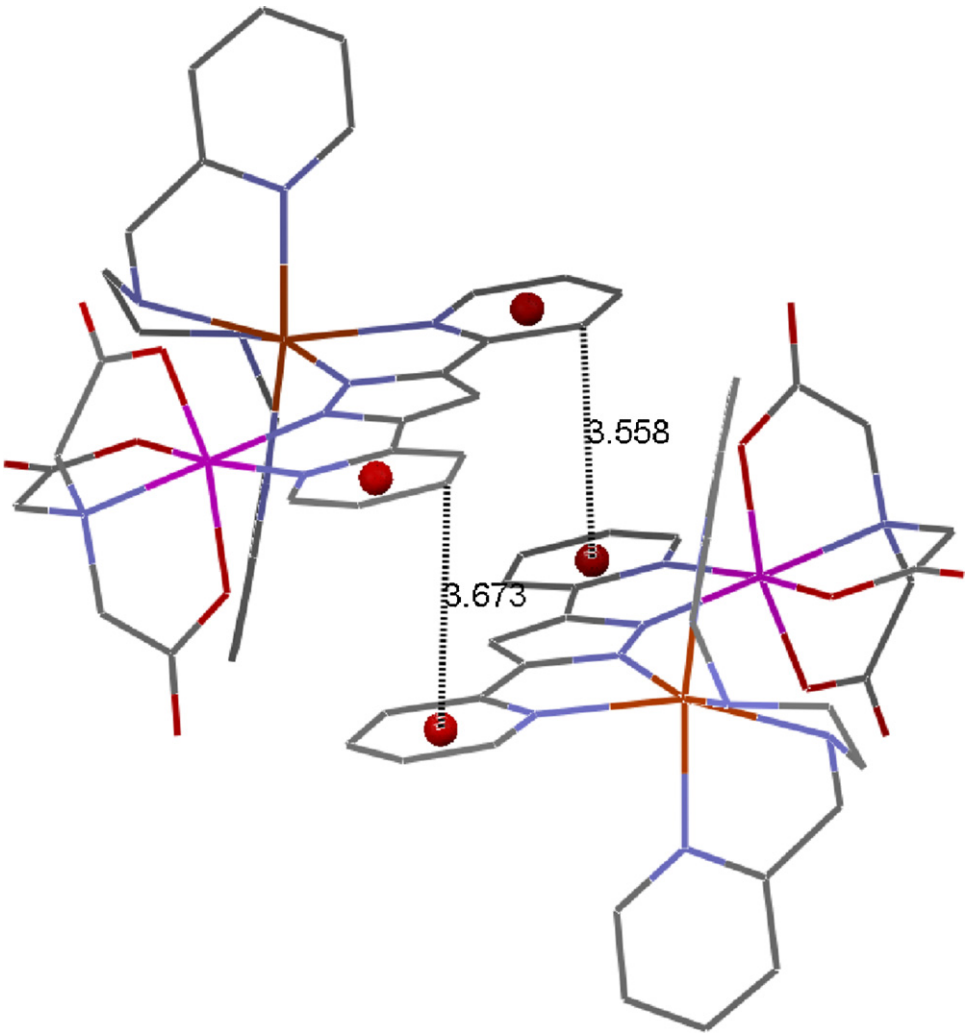

Fig. 40. Ball and stick representation of complex **43**·H_2O·3DMF showing the π–π stacking between L^{21} strands of two neighboring molecules. Anions, solvent molecules and hydrogen atoms are omitted for the sake of clarity. This figure was generated from data obtained from the CCDC as published originally in reference [83].

temperature. The Fe···Fe distance decreases with temperature (4.24 and 4.07 Å at 296 and 100 K, respectively). There are π–π interactions between the ligand strands of neighboring molecules. These are face-to-face and face-to-edge π stacking interactions between the pyrazolate ring and the pyridyl ring of a neighboring molecule (Fig. 38) [80]. These interactions account for the complete and abrupt ST observed for this complex.

Kaizaki and co-workers also synthesized an analogous complex of **41**, complex *trans*-$[Fe_2(\mu\text{-}L^{21})_2(NCBH_3)_2(4phPy)_2]$ (**42**) where 4phPy = 4-phenylpyridine. This complex was synthesized in the same manner as **41** but using an excess of 4-phenylpyridine, isolating a powder sample (no colour was reported) [82]. Interestingly the magnetic properties are quite different from complex **41**. Complex **42** undergoes a relatively abrupt and two step ST upon cooling (it is not clear what type of sample was used for the magnetic measurements). The authors were able to crystallise complex **42**, but the method of crystallization is not explicit in the original paper. X-ray crystal structure determinations at 100, 200 and 296 K helped to determine that the ST occurs from a [HS–HS] state to a [LS–LS] state through a [HS–HS]:[LS–LS] 1:1 mixed state at 200 K. The complex crystallizes in the P-1 space group and there is no phase change during the ST. At 100 and 296 K there is only one crystallographic type of iron(II) centre, with average Fe–N bond lengths of 1.979 and 2.167 Å respectively, which are consistent with the [LS–LS] and [HS–HS] states respectively.

At 200 K the cell volume has doubled and there are two different iron(II) centres present. The average Fe-N bond lengths of 2.000 and 2.116 Å for the two different iron(II) centres showed that at this temperature the [LS–LS] and [HS–HS] states co-exist in a 1:1 mixture [80].

Kaizaki and co-workers [71] studied the effect on the SCO of the choice of substituent present on the pyridine rings that occupy the apical positions in two sets of *trans*-$[Fe_2(\mu\text{-}L^{21})_2(NCE)_2(X\text{-}Py)_2]$ complexes. The first set corresponds to NCE = $NCBH_3$ and the second set corresponds to NCE = NCS. In both cases X-Py = 4-methylpyridine (4-MePy), 4-(*N*,*N*,-dimethylamino)pyridine (4-Me_2Npy), pyridine (py), 3-methylpyridine (3-Mepy), 3-chloropyridine (3-Clpy) or 3-bromopyridine (3-Brpy). The complexes containing $NCBH_3^-$ have a higher $T_{1/2}$ than the NCS^- analogues, due to the stronger ligand field imposed by $NCBH_3^-$. Interestingly, for both sets of complexes they found a linear correlation between the Hammett constant (σ^n: electron donating substituents have a negative value, electron withdrawing ones have a positive value, *H* is zero) and the $T_{1/2}$. Specifically, as the substituted pyridine was altered the $T_{1/2}$ increased as follows: 4-MePy < 4-Me_2Npy < py < 3-Mepy, 3-ClPy ≤ 3Brpy. This is consistent with the more electron withdrawing substituents increasing the π-backbonding and decreasing the σ-bonding of the pyridine ligands, stabilising the LS-state and therefore increasing the transition temperature. This study is an important one as it is one of very few to examine *systematic* variations in a ligand substituent in a *closely related family* of complexes, and it is certainly a rare case of identifying such a correlation. Such studies open up the possibility of *predicting the* $T_{1/2}$ of the SCO complex by consideration of the nature of the proposed substituent on the pyridine ligand *before actually preparing it*. This is highly desirable in SCO chemistry, if we are to move from good luck to good management of the properties obtained.

In order to study the interaction between the pyrazolate-bridged metal centres, Kaizaki and co-workers [83] also synthesized the *dinuclear heterometallic* complex $[(nta)Cr(\mu\text{-}L^{21})Fe(picen)](BF_4)$ (**43**) where nta = nitrilotriacetic acid and picen = *N*,*N*′-bis(2-pyridylmethyl)ethylendiamine. Complex **43** was synthesized, under a N_2 atmosphere, by reacting one equivalent of $[Cr(nta)(HL^{21})]\cdot 3H_2O$ with one equivalent of cryptand [2,2,2] (4,7,13,16,21,24-hexaoxa-1,10-diazabicyclo[8,8,8]hexacosane) in methanol, then adding one equivalent of $Fe(BF_4)\cdot 6H_2O$, then one equivalent of picen, and stirring overnight. The resulting yellow-brown solid was used in the magnetic measurements. Recrystallization from DMF by diethyl ether vapour diffusion under N_2, afforded brown plates of $[(nta)Cr(\mu\text{-}L^{21})Fe(picen)](BF_4)\cdot H_2O\cdot 3DMF$ (**43**$\cdot H_2O\cdot 3DMF$) suitable for X-ray crystallography (see below).

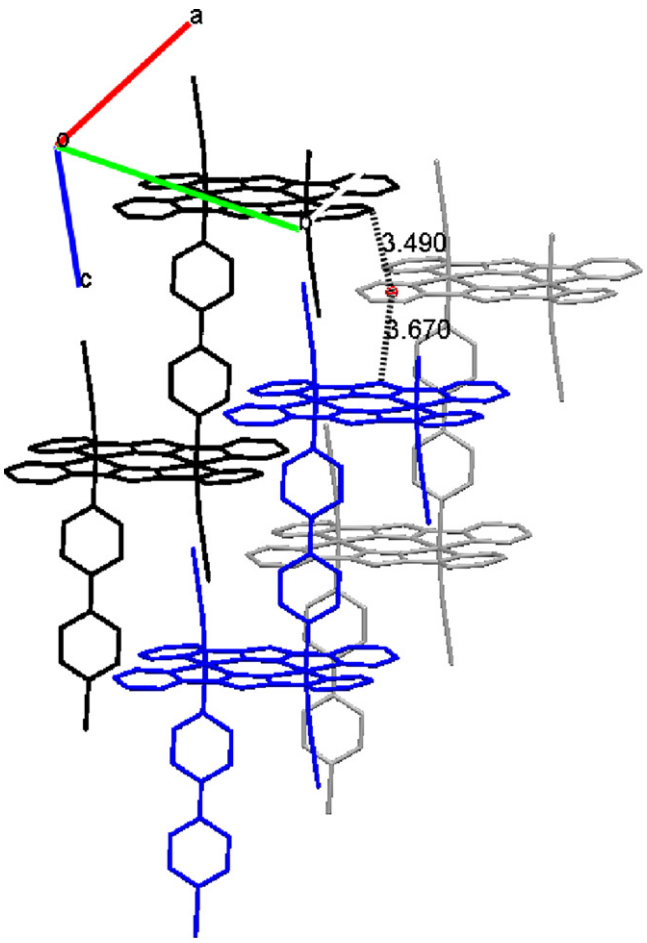

Fig. 41. Face to face π–π interactions between the pyridine-pyridine and pyridine-pyrazole moieties of $(L^{21})^-$ formed between different polymeric chains (black, blue and gray) in the crystal packing of complex **44**. The methanol solvent molecule and the hydrogen atoms are omitted for the sake of clarity. This figure was generated from data obtained from the CCDC as published originally in reference [84].

A powder sample of complex **43**$\cdot H_2O\cdot 3DMF$ presents a gradual and almost complete ST with $T_{1/2} \approx 250$ K. The thermal ST was characterized by ^{57}Fe Mössbauer spectroscopy. The spectrum at 298 K shows the characteristic doublet for a HS iron(II) centre (δ_{iso} = 0.966 and ΔE_Q = 2.08 mm s^{-1}), while at 77 K the parameters are typical of the LS state (δ_{iso} = 0.282 and ΔE_Q = 0.486 mm s^{-1}) [83].

The heterodimetallic complex **43**$\cdot H_2O\cdot 3DMF$ crystallizes in $P2_1/n$ space group. The ligand $(L^{21})^-$ bridges the Cr(III) and Fe(II) centres via the pyrazolate moiety. The Cr(III) is bonded to the tetradentate nta ligand through the central tertiary amine, and the three O-donor atoms in a *mer* fashion, and is also bonded to two nitrogen donor atoms of the $(L^{21})^-$ ligand, one from the bridging pyrazolate moiety and the other from a pyridine arm. The iron(II) centre is coordinated to a tetradentate picen ligand, through two secondary amines and to two pyridine rings, and also to two nitrogen donor atoms of the $(L^{21})^-$ ligand, one from the bridging pyrazolate moiety and the other from a pyridine arm. Interestingly there is an intramolecular hydrogen bonding interaction between one of the protons of the secondary amine in the picen

Table 4
Summary of some structural and magnetic parameters for the structurally characterized SCO-active iron(II) complexes of pyrazole-pyridine/pyrazine containing ligands analysed in this paper.

Complex	T (K)	Spin state	Space group	Colour	$T_{1/2}$ (K)	$\Delta T_{1/2}$ (K)	Ref.
$[Fe(L^1)_2][BF_4]_2$ (**1**)	240 290	LS HS	$P2_1$ $P2_1$	Dark brown Yellow	261	3	[26,27]
1·2.9CH_3NO_2·0.25H_2O	150	LS	$P2_12_12_1$	Dark brown	261	3	[26]
$[Fe(L^1)_2][Co(C_2B_9H_{11})_2]_2$ (**2**)	150 300	LS HS	$Pca2_1$ $Pca2_1$	Not stated Orange	318 (incomplete)	0	[39]
$[FeL^1][ClO_4]_{0.30}[BF_4]_{1.70}$ (**4**)	150 300	LS HS	$P2_1$ $P2_1$	Dark brown Yellow	258	0.6	[40]
$[FeL^1][ClO_4]_{0.98}[BF_4]_{1.02}$ (**5**)	150 300	LS HS	$P2_1$ $P2_1$	Dark brown Yellow	253	1.1	[40]
$[FeL^1][ClO_4]_{1.68}[BF_4]_{0.32}$ (**6**)	150 150	LS LS	$C2/c$ $P2_1/n$	Dark brown Dark brown	250	1.6	[40]
$[Fe(L^2)_2][BF_4]_2$ (**8**)	300	HS	$P2_1/n$	Orange-yellow	271	0	[45,46]
$[Fe(L^2)_2][ClO_4]_2$ (**9**)	30 30 340	LS HS[a] HS	Cc Cc Cc	Brown Yellow Yellow	284	0	[45,46]
$[Fe(L^3)_2](ClO_4)_2$ (**10**)	30 250	LS HS	$P\bar{4}2_1c$ $P2_12_12_1$	Dark-brown-yellow Yellow	233	3	[46]
$[Fe(L^4)_2](BF_4)_2$ (**11**)	220 300	LS HS	$P\bar{4}2_1c$ $P2_1$	Brown Yellow	$T_{1/2}\uparrow = 203$ $T_{1/2}\downarrow = 200$	3	[47]
$[Fe(L^5)_2](BF_4)_2$ (**12**)	300	HS	$P\bar{4}2_1c$	Yellow	$T_{1/2}\uparrow = 252$ $T_{1/2}\downarrow = 254$	2	[47]
$[Fe(L^6)_2][BF_4]_2$·3$MeNO_2$ (**13**$[BF_4]_2$·3$MeNO_2$)	150 300	LS HS	$P2_1/n$ $P2_1/n$	Brown Yellow	198	0	[48]
$[Fe(L^7)_2][BF_4]_2$ (**14**$[BF4]_2$)	30 290	LS HS	$I\bar{4}$ $I\bar{4}$	Brown Yellow	235	0	[48]
$[Fe(L^7)_2][ClO_4]_2$ (**14**$[ClO_4]_2$)	30 290	LS HS	$I\bar{4}$ $I\bar{4}$	Brown Yellow	196 133 (2 steps)	0	[48]
$[Fe(L^{10}H^+)(L^{10})](ClO_4)_3$·MeOH (**16**)	180	LS	$P2_1/c$	Red	286	2	[52]
$[Fe(L^{11})_2](ClO_4)_2$·2CH_3CN (**17**)	150	LS	$P2/c$	Red	$T_{1/2}\uparrow = 162$ $T_{1/2}\downarrow = 196$ (2 steps)	34	[53]
$[Fe(L^{11})_2](BF_4)_2$·2CH_3CN (**18a**) (orange polymorph)	180	LS	$P2/c$	Red	$T_{1/2}\uparrow = 218$ $T_{1/2}\downarrow = 224$	6	[53]
$[Fe(L^{11})_2](BF_4)_2$·2CH_3CN (**18b**) (red polymorph)	180	LS	$Pna2_1$	Red	Not stated	Not stated	[53]
$[Fe(L^{12})_2](ClO_4)_2$ (**19**)	180	LS	$Pbcn$	Brown	333	0	[55]
$[Fe(L^{13})_2](ClO_4)_2$ (**20**)	180	LS	Pcca	Brown	281	0	[55]
$[Fe(L^{14})_2](ClO_4)_2$·2CH_3CN (**21**)	180 298	LS:HS (1:1) HS	$C2/c$ $C2/c$	Dark orange Light orange	Not stated	0	[55]

Table 4 (*Continued*)

Complex	T (K)	Spin state	Space group	Colour	$T_{1/2}$ (K)	$\Delta T_{1/2}$ (K)	Ref.
[Fe $(H_2L^{15})_2$](BF$_4$)$_2$·3H$_2$O (**22**·3H$_2$O)	RT	LS	*C*2/*c*	Red brown	$T_{1/2}\uparrow$ = 180 $T_{1/2}\downarrow$ = 170	10	[58]
[Fe(H_2L^{15})$_2$]I$_2$·4H$_2$O (**23**·4H$_2$O)	RT	LS	*P*-1	Red brown	Not stated	-	[58]
[Fe(H_2L^{15})$_2$](SCN)$_2$·2H$_2$O (**24**·2H$_2$O)	RT	HS	*P*-1	Yellow	First step: $T_{1/2}\uparrow$ = 256 $T_{1/2}\downarrow$ = 247 Second step $T_{1/2}\uparrow$ = 219 $T_{1/2}\downarrow$ = 247	1st step: 9, 2nd step: 24	[59]
[Fe(H_2L^{15})$_2$](SeCN)$_2$ (**25**)	RT	HS	*P*-1	Orange yellow	321	0	[59]
[Fe(H_2L^{15})$_2$](CF$_3$SO$_3$)$_2$·3H$_2$O (**26**·3H$_2$O)	RT	LS	*P*-1	Yellow	$T_{1/2}\downarrow \approx$ 285 K $T_{1/2(\mathbf{1})}\uparrow \approx$ 150 K $T_{1/2(2)}\uparrow \approx$ 285 K	1st step: ≈30, 2nd step: ≈100	[62,63]
[Fe(H_2L^{15})$_2$][Fe(CN)$_5$(NO)] (**27**)	100 294	LS HS	*Pnca* *P*4/*ncc*	Orange Yellow	$T_{1/2}\uparrow$ = 181 $T_{1/2}\downarrow$ = 184	3	[64]
[Fe(H_2L^{15})$_2$][Cr(bpy)(ox)$_2$]$_2$·2H$_2$O (**28**·2H$_2$O)	180	HS:LS (1:1)	*P*-1	Red	$T_{1/2}\downarrow$ = 353	0	[65]
28′·2H$_2$O	180	HS	*P*-1	Red	$T_{1/2}\downarrow$ = 353	0	[65]
[Fe(H_2L^{15})$_2$][Cr(phen)(ox)$_2$]$_2$·0.5H$_2$O·0.5MeOH (**29**·0.5H$_2$O·0.5MeOH)	180	HS:LS (1:1)	*P*-1	Orange	370	0	[66]
[Fe$_2$(H_2L^{15})$_2$(μ-bpy)(SCN)$_4$]·2MeOH (**30**)	293	[HS-HS]	$P2_1/n$	Red	120-70 (gradual)	0	[67]
[Fe(L^{16})$_2$](ClO$_4$)$_2$·H$_2$O (**31**)	RT	LS	$P2_1$	Not Stated	≈ 210	0	[68,69]
[Fe(HL^{18})$_3$](CF$_3$SO$_3$)$_2$·2H$_2$O (**33**·2H$_2$O)	RT	HS	$P2_1/c$	Red brown	$T_{1/2}\uparrow$ = 241 $T_{1/2}\downarrow$ = 229	12	[72]
{[Fe(HL^{18})$_2$(NCSe)$_2$](μ-OH$_2$)(H$_2$O)$_2$}·H$_2$O·MeOH (**34**)	298	HS	*Pbcn*	Yellow	≈125	0	[73]
[Fe$_2$(HL^{18})$_2$(μ-L^{18})$_2$(NCSe)$_2$]·2H$_2$O (**35**)	123 298 123	HS:LS (4:1) [HS:HS] [LS:LS]	*Pbca* *Pbca* *Pbca*	Yellow Yellow-orange	225	0	[74]
[Fe(L^{19})$_2$](ClO$_4$)$_2$·C$_7$H$_8$ (**36**·C$_7$H$_8$)	270 240 120	HS HS LS	$P2_1/n$ $P2_1/n$ $P2_1/n$	yellow Yellow- orange	$T_{1/2}\uparrow \approx$ 233 $T_{1/2}\downarrow \approx$ 231	2	[76]
[Fe(L^{20})$_2$](BF$_4$)$_2$·MeOH (**37**·MeOH)	25 25 Quench- cooled 123	LS HS HS:LS (1:1)	*Pn* *Pn* *Pn*	red	Step 1 $T_{1/2} \approx$ 197 Step 2 $T_{1/2}\uparrow$ = 91 $T_{1/2}\downarrow$ = 98	7	[77]
[Fe(L^{20})$_2$](ClO$_4$)$_2$·EtOH (**38**·EtOH)	123	LS	$P2_1/n$	Red	250	0	[77]
trans-[Fe$_2$(μ-L^{21})$_2$(NCBH$_3$)$_2$(Py)$_2$] (**41**)	100 296	[LS-LS] [HS-HS]	$P2_1/n$ $P2_1/n$	Red Red	205	0	[80]
trans-[Fe$_2$(μ-L^{21})$_2$(NCBH$_3$)$_2$(4phPy)$_2$] (**42**)	100 200 296	[LS-LS] [LS-LS]:[HS-HS] 1:1 [HS-HS]	*P*-1 *P*-1 *P*-1	Black Red Red	200	0	[82]
[(nta)Cr(μ-L^{21})Fe(picen)](BF$_4$) (**43**)	296	[HS-HS]	$P2_1/n$	Brown	250	0	[83]
trans -[Fe$_2$(μ-L^{21})(μ-bpy)(NCS)$_2$]$_n$·MeOH (**44**)	150 200	[LS-LS] [HS-HS]	*P*-1 *P*-1	Black Orange	162	2	[84]

[a] Light induced metastable HS state.

ligand and one of the carboxylate units of the nta ligand (Fig. 39). The coordination sphere around the iron(II) centre is highly distorted: the N–Fe–N bond angles are almost 10° away from the ideal octahedral angles of 90° and 180°. The average Fe–N bond length, 2.203 Å, is typical of iron(II) in the HS state. As expected, there are intermolecular π stacking interactions between the two pyridyl moieties of the $(L^{21})^-$ strands in pairs of neighboring complexes, and these result in discrete dimers within the crystal lattice (Fig. 40).

In an attempt to understand the interactions that occur between neighboring SCO-active molecules during a ST, Kaizaki and co-workers [84] also synthesized the 1D polymeric complex *trans*-$[Fe_2(\mu\text{-}L^{21})(\mu\text{-bpy})(NCS)_2]_n\cdot$MeOH (**44**) where bpy = 4-4′-bipyridine. Complex **44** was synthesized in methanol, under a nitrogen atmosphere, by layering a methanolic solution containing HL^{21} and bpy over a 10% methanol solution of tetra-*n*-butylammonium hydroxide. The layers slowly mixed at room temperature and after 1 month brown crystals suitable for X-ray crystallography formed.

Magnetic susceptibility studies of the crystalline material showed that complex **44** undergoes an abrupt and almost complete ST upon cooling. In the warming mode a small hysteresis loop of 2 K width is observed ($T_{1/2}$ = 162 K). The ST was corroborated by VT ^{57}Fe Mössbauer spectroscopy. At 79.5 K the LS state was characterized by a doublet with parameters δ_{iso} = 0.505 and ΔE_Q = 0.573 mm s^{-1}. Whereas at 297 K only one doublet, characteristic of HS iron(II), is seen (δ_{iso} = 1.00 and ΔE_Q = 2.45 mm s^{-1}), confirming the ST. From these results it is clear that the ST in this polymer of dinuclear complexes occurs from a [HS–HS] to a [LS–LS] state. Both spin states were characterized by X-ray crystallography. Complex **44** crystallizes in the *P*-1 space group and is isostructural with complexes **41** and **42**. In this case the axially bridging bpy ligand connects two dinuclear cations, forming a linear polymeric structure. There are face to face π–π interactions between the pyridine rings of the $(L^{21})^-$ ligands of neighboring molecules, and face to face π–π interactions between the pyrazole ring and the pyridine moiety in neighboring molecules in different polymeric chains (Fig. 41) [84].

4. Concluding remarks

In this review the synthesis, characterisation and magnetic properties of the 42 structurally characterized SCO-active iron(II) complexes of pyrazole-pyridine/pyrazine containing ligands has been detailed and analysed. According to the CSD (5.31, update September 2009) there are at least 90 structurally characterized iron(II) complexes of the ligands analysed in this review but only half of them are SCO-active. A summary of some of the magnetic and structural properties is presented in Table 4.

The six classes of ligands analysed in this review contain at least one pyridine or pyrazine moiety attached to either the C or N atom of the pyrazole ring, either directly or indirectly. The iron(II) complexes of the more rigid terdentate ligands 2,6-bis(pyrazol-1-yl)pyridine/pyrazine ($N_{pyrazole}$–$C_{pyridine}$ connection) and 2,6-bis(pyrazol-3-yl)pyridine ($C_{pyrazole}$–$C_{pyridine}$ connection) have varied and interesting SCO-properties. In the case of the $N_{pyrazole}$–$C_{pyridine}$ connected ligands a wide range of substitutions in the ligand skeleton has been achieved, therefore some tuning and modification of SCO properties has been done in this way. For this system the effect of the anion and crystallization solvent on the SCO properties has also been analysed, showing how sensitive SCO is towards the choice of both anion and solvent. Meanwhile complexes of the $C_{pyrazole}$–$C_{pyridine}$ connected 2,6-bis(pyrazol-3-yl)pyridine ligands (H_2L^{15}) present solvent dependent SCO activity. Future work with this class of ligand should include the introduction of substituents in the ligand structure in order to tune the SCO properties.

A more flexible, and longer armed version of the ligands described above is 2,6-bis(pyrazol-1-ylmethyl)pyridine (L^{16}), a terdentate ligand that generates two adjacent 6-membered chelate rings (either side of the pyridine ring) on binding. In principle, this ligand could be functionalised more easily than its more rigid analogues and therefore a family of pre-designed iron(II) SCO active complexes could be prepared. However, it is interesting to note that the methyl-substituted ligand L^{17} resulted in an iron(II) complex that was locked in the HS state, probably due to steric effects.

The ligand 2-(pyrazol-3-yl)pyridine (HL^{18}) can act as a bidentate ligand, forming a 5-membered chelate ring on binding. The result is either tris-bidentate complexes or, on deprotonation of the NH group of the pyrazole ring, polynuclear complexes readily form. The SCO chemistry of the polynuclear complexes of the deprotonated ligand is more interesting than that of the monometallic complexes of the neutral ligand. Despite this, there is only one dinuclear SCO active complex structurally characterized to date (complex **35**), probably due to the difficulties associated with the clean isolation of dinuclear systems using this ligand, which has a relatively low denticity and can generate a relatively wide range of possible structural types of complex. Di- and poly-metallic systems are very important in order to understand the effect on SCO of the communication between the pyrazolate-bridged iron centres so there is considerable interest in such species.

The *N*-blocked analogue of HL^{18}, 2-(1-picolylpyrazol-3-yl)pyridine (L^{19}), is a terdentate ligand with chemistry similar to that of the 2,6-bis(pyrazol-1-ylmethyl)pyridine (L^{16}) ligand, despite it featuring a central pyrazole (cf. pyridine) and a combination of adjacent 5- and 6-membered chelate rings (cf. both 6-membered). There is only one structurally characterized complex of ligand L^{19} (complex **36**·C_7H_8, $T_{1/2}\uparrow \approx 233$, $T_{1/2}\downarrow \approx 231$ K). This ligand better stabilised the HS state, indicating that it confers a weaker ligand field towards iron(II) centres, than the analogous ligand of the more rigid family, 2,6-(pyrazol-1-yl)pyridine family, L^1 ($T_{1/2}$ = 261 K). Use of the pyrazine-analogue of L^{19}, L^{20}, resulted in a, differently solvated, iron(II) complex (**38**·EtOH) with no hysteresis loop (the potential of greater intermolecular interactions being facilitated by the 'spare' nitrogen atoms was not realised).

Finally, the deprotonated bis-bidentate ligand 3,5-bis(pyrid-2-yl)pyrazolate $(L^{21})^-$ affords dimetallic systems in which the iron(II) centres are doubly-bridged by pyrazolate units and the apical positions are available for coordinating solvent and/or anion molecules, facilitating the tuning of the SCO properties. Another way to tune the properties of these dinuclear iron(II) complexes would be to introduce substituents in the 4-position of the pyrazole moiety or somewhere in the pyridine rings of HL^{21}.

Some of the complexes presented in this review showed the LIESST effect at very low temperatures. Attempts to use pyrazole moieties in the synthesis of highly constrained ligands may ultimately result in complexes with higher *T*(LIESST), for example at liquid nitrogen temperatures (at present even this is an ambitious target). However, a survey of 60 SCO complexes by Letard and co-workers [42] revealed, along with the expected correlation between the observed $T_{1/2}$ and *T*(LIESST) values (Eq. (1)), a wide range of *T*(LIESST) values, ca. 20–140 K, so clearly higher temperatures than have been seen for the pyrazolate complexes presented above have been observed for other ligand classes. In addition, they showed that the *T*(LIESST) value appears depend on the exact nature of the inner coordination sphere provided by the ligand (they examined monometallic and network complexes of mono-, di-, tri- and tetra-dentate ligands).

The first systematic variation of ligand substituents in such complexes, by Kaizaki and co-workers [71], revealed a correlation between the Hammett constant of the substituent and $T_{1/2}$

observed for the resulting diiron(II) complex. This indicates that one of the longer term aims in SCO, the prediction and tuning of the nature of the SCO event, is not entirely unrealistic. Certainly establishing a degree of predictability and tuneability – prior to synthesis and characterisation – is highly desirable if such complexes are to form the basis for the production of useful nanodevices, which are likely to need to operate at, or near, room temperature.

Acknowledgements

This work was supported by grants from the University of Otago and the MacDiarmid Institute, including the award of a MacDiarmid-funded PhD scholarship to JO.

References

[1] S. Trofimenko, Chem. Rev. 72 (1972) 497.
[2] F. Mani, Coord. Chem. Rev. 120 (1992) 325.
[3] G.L. Monica, G.A. Ardizzoia, Prog. Inorg. Chem. 46 (1997) 151.
[4] R. Mukherjee, Coord. Chem. Rev. 203 (2000) 151.
[5] M.D. Ward, J.A. McCleverty, J.C. Jeffery, Coord. Chem. Rev. 222 (2001) 251–272.
[6] C. Pettinari, R. Pettinari, Coord. Chem. Rev. 249 (2005) 525–543.
[7] C. Pettinari, R. Pettinari, Coord. Chem. Rev. 249 (2005) 663–691.
[8] M.A. Halcrow, Coord. Chem. Rev. 249 (2005) 2880.
[9] M.A. Halcrow, Coord. Chem. Rev. 253 (2009) 2493.
[10] M.A. Halcrow, Dalton Trans. (2009) 2059–2073.
[11] J. Klingele, S. Dechert, F. Meyer, Coord. Chem. Rev. 253 (2009) 2698.
[12] A. Bousseksou, G. Molnar, J.A. Real, K. Tanaka, Coord. Chem. Rev. 251 (2007) 1822.
[13] P. Gütlich, H.A. Goodwin, Top. Curr. Chem. 233 (2004) 1.
[14] P. Gütlich, Y. Garcia, H.A. Goodwin, Chem. Soc. Rev. 29 (2000) 419.
[15] J.A. Real, A.B. Gaspar, M.C. Muñoz, Dalton Trans. (2005) 2062.
[16] S. Brooker, J.A. Kitchen, Dalton Trans. (2009) 7331.
[17] O. Kahn, Chem. Br. 2 (1999) 24.
[18] Y. Garcia, P.J. van Koningsbruggen, G. Bravic, P. Guionneau, D. Chasseau, G.L. Cascarano, J. Moscovici, K. Lambert, A. Michalowicz, O. Kahn, Inorg. Chem. 36 (1997) 6357.
[19] J.-F. Letard, P. Guionneau, L. Capes, Top. Curr. Chem. 235 (2004) 221.
[20] J.A. Kitchen, S. Brooker, Coord. Chem. Rev. 252 (2008) 2072–2092.
[21] F.H. Allen, Acta Crystallogr., Sect. B 58 (2002) 380.
[22] F.H. Allen, S.A. Bellard, M.D. Brice, B.A. Cartwright, A. Doubleday, H. Higgs, T. Hummelink, B.G. Hummelink-Peters, O. Kennard, W.D.S. Motherwell, J.R. Rodgers, D.G. Watson, Acta Crystallogr., Sect. B 35 (1979) 2331.
[23] G.J. Long, D. Grandjean, D.L. Reger, Top. Curr. Chem. 233 (2004) 91.
[24] H.A. Goodwin, Top. Curr. Chem. 234 (2004) 23.
[25] T. Ayers, S. Scott, J. Goins, N. Caylor, D. Hathcock, S.J. Slattery, D.L. Jameson, Inorg. Chim. Acta 307 (2000) 7–12.
[26] J.M. Holland, J.A. McAllister, C.A. Kilner, M. Thornton-Pett, A.J. Bridgeman, M.A. Halcrow, J. Chem. Soc., Dalton Trans. (2002) 548.
[27] J.M. Holland, J.A. McAllister, Z. Lu, C.A. Kilner, M. Thornton-Pett, M.A. Halcrow, Chem. Commun. (2001) 577.
[28] A.H.R. Al-Obaidi, K.B. Jensen, J.J. McGarvey, H. Toftlund, B. Jensen, S.E.J. Bell, J.G. Carroll, Inorg. Chem. 35 (1996) 5055.
[29] L.J. Wilson, D. Georges, M.A. Hoselton, Inorg. Chem. 14 (1975) 2968.
[30] H. Toftlund, S. Yde-andersen, Acta Chem. Scand. 35A (1981) 575.
[31] N. Ortega-Villar, A. Thompson, M.C. Muñoz, V.M. Ugalde-Saldívar, A.E. Goeta, R. Moreno-Esparza, J.A. Real, Chem. Eur. J. 11 (2005) 5721–5734.
[32] W. Linert, M. Konecny, F. Renz, J. Chem. Soc., Dalton Trans. (1994) 1523.
[33] K.A. Reeder, E.V. Dose, L.J. Wilson, Inorg. Chem. 17 (1978) 1071.
[34] B. Weber, F.A. Walker, Inorg. Chem. 46 (2007) 6794.
[35] D.F. Evans, T.A. James, Dalton Trans. (1979) 723.
[36] N.G. White, H.L.C. Feltham, C. Gandolfi, M. Albrecht, S. Brooker, Dalton Trans. 39 (2010) 3751.
[37] V.A. Money, I.R. Evans, M.A. Halcrow, A.E. Goeta, J.A.K. Howard, Chem. Commun. (2003) 158.
[38] V.A. Money, J.S. Costa, S. Marcen, G. Chastanet, J. Elhaik, M.A. Halcrow, J.A.K. Howard, J.-F. Letard, Chem. Phys. Lett. (2004) 273.
[39] J. Elhaik, M.A. Halcrow, C.A. Kilner, Dalton Trans. (2006) 823.
[40] C. Carbonera, C.A. Kilner, J.-F. Létard, M.A. Halcrow, Dalton Trans. (2007) 1284.
[41] D.M.P. Mingos, A.L. Rohl, J. Chem. Soc., Dalton Trans. (1991) 3419.
[42] J.-F. Létard, P. Guionneau, O. Nguyen, J.S. Costa, S. Marcén, G. Chastanet, M. Marchivie, L. Goux-Capes, Chem. Eur. J. 11 (2005) 4582–4589.
[43] J.-F. Letard, J. Mater. Chem. 16 (2006) 2550.
[44] J.-F. Letard, P. Guionneau, L. Rabardel, J.A.K. Howard, A.E. Goeta, D. Chassaeu, O. Kahn, Inorg. Chem. 37 (1998) 4432.
[45] V.A. Money, J. Elhaïk, M.A. Halcrow, J.A.K. Howard, Dalton Trans. (2004) 1516.
[46] C. Carbonera, J.S. Costa, V.A. Money, J. Elhaïk, J.A.K. Howard, M.A. Halcrow, J.-F. Létard, Dalton Trans. (2006) 3058.
[47] R. Pritchard, C.a. Kilner, M.A. Halcrow, Chem. Commun. (2007) 577.
[48] J. Elhaïk, V.A. Money, S.A. Barrett, C.A. Kilner, I.R. Evans, M.A. Halcrow, Dalton Trans. (2003) 2053.
[49] V.A. Money, J. Elhaïk, I.R. Evans, M.A. Halcrow, J.A.K. Howard, Dalton Trans. (2004) 65.
[50] B.J. Childs, D.C. Craig, K.A. Ross, M.L. Scudder, H.A. Goodwin, Aust. J. Chem. 47 (1994) 891.
[51] J. England, R. Gondhia, L. Bigorra-Lopez, A.R. Petersen, A.J.P. White, G.J.P. Britovsek, Dalton Trans. (2009) 5319–5334.
[52] C. Rajadurai, F. Schramm, S. Brink, O. Fuhr, M. Ghafari, R. Kruk, M. Ruben, Inorg. Chem. 45 (2006) 10019.
[53] C. Rajadurai, Z. Qu, O. Fuhr, B. Gopalan, R. Kruk, M. Ghafari, M. Ruben, Dalton Trans. (2007) 3531–3537.
[54] R.A. Nyquist, Appl. Spectrosc. 44 (1990) 1405–1407.
[55] N.T. Madhu, I. Salitros, F. Schramm, S. Klyatskaya, O. Fuhr, M. Ruben, Compt. Rendus Chim. 11 (2008) 1166.
[56] K.H. Sugiyarto, H.A. Goodwin, Aust. J. Chem. 41 (1988) 1645.
[57] T. Buchen, P. Gütlich, H.A. Goodwin, Inorg. Chem. 33 (1994) 4573.
[58] K.H. Sugiyarto, D.C. Craig, A.D. Rae, H.A. Goodwin, Aust. J. Chem. 47 (1994) 869.
[59] K.H. Sugiyarto, M.L. Scudder, D.C. Craig, H.A. Goodwin, Aust. J. Chem. 53 (2000) 755.
[60] A. Bhattacharjee, V. Ksenofontov, K.H. Sugiyarto, H.A. Goodwin, P. Gutlich, Adv. Funct. Mater. 13 (2003) 877.
[61] A. Bhattacharjee, J. Kusz, M. Zubko, H.A. Goodwin, P. Gütlich, J. Mol. Struct. 890 (2008) 178.
[62] K.H. Sugiyarto, K. Weitzner, D.C. Craig, H.A. Goodwin, Aust. J. Chem. 50 (1997) 869.
[63] T. Buchen, P. Giitlich, K.H. Sugiyarto, H.A. Goodwin, Chem. Eur. J. 9 (1996) 1134.
[64] K.H. Sugiyarto, W.-A. McHale, D.C. Craig, A.D. Rae, M.L. Scudder, H.A. Goodwin, Dalton Trans. (2003) 2443.
[65] M.C. Giménez-López, M. Clemente-León, E. Coronado, F.M. Romero, S. Shova, J.-P. Tuchagues, Eur. J. Inorg. Chem. (2005) 2783.
[66] M. Clemente-León, E. Coronado, M.C. Giménez-López, F.M. Romero, Inorg. Chem. 46 (2007) 11266.
[67] D. Fedaoui, Y. Bouhadja, A. Kaiba, P. Guionneau, J.-F. Létard, P. Rosa, Eur. J. Inorg. Chem. (2008) 1022.
[68] A.A. Watson, D.A. House, P.J. Steel, Inorg. Chim. Acta 130 (1987) 167.
[69] S. Mahapatra, R.N. Mukherjee, Polyhedron 12 (1993) 1603.
[70] S. Mahapatra, R.J. Butcher, R. Mukherjee, Indian J. Chem. 40A (2001) 973.
[71] S. Kaizaki, K. Nakano, N. Suemura, K. Yoneda, S. Kawata, Dalton Trans. (2005) 740.
[72] L.S. Harimanow, K.H. Sugiyarto, D.C. Craig, M.L. Scudder, H.A. Goodwin, Aust. J. Chem. 52 (1999) 109.
[73] B.A. Leita, B. Moubaraki, K.S. Murray, J.P. Smith, Polyhedron (2005) 2165.
[74] B.A. Leita, B. Moubaraki, K.S. Murray, J.P. Smith, J.D. Cashion, Chem. Commun. (2004) 156.
[75] S. Singh, V. Mishra, J. Mukherjee, N. Seethalekshmi, R. Mukherjee, Dalton Trans. (2003) 3392.
[76] V. Mishra, R. Mukherjee, J. Linares, C. Balde, C. Desplanches, J.-F. Létard, E. Collet, L. Toupet, M. Castro, F. Varret, Inorg. Chem. 47 (2008) 7577.
[77] B.A. Leita, S.M. Neville, G.J. Halder, B. Moubaraki, C.J. Kepert, J.-F. Létard, K.S. Murray, Inorg. Chem. 46 (2007) 8784.
[78] N. Suemura, M. Ohama, S. Kaizaki, Chem. Commun. (2001) 1538.
[79] G.B. Kauffman, R.A. Albers, F.L. Harlan, Diidothiocyanatotetrapyridine and Diisothiocyanatodipyridine Complexes of Dipositive First-Transition-Metal Ions (Manganese, Iron, Cobalt, Nickel, Copper, and Zinc), vol. 12, McGraw-Hill, 1970.
[80] K. Nakano, N. Suemura, S. Kawata, A. Fuyuhiro, T. Yagi, S. Nasu, S. Morimoto, S. Kaizaki, Dalton Trans. (2004) 982.
[81] C.J. Schneider, J.D. Cashion, B. Moubaraki, S.M. Neville, S.R. Batten, D.R. Turner, K.S. Murray, Polyhedron 26 (2007) 1764.
[82] K. Nakano, S. Kawata, K. Yoneda, A. Fuyuhiro, T. Yagi, S. Nasu, S. Morimoto, S. Kaizaki, Chem. Commun. (2004) 2892.
[83] K. Ni-iya, A. Fuyuhiro, T. Yagi, S. Nasu, K. Kuzushita, S. Morimoto, S. Kaizaki, Bull. Chem. Soc. Jpn. 74 (2001) 1891–1897.
[84] K. Yoneda, K. Adachi, S. Hayami, Y. Maeda, M. Katada, A. Fuyuhiro, S. Kawata, S. Kaizaki, Chem. Commun. (2006) 45.